EXPERIMENTAL INVESTIGATION OF SMALL WATERSHED FLOODS

by

E. F. Schulz
V. M. Yevjevich

June, 1970

Colorado Water Resources Research Institute
Completion Report No. 18

EXPERIMENTAL INVESTIGATION OF SMALL WATERSHED FLOODS

Completion Report 18

OWRR Project B-030-COLO

June 30, 1970

by

E. F. Schulz and V. M. Yevjevich
Department of Civil Engineering
Colorado State University

submitted to

Office of Water Resources Research
U. S. Department of Interior
Washington, D. C.

The work upon which this report is based was supported (in part) by funds provided by the United States Department of the Interior, Office of Water Resources Research, as authorized by the Water Resources Research Act of 1964, and pursuant to Grant Agreement No. 14-01-0001-1885.

NATURAL RESOURCES CENTER
Colorado State University
Fort Collins, Colorado

Norman A. Evans, Director

June, 1970

CER69-70EFS-VY38

ABSTRACT

EXPERIMENTAL INVESTIGATION
OF SMALL WATERSHED FLOODS.

An outdoor experimental rainfall-runoff facility was constructed at Colorado State University. Initially the watershed consisted of a conic section having an interior angle of 120°, a radius of 110 feet and a uniform slope of 5%. The surface of the watershed was stabilized by covering with a sheet of butyl rubber. The rainfall is simulated by overlapping sets of rainfall patterns from 164 sprinkler heads set at 10 feet above the surface of the watershed. Rainfall intensities of approximately 0.5, 1.0, 2.0 and 4.0 inches per hour can be produced by utilizing various combinations of sprinkler heads. At the present time the experimental rainfall is uniformly distributed in time and space over the watershed. In the future almost any variation of distribution is possible since each of the 164 sprinklers can be individually controlled according to any program. The runoff is measured through a 1.5-ft. H-flume equipped with a modified FW 1 water stage recorder. The time scale has been speeded up so that the smallest scale division corresponds to 5 seconds of time. Experiments on butyl rubber surface have demonstrated that the kinematic wave theory can be applied to computing the output hydrograph from the conic sector by considering the watershed as a 5-element kinematic cascade where each succeeding element is narrower than the previous element. For the case of the converging flow on the conic section, it was found that the flow can no longer be characterized as laminar. Research work is continuing.

Schulz, E. F., and V. M. Yevjevich

EXPERIMENTAL INVESTIGATION OF SMALL WATERSHED FLOODS

KEY WORDS: - *Rainfall-Runoff, *Hydrologic Models, *Rainfall Simulator, Hydrology, Surface Detention, Experimental Watershed, *Kinematic Wave Theory, Kinematic Cascade, Laminar Flow, Turbulent Flow.

EXPERIMENTAL INVESTIGATION OF SMALL
WATERSHED FLOODS

This report presents the developments and summarizes the results of the research up to the termination of Project B-030-COLO on 30 June 1970. Certain aspects of the research work is continuing. The research support we have received from the Office of Water Resources Research has aroused some interest on the part of other public and private agencies. The facility has the benefit of a moderate amount of support from the Agricultural Research Service, and the Department of the Army. The matching funds have been provided through the Colorado State University Experiment Station.

OBJECTIVES

The objectives of this research project were 1) to develop an experimental facility wherein various theories and analytical methods could be evaluated and 2) test analytical theories and 3) merge the analytical models with observations of floods from small natural watersheds. The long term objectives of the experimental rainfall-runoff facility is to bridge the results between the small scale, "low-noise" experiments with the larger scale randomized data from natural watersheds.

The basic design of the experimental facility has been described in reports issued in connection with a previous project and will be brought current in this discussion. The results of experiments in connnection with the Kinematic Wave Theory will be briefly summarized.

During the period of the current project considerable research effort was devoted to the design, testing and development of a practical rainfall simulator system. Initially it was desired to create a reproducible storm having a uniform areal distribution of rainfall at a uniform intensity for whatever duration required to bring various elements of the catchment to an equilibrium rate of runoff. As the basic knowledge about the rainfall-runoff process matured the areal and time distributions within the duration of the model storm would be varied. The design and testing of the rainfall system is presented in detail in a report included as Appendix I.

SUMMARY OF FINDINGS

Initially effort was devoted to develop a rainfall simulator which would duplicate some of the natural atmospheric processes in producing the rainfall. In addition it was thought that any structure of the rainfall simulator must not interfere with the trajectory of any raindrop falling on the experimental catchment. This meant that the simulators must either be around the periphery of the catchment or would have to be suspended above the catchment.

The effort to produce a rainfall simulator over a catchment of so great extent proved to be unsuccessful. It was decided to build a simulator over the upper conic section of the watershed based on the rainfall simulator built in Israel and reported by A. Shachori and I. Seginer. This design was based on the overlapping patterns of rainfall from a number of adjacent individual sprinklers.

Extensive tests were made on various types and designs of sprinklers and nozzles used for lawn irrigation. Several of the nozzles were thoroughly tested over practical ranges of operating pressure and distance above the ground. The model 78c Rain Jet nozzle operating at a pressure of 28 psi and 10 feet above the ground was selected for use.

Overlapping patterns from adjacent nozzles were combined by means of a computer program to find the optimum spacing of nozzles. A test was conducted on a small number of nozzles to verify experimentally the computer predicted rainfall distribution. The final design was based upon overlapping patterns from sprinklers equally spaced at 40 foot a distance. Higher intensities were obtained by increasing the density of the nozzles. The nozzles were spaced at 10-foot intervals along a 2-inch aluminum supply line. These

aluminum supply lines were spaced at 17.5 - foot intervals along the long axis of the watershed. Additional features of testing and design of the rainfall simulator are given in Appendix I.

Kinematic Wave Experiments

The butyl covered upper conic sector was used as watershed to test various aspects of the kinematic wave theory. The rainfall was uniformly distributed over the catchment but since the flow is converging, the depth of flow is increasing. As a result, the flow passed from a laminar flow in the headwaters to a turbulent flow at the outlet where the runoff hydrograph is measured.

It was found that the conic watershed could be represented by a kinematic cascade of five elements of decreasing width. A finite-difference solution based on a rectangular grid was used to solve the kinematic cascade. Three finite-difference methods were used, they were:

1. Lax-Wendroft (Single-Step),
2. Upstream Differencing,
3. Brakensiek's Four Point Method.

A comparison of these results are shown in the report included as Appendix II. The results presented in Appendix II were based on tests on the 120° butyl covered conic section having a 110-foot length of overland flow.

Some experiments were conducted with shorter lengths of overland flow and with sectors of 30°. The butyl surface was roughened by scattering gravel over the surface. Some of these data for the smaller watersheds and for the smaller rainfall intensities have been difficult to interpret because of stilling - well lag on the runoff recorder and because of uncertainty with regard to the time of beginning and ending of the rainfall with respect to the time scale of the runoff hydrograph. The runoff recorders have been

modified and improved to eliminate these uncertainities and some of the data will be repeated during the coming season. A summary of the other runs is included in the report presented as Appendix III.

CONCLUSIONS

The facility has been in operation and has verified the validity of the Kinematic Wave Theory as applied to the concept that the conic watershed can be considered as a series of cascades.

Weakness in the design of some of the instruments have been located and corrected. The watershed in now being enlarged to add two intersecting plane sectors to the conic sector. A variety of experiments dealing with the mathematical modelling of flood runoff, channel morphology in an erodible material and the routing of pollutants in a watershed system will be investigated during the coming summer.

LIST OF APPENDICES

COLORADO STATE UNIVERSITY

EXPERIMENTAL RAINFALL-RUNOFF FACILITY

Design and Testing of Rainfall System

by

M. E. Holland

prepared for
U. S. Department of the Interior
Office of Water Resources Research
under matching grant
No. B-030-COLO.
and
Colorado State University Experiment Station
Fort Collins, Colorado

November 1969

CER 69-70 MEH 21

ACKNOWLEDGEMENTS

The research reported in this paper is supported by the United States Department of the Interior, Office of Water Resources Research under Matching Grant No. B-030-COLO. and by the Colorado State University Experiment Station. The United States Department of Agriculture, Agricultural Research Service, has cooperated in the development of the facility.

Portions of this report have been prepared as internal reports by graduate research assistants working on the project. The contributions of C. B. Cluff on the drop size study and R. E. Smith on the modification of the capacitance raingage are especially of note. George Smith, Associate Professor of Civil Engineering, and David Woolhiser, Research Hydraulic Engineer with the Agricultural Research Service, also have assisted in the preparation of this report.

were lowered slightly to further reduce the interaction, but the problem was not completely removed.

A more serious problem was found to be the concentration that occurred at the ends of the sweep of the nozzles. There is a certain amount of time required to stop the nozzles and reverse the direction of movement. As the speed of movement increases to provide a more uniform distribution in time, the proportion of time required to reverse the movement becomes greater. Large concentrations develop at the ends of the sweep. This could not be lessened without causing the time distribution to be worsened.

The above problems, coupled with the sensitivity of the jets to the wind, led to the rejection of the rain gun system. The wind effect is partly shown in Figure 7, where the lower part of the facility, at the right edge of the figure, is receiving no rainfall. The break-up of the jet to reduce other problems only intensifies the sensitivity to wind. This sensitivity is greatest for the lower intensities, which would be a frequent part of the testing anticipated on the facility.

Grid System

When the preliminary survey of literature was made, the grid system was rejected because of the cost of the structural support required to hold the nozzles and water supply lines above the facility. During the fall and winter of 1968-69, a modification of the grid system was given further consideration. The system used by Shachori and Seginer (5) used supply lines laid along the ground with the nozzles raised by small pipes to a height of 2 meters. Thus, no additional structural support is required. The design that was considered for the experimental facility

Figure 7. Testing of Irrigation Guns

Figure 8. Test for Distribution of Intensities for a Nozzle with Circular Pattern

CONSTRUCTION OF AN EXPERIMENTAL RAINFALL-RUNOFF FACILITY

Chapter 1

INTRODUCTION

The advantages of controlled experimentation into the problems of flood runoff, as distinct from the use of actual storm and flood data on natural catchments, are sufficiently great that many attempts have been made to utilize laboratory experiments in the study of runoff processes (1,2,3). Rainfall simulators have been used in the past mainly for studies of infiltration, detention storage, and overland flow. Hydrologists have long felt the desire to use rainfall in such a way that results obtained from a rainfall-runoff simulator could readily be applied to natural catchments. However, the size, complexity and cost of a structure suitable for study of the whole runoff cycle, and the inherent difficulties of extrapolating results from a "model" catchment to a natural catchment have discouraged the use of rainfall-runoff simulators for these purposes.

The rainfall-runoff experimental facility described in this paper makes possible the study of a number of processes that cannot be studied by small-scale laboratory models because of the problems of achieving dynamic similarity of hydrologic events. The philosophy and the general classes of problems that can be studied on the experimental facility have been presented previously (4) and will not be discussed in detail here. However, a brief review of the history of the development of this facility will be presented before the facility itself is described.

Development and use of the experimental facility is one phase of a three-phase research program into floods on small catchments. The other two phases are:

(i) The collection and processing of rainfall, streamflow, and catchment data for a large number of flood events that have been recorded

on small catchments throughout the world, and the storing of these data on punched cards and magnetic tape for ready use and distribution, and,

(ii) Theoretical studies of the relation between flood hydrographs and the factors that affect them, as well as the study of statistical and other techniques that can be used for the analysis of data from experimental investigations as well as from natural catchments. The three phases of the research program operate in a complementary fashion to permit the application of data and analysis techniques from a spectrum of sources to the study of the rainfall-runoff relationships in natural watersheds.

OBJECTIVES AND CRITERIA

The rainfall-runoff experimental facility was established in the early 1960's as a part of the three-phase approach to the study of floods from small watersheds. Although the rainfall-runoff simulator was originally conceived as a tool in the study of floods, it soon became clear that such a device could be useful in studying other hydrologic problems not related, or only indirectly related to flood estimation. These include such things as erosion studies and studies of the travel and dissipation of pollutants (chemical, biological and radioactive) in the watershed environment. The potential uses in these areas are discussed in more detail in the previous report (4). The aspects of interest for this report are the advantages in using the experimental facility and requirements that such uses place on the facility.

All the advantages in studying simulated rainfall-runoff events on an artificial catchment rather than naturally-occurring events on natural catchments derive from the fact that the simulated event can be controlled, whereas the natural event cannot. Briefly, the advantages are: (a) the potential homogeneity of any factor; (b) the controlled variability of any

factor; (c) the time factor in obtaining results; and (d) the convenience in experimentation. These will be explained more fully below.

Homogeneity. Whereas in nature all variables in general are variable in either space or time or both, in a rainfall-runoff simulator, any one or all variables can be made homogeneous over the whole area of the simulator and throughout the period of a test. This capability should be helpful in isolating the effect of a variable, since it will avoid the necessity of developing and using "average" or "index" measures of variables, or sampling variables across the area or in time. For example, if main stream slope is made uniform for a particular test, there will be no doubt about the appropriate measure of this variable as there is in the case of natural streams. This doubt has led to the development and use of at least four different measures of main stream slope, two being purely geometrical, and the others allowing for the effects of slope changes on velocity of flow. No one method is widely accepted, so the avoidance of this confusion will be an advantage for the artificial stream. The advantage applies to all characteristics of both the rainfall and the catchment.

This capacity for homogeneity of variables will also be useful in providing standard conditions against which results for non-homogeneous conditions can be compared. For instance, it seems logical to run tests in which rainfall intensity is approximately uniform with respect to time and area (although this never occurs in nature) to provide a yardstick against which the results of rainfalls of varying degree of non-uniformity can be compared.

Variability. An obvious advantage of the artificial event over the natural is the ability to change any particular variable between tests, while keeping all other variables unchanged. This variability between tests is not to be confused with the homogeneity or otherwise of a variable within a

test, which was discussed in the preceding paragraphs. Any particular variable can be either homogeneous or non-homogeneous over the area of the simulator or throughout the duration of a test, but it is important to be able to vary its value or average value over a wide range in a series of tests (without varying any other independent variable) to isolate its effect on whatever dependent variable (such as flood peak) is being studied. This is impossible to do on natural catchments and so it has been impossible to isolate the effect of any one variable with confidence.

In nature, it is necessary to use data from many catchments in order to get a range of values of any one variable, but use of many catchments also results in a range of all other independent variables. Thus, extracting the effect of any one variable becomes an inaccurate process, especially if, as is usual, the number of catchments and runoff events used is small.

Time Factor. A major disadvantage and inconvenience in most hydrologic studies is the relative paucity of data that arises from the relative shortness of most hydrologic records. Since, with an artifical rainfall simulator, it is not necessary to wait for natural storms to occur, a large body of data can be obtained in a short time. This is an important advantage of the use of simulated events.

Convenience. The location of the experimental facility at the Engineering Research Center makes workshop, laboratory, storage, office and data digitizing facilities readily available. The faculty members can supervise and monitor the progress of experiments during each day. Continual contact can be had with the experimental effort.

REQUIREMENTS FOR FACILITY

The requirements for the experimental facility may be presented in three general classes: (1) control of rainfall, (2) measurement of variables and (3) modification of basin characteristics.

1. Control of Rainfall

Uniformity and reproducibility. The controlled application of rainfall is the most important feature of the rainfall-runoff simulator. This is the characteristic that distinguishes the facility from experimental watersheds. The basic requirements of the artificial rainfall are areal uniformity and reproducibility. The facility should be capable of producing an approximately uniform spatial distribution of rainfall over the basin to minimize the masking of the basin response by rainfall variations. A perfectly uniform distribution will not be achieved, but a close approximation should be possible. Natural rainfall is never completely uniform, but the more nearly uniform the rainfall is over the entire basin, the more easily the effects of the watershed response may be evaluated from the experimental data.

The reproducibility of rainfall conditions is more important than uniformity. A repetition of an experiment under identical conditions is frequently useful to confirm results for the observed trial or to fill in measurements that may have been missed when an instrument did not operate properly. It is not necessary that a specified distribution be achieved without a trial-and-error approach, but once the control settings for a given pattern of rainfall have been determined, it should be possible to reproduce the conditions with a high degree of reliability at any later time by making the appropriate control settings.

For many studies it will be convenient to have the ability to vary the input in time and space. The experimental facility does include some provision for this.

For erosion studies, the artifical rainfall should approximate the spectrum of impact energies of natural raindrops. This will be difficult to achieve over the full range of input intensities.

2. Measurement of Variables

General requirements. The distribution of parameters and variables in both space and time are needed to interpret the response of the watershed system. If control of the input and state parameters of the system were perfect, their measurement would be of only minor significance because the values could be determined from the control specifications. Since the control is imperfect and the uniformity of rainfall can only be estimated before the facility is operated, the measurements will be quite important.

The instrument readings from all instruments should be transmitted to one location for observation and as much of the data as possible should be recorded automatically. This is needed because the changes in the variables may frequently occur faster than a person can take down values. Also, when the data are recorded automatically, there is less chance of error in recording values. Since most of the data will be analyzed with a computer, direct digital recording should be utilized as much as possible to speed the assembly of the basic data into form for computer input.

3. Controlled Parameter Variations

The third requirement of the rainfall-runoff experimental facility is the ability to vary the basin parameters in a controlled manner. The shape of the basin and the stream configuration represent large scale parameters that can be varied, and the surface roughness and detention characteristics represent more readily variable parameters. The large scale parameters will be modified by using earth-moving equipment to reshape the basin, so they will be varied less frequently than the other variables.

The major points that should be recognized in scheduling parameter variations are (a) that the research plan should be designed so the more easily varied parameters are modified as much as possible

before the major features such as shape and stream network are changed; (b) that the ranges and step sizes of parameter variations should be adjusted as experimental data clarifies the relative significance of various factors; and (c) the processes may be more readily evaluated if they can be physically isolated in the basin.

PRELIMINARY STUDIES OF FEASIBILITY

The initial investigations of the concept of the experimental facility were supported by the Colorado Agricultural Experiment Station, now called the Colorado State University Experiment Station. These efforts included the selection of the location for the facility, the review of literature concerned with the use of rainfall simulators in erosion, infiltration and overland flow studies and the determination of how the slopes and overall shape of the catchment would be changed.

The location of the experimental facility was determined on the basis of water supply, shop, office and automatic analog-to-digital data conversion facilities. All of these facilities are readily available at the CSU Engineering Research Center, Foothills Campus. A site that could contain the one-acre facility was available adjacent to the Research Center and was selected. The water supply for the hydrologic and hydraulic facilities comes from Horsetooth Reservoir, beside which the Engineering Research Center is located. A 36-inch supply line brings an ample supply to the facilities.

The literature review on rainfall simulators revealed that simulators have been used for a number years for erosion and infiltration studies and for small-scale laboratory experiments in overland flow. No system was found in the preliminary reviews that could be

efficiently adapted to the proposed facility. A tentative design based on large fog nozzles mounted on towers was formulated during this period, but a continuing review was made of other potential systems. The existing system was adapted from one found later in the study.

The final decision in the feasibility phase of the research concerned the method of changing the slopes and shape of the catchment. Small-scale laboratory models can utilize platforms that are tilted to provide the desired slopes. The 3-foot diameter, 800-foot long pipe at the Engineering Research Center facilities, had also been provided with slope adjustment. However, because of the large area involved in the proposed facility, the platform would be very costly. It was decided, instead, to use earthmoving equipment to mold the large-scale features of the facility. A number of experiments can be run with small-scale features varied before a major change is required.

OWRR GRANT-PHASE I

In 1966 the Department of the Interior, Office of Water Resources Research, provided a matching grant for Phase 1 of the design, construction and use of the experimental facility. The work during this two-year period consisted of making a concise formulation of the philosophy of use and objectives of the experimental facility, conducting preliminary design studies and installing the major facilities, such as the water supply lines from the 36-inch main to the experimental facility. The results of this work are reported in a previous report (4) and only a few points will be touched here.

The first design project was the main supply line for the facility. A 26-inch diameter main ran past the site of the facility carrying water

from the 36-inch main to the Hydromachinery Laboratory. A 10-inch line was connected to the 26-inch main and was laid around the site of the facility. The 10-inch line lies outside the experimental runoff area except at the upper end where it had to cross the area. Thus, whatever rainfall system was later installed could be supplied from both sides of the facility. The main control valves were installed in the 10-inch line and a drain line was located between the 10-inch line and a creek draining the site. The drain line can be used to empty the 10-inch line or to control the pressures in the line by diverting part of the flow at times.

Although no attempt was made to model a specific watershed, it was necessary to decide on a shape and slope for the Facility representative of typical small watersheds. Rather than make a capricious decisic it was decided to study the shapes and slopes of actual watersheds for whi data were available.

Sixty-one small watershed were studied to determine a representative shape. For the initial geometric shape of the Facility it was decided to compromise between the results obtained in the survey of the small watersheds in nature and the natural shape of the selected Facility site. Furthermore, it was decided to simplify the initial shape and drainage characteristics as much as possible. The less complex the geometrical shape of the basin, the less difficulty will occur in data analysis. The shape selected is composed of two intersecting planes and an upper conic section. Each of the sections can be readily described by a simple mathematical function.

The preliminary shaping of the facility was performed after the 10-inch supply line had been installed. The slopes were broughtapproximately to their design values so that settling could take place before the final adjustments were made.

The tests of rainfall systems during Phase I were related mainly to nozzles that could be used in the tower system. A number of tests were performed on individual nozzles under varying wind conditions to determine the distributions of intensities. The testing program will be discussed more in Chapter 2. A rotating head was designed to provide a more uniform spatial distribution with the nozzles. The intensities of rainfall that would occur with several of the towers operating were rather high, so alternative systems were still being considered.

The necessary prerequisites in the operation of the facility are the simulation of natural precipitation, and the subsequent measurement of the precipitation and runoff. Precipitation measurement should be as accurate as possible and should be continuous during any given simulated storm. To accomplish the objective of both accuracy and sensitivity, the capacitance gage system for measuring and recording very small surface waves was adapted to a standard precipitation gage. The capacitance gage senses the depth of water at a given instant of time. The depth is transmitted as an electric signal either to a magnetic tape recorder or directly to the analog-to-digital converter. The latter records the data on punch cards for analysis by computer.

In addition to precipitation, it will be necessary to measure the runoff amount produced by a given rate of precipitation. The H-flume developed by the Agriculture Research Service was chosen for the purpose. The principal reasons for selecting the H-flume were: (a) simplicity in design and construction, (b) freedom of passage of debris through the measuring section, and (c) below surface construction of the head box minimizing the formation of backwater at the measuring structure.

OWRR GRANT-PHASE 2

The second phase of the construction of the experimental facility was funded under a two-year matching grant by OWRR in 1968. The level of funding was less than had originally been planned for, and therefore only the upper conic section could be developed to demonstrate the use of the facility.

The primary emphasis during the first year of Phase 2 was on the selection of the final rainfall system. Two alternatives to the tower system were examined. One was the use of large irrigation guns located outside the catchment area. These guns left the area free of obstructions, but had significant disadvantages that led to the rejection of this approach. The second alternative was based on small-diameter aluminum irrigation pipe with small sprinklers, such as are used in lawn sprinkler systems. A number of sprinklers were investigated, and one was found that performed acceptably. The individual nozzles were tested in the laboratory to determine the distribution of intensities. A computer program was then used to simulate the operation of a number of nozzles with overlapping patterns. A coefficient of variation of about 10% was found to be possible for a range of intensities from 0.5 to 4 inches per hour.

A pilot system was field tested and found to be satisfactory. The full system for the upper conic section was installed during the second summer of Phase 2, and an initial set of experiments were run during the fall.

During Phase 2, a cooperative effort by the Department of Agriculture, Agricultural Research Service, became a part of the experimental research. This cooperation included professional

and graduate research assistant work on the development of the facility and provision of equipment such as chart-recording gages for rainfall and streamflow. The chart-recording gages provide immediate graphical presentation of data to supplement the digitized records.

The treatment of the surface of the facility to make it impermeable was changed in Phase 2. Originally, the covering of the facility with butyl material had been rejected on the basis of cost. However, the availability of a quantity of butyl on surplus made it economically feasible to use. The upper conic area was, therefore, covered with butyl after the final shaping was performed.

The capacitance raingages, which had performed satisfactorily in the laboratory, were found to have instabilities when installed in the field. A number of tests by project personnel resulted in the use of larger probes with heat-shrink plastic coatings instead of enamel. Several gages have been modified and appear to be operating satisfactorily in the field.

The upper conic section is essentially complete and has been used for a series of tests in the cooperative effort of CSU and the ARS. The tests varied the area of the catchment contributing runoff by (a) separating off a 30^0 sector, giving data from 30^0, 90^0 and 120^0 sectors, and (b) by using shorter radii than the 110-foot radius of the basic sector. In addition, a series of tests was run with small-size gravel providing roughness and surface detention effects.

The following chapters of this report describe the development of the major components of the experimental facility in more detail. Chapter 2 discusses the rainfall system, Chapter 3 presents the instru-

mentation for measuring rainfall and runoff and Chapter 4 discusses the shapes and surface treatment of the facility.

POTENTIAL APPLICATIONS

The experimental facility has potential, not only in studies of watershed response as reported in Chapter 5, but also in other investigations. Two such uses are included in research that has already been funded this year. One study concerns the quality of water running off from waste piles of oil shale in Colorado. Part of the research will use the facility to provide artificial rainfall on oil shale material and collect the runoff for chemical analysis. The other project is a study of the geomorphological development of river basins. An erodable material will be used and several drainage systems will be developed. This project is funded through the Geology Department at CSU, but is of interest in Hydrology as well.

The potential of the rainfall-runoff facility is indicated by the nature of the research that has already begun to develop around it. The results from these initial studies will stimulate additional research efforts. The facility will be of very great value in the study of many processes of watershed response in runoff, water quality and geomorphology that are now either obscure or neglected.

Chapter 2

ARTIFICIAL RAINFALL SYSTEM

Preliminary Studies

The artificial rainfall system is such an important part of the experimental facility that considerable research and test studies were performed before the final design was achieved. A review was made of literature concerning the use of rainfall simulators in laboratory studies of overland flow and field studies of erosion and infiltration. Based on this review the following factors were considered to be important in the design of the system: (1) distribution of intensities in time and space, (2) distribution of drop sizes compared to the drop size distribution of natural rainfall, (3) cost of constructing the system, (4) convenience and flexibility of the system in providing a variety of inputs under a range of field conditions and (5) the degree of interference with access to the catchment and with operation of other hydraulic facilities at the Engineering Research Center.

The intensities and drop sizes are related because large nozzles tend to produce larger drop sizes and higher intensities, while smaller nozzles can generally provide more uniformity and greater flexibility in the choice of intensities. A number of indices of the uniformity of rainfall have been described in the literature. For the purpose of comparing different systems, the coefficient of variation of the spatial distribution of intensities was used. The criterion for acceptance of the uniformity of an input was set as a coefficient of variation less than 0.10 over the range of intensities to be used for the rainfall tests. The criterion for drop sizes is more difficult to specify. The point of interest is the distribution of impact energies for erosion. The effect

of rainfall is modified by the protective influences of natural vegetation and the overland flow water depth in natural watersheds. Another factor to be considered in selecting the rainfall system is the sensitivity of the input to wind. The facility will be subject to a certain amount of wind at all times. If the system is highly sensitive to wind, there will be more times that the facility must be shut down and there will be more difficulty in reproducinginput patterns.

Combining the criteria for the rainfall system with the study of simulators that had been used previously led to the selection of three types of rainfall systems for further study. A system of fog nozzles on towers about 30 to 50 feet high was the first system investigated in detail. The second type of simulator was the large-diameter irrigation gun system that has been used for irrigating large fields. The third system was based on the concept of a grid of small nozzles over the catchment. This type was originally rejected because of the cost of the supporting structure, but a modification of this type was found to be feasible and was given further testing.

Fog Nozzle, Tower System

The system utilizing fog nozzles of the type used in fire fighting seemed to offer the most potential for adaptation to the needs of the facility. The first studies were therefore conducted with these nozzles. A number of nozzles were obtained from government surplus and laboratory studies were performed to determine the flow characteristics of the nozzles under various line pressures. The head loss through the nozzle and the flow ra at each pressure and at each position of the nozzle, from the smallest opening to the full open position, were determined. It was found that

the discharge was the same for all openings at a given pressure and the loss characteristics were similar for all pressures. Thus, the nozzles could be modeled by the standard hydraulic principles to extend experimental results with computer analyses.

The fog nozzles have too long a trajectory for the jet to be tested in the laboratory to determine the distribution of intensities that will be generated. Therefore, an outdoor testing rig was constructed as shown in Figure 1. A framework on the right side of the figure provides support for the nozzle at a height of about 8 to 10 feet above ground. Water was supplied to the test site by the large supply line from Horsetooth Reservoir. The water was pumped through a fire hose to the nozzles. For some of the tests an elevation greater than 10 feet was required. A 2-inch diameter steel pipe was temporarily supported by a crane for this series of tests, and heights up to 50 feet were tested. A grid of cans was set up to collect the precipitation from the nozzle during a measured length of time. The nozzle was oriented at various positions from horizontal to vertical to provide varying trajectories.

Examples of the test results from three of these runs are shown in Figures 2, 3 and 4. The isohyets of the depths of water collected in the cans are drawn on these figures. In the first example the nozzle is located in the lower righthand corner and is oriented in a horizontal direction. It is seen that the larger drop sizes provide a concentration of input in the area where the main jet is directed, and a decreasing amount is carried beyond and to the sides of the main jet. The degree of spreading that occurs depends on the opening of the nozzle.

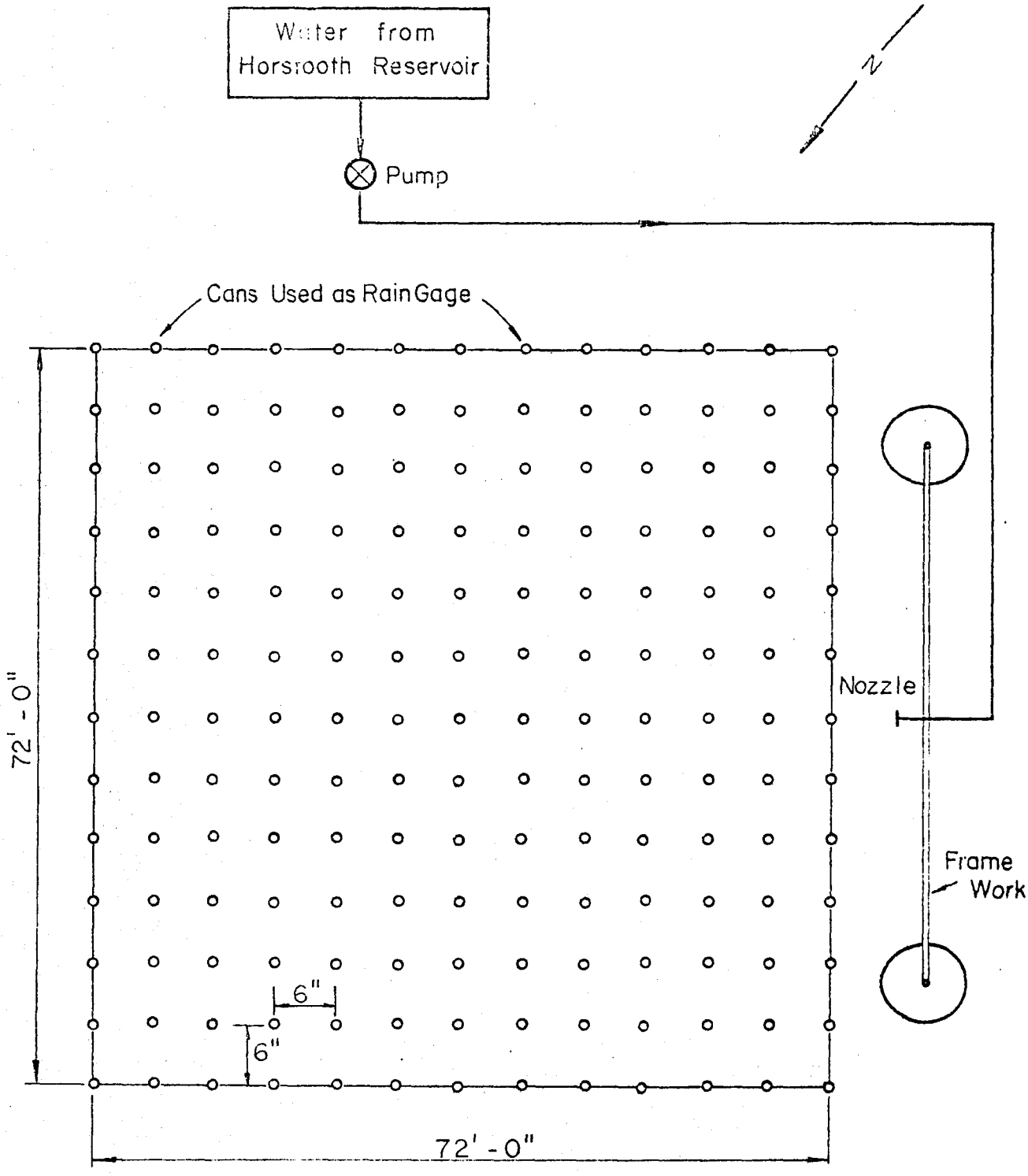

Figure 1 Testing Rig and Measurement Grid for Testing Fog Nozzles

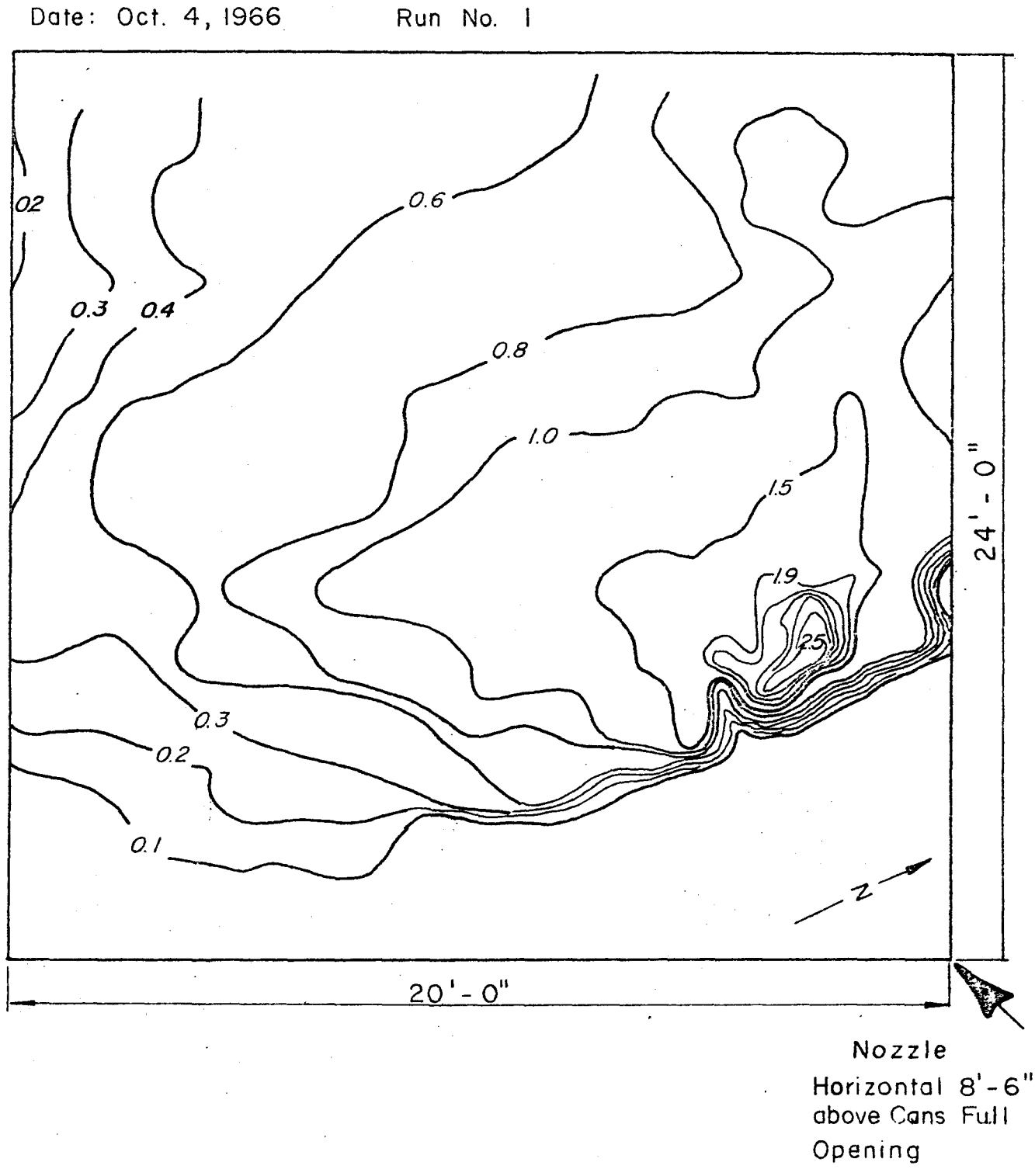

Figure 2 Distribution of Precipitation from a Nozzle Directed Horizontally

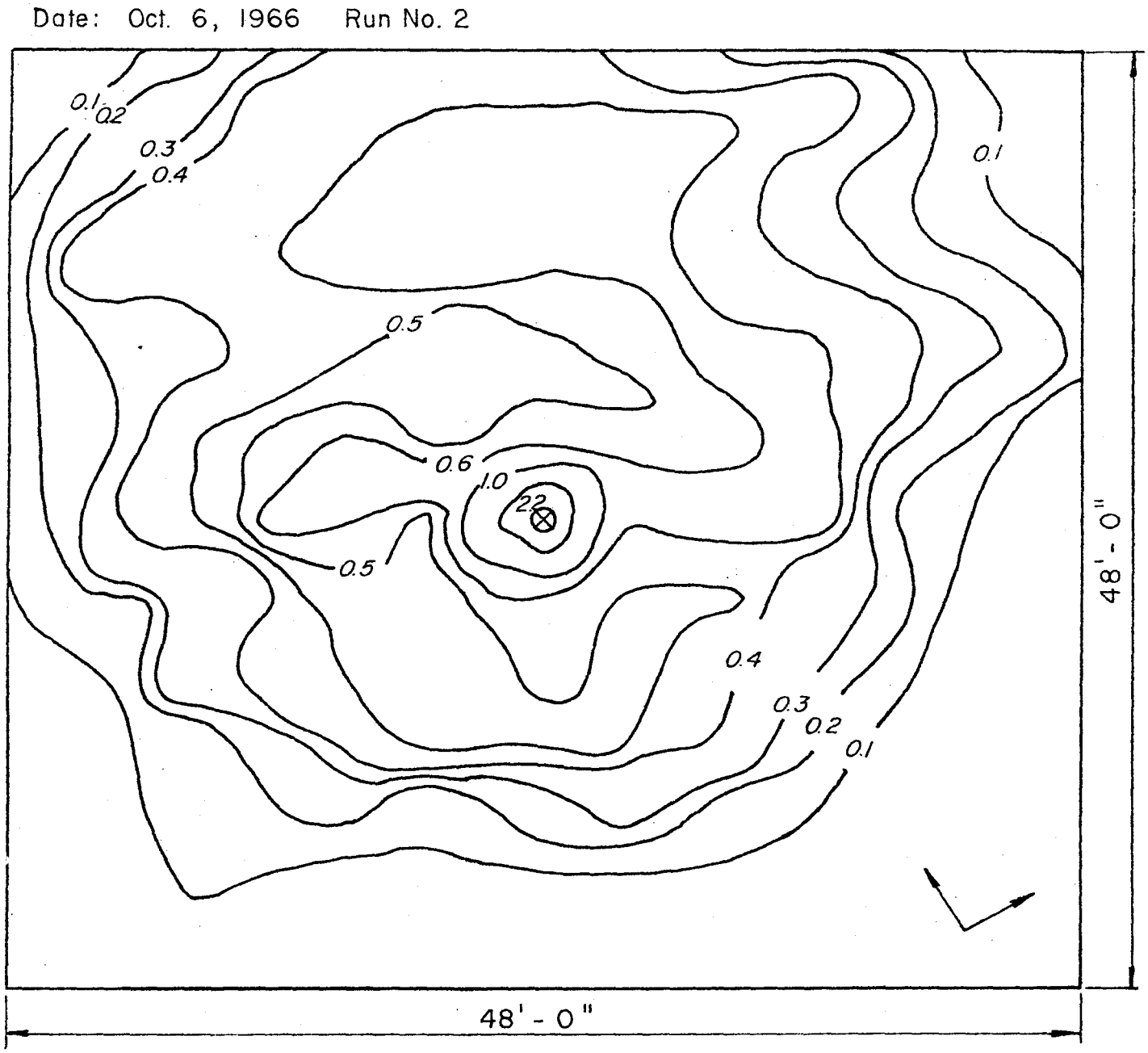

Figure 3 Distribution of Precipitation from a Nozzle Directed Vertically

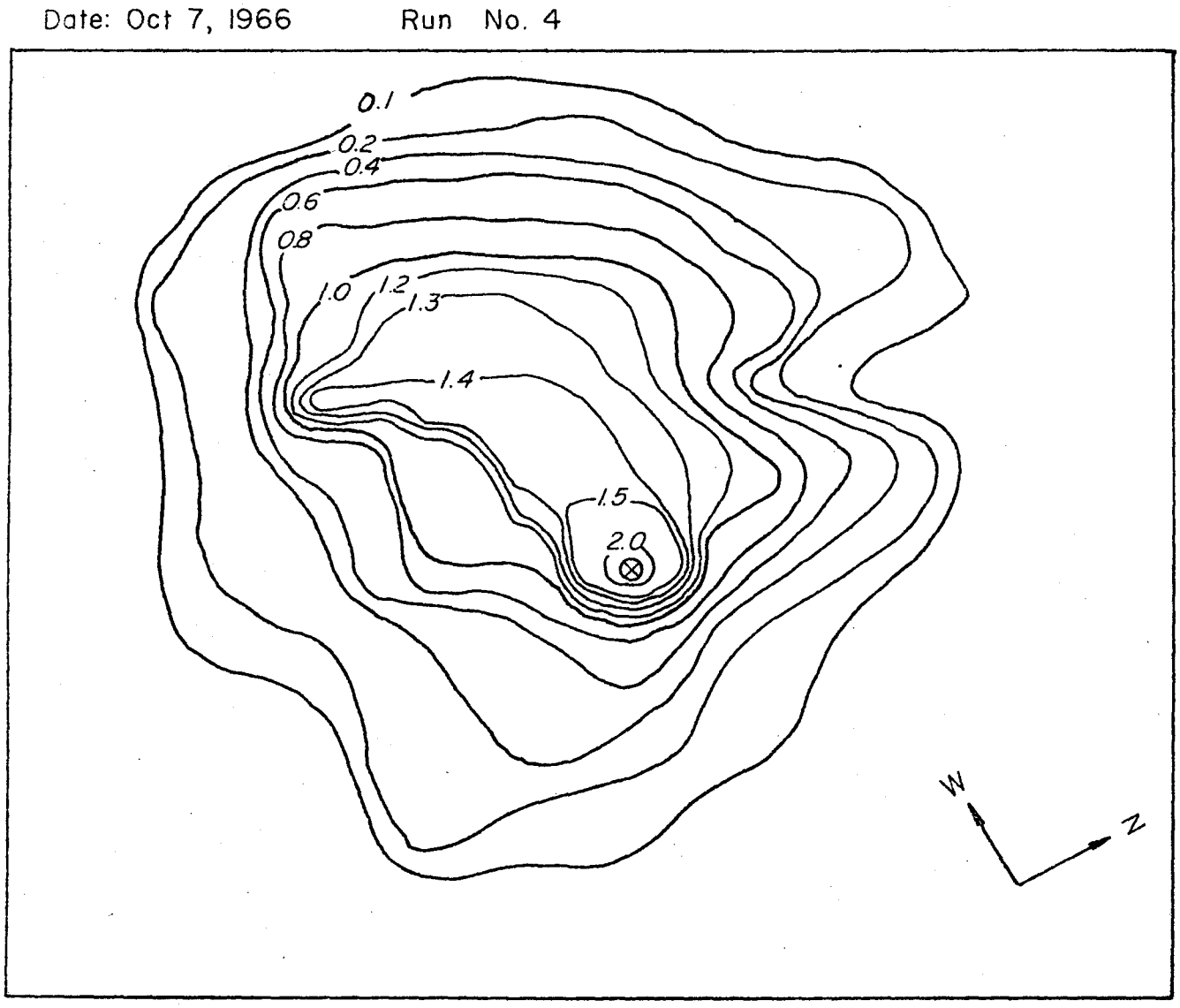

Figure 4 Distribution of Precipitation from a Nozzle at 45° from Horizontal

The second example shows a nozzle in the center of the measurement grid and oriented vertically. The isohyets show the general radial character of this distribution, grading from a high intensity at the nozzle to zero as you move away from the nozzle. A slight wind effect is noticeable in this test. There is a shift of the isohyets toward the top of the figure from the radial symmetry that would be expected in the absence of wind. Note that the higher intensities are less affected than the lower intensities. This supports the hypothesis that the higher intensities are in areas that have larger drop sizes. The smaller drops are affected more strongly by the wind.

The 45-degree orientation is shown in the third example. A large concentration still occurs in the immediate vicinity of the nozzle. However, the distribution is more uniform a short distance away from the nozzle and the highest concentrations occur slightly removed from the nozzle. The center of the pattern shows greater uniformity than in the case of the vertical orientation.

The effect of the wind was investigated more fully in a set of tests is which the wind speed and direction were measured several times during each run. Figures 5 and 6 show the isohyets from a few of these tests. The runs illustrated are made with the nozzle at different elevations. This shows that the effect of the wind is greater at the higher elevations. Part of this is due to the greater degree of breaking up of the large drops into smaller drops as the fall is increased. A second factor is the higher velocities of wind that occur at greater heights above the ground. The velocity measurements were all made at about the same height, so the wind speeds actually acting on the nozzle is greater at the higher heights than the measured wind speed indicates.

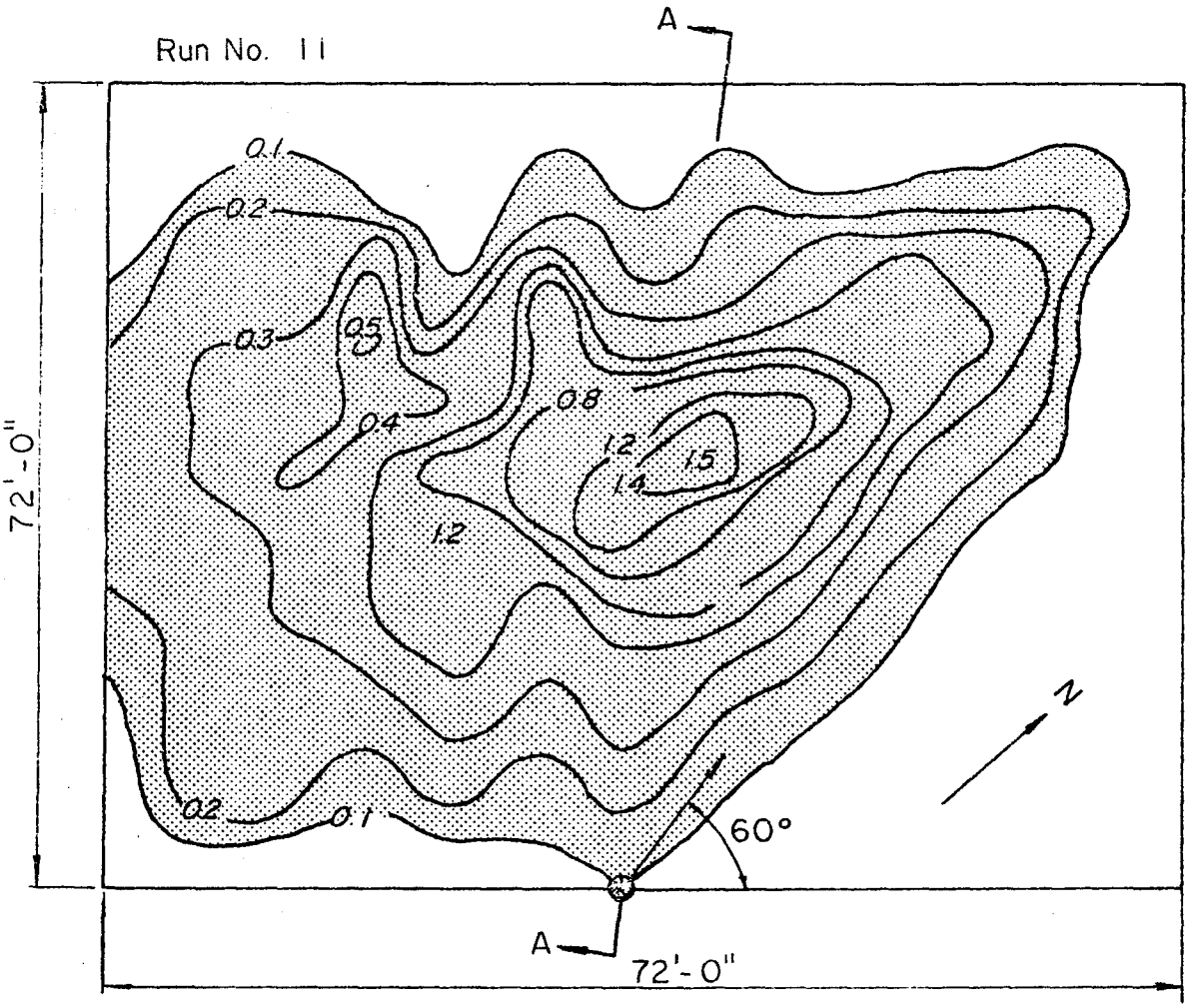

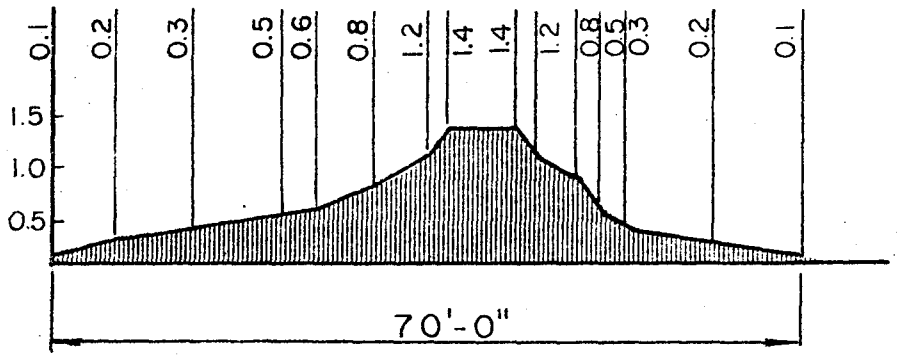

SECTION A—A

Nozzle Position and Direction
Nozzle Opening : half
Nozzle Height : 30'-0"
Wind Speed : 3 - 6 - 2 - 3 - 3 - 2 - 2 - 1 - 0 - 1 mph
Wind Direction: SE
Time : 10 minutes

Figure 5 Effect of Light Wind on Precipitation Distribution of Nozzle 30 feet High

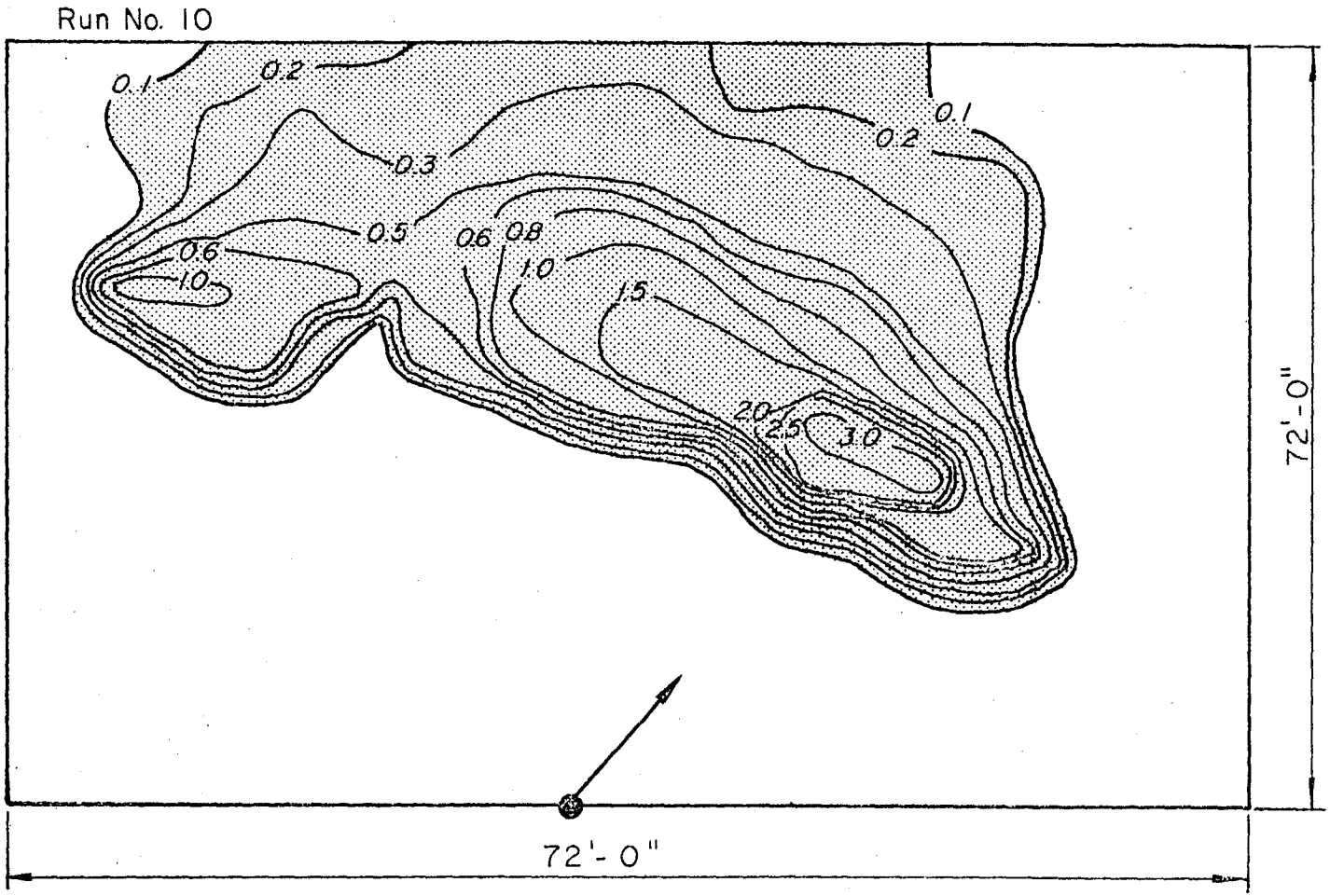

Nozzle Position and Direction:

Nozzle Opening : half

Nozzle Height : 20'-0"

Wind Speed : 8-10-5½-8½-5-6-10-6½-5½ mph

Wind Direction : SE

Time : 10minutes

Figure 6 Effect of Stronger Wind on Precipitation of Nozzle 20 feet High

The greater influence of the wind on the areas of lower intensity is still shown in these results.

Another effect of increasing the height of the nozzles is to increase the area of coverage. Part of this is due to the influence of the wind on the smaller drop sizes. The effect is to cover more area with relatively low intensities, so the average intensity over the original area of coverage is not changed much. The increased area covered tends to counter some of the disadvantages of increased height, but is not a dominating influence by itself.

The testing program also provided data for comparing the effectiveness of the different nozzle openings. The smallest opening gives the concentrated jet that has a long, narrow distribution. This pattern is not satisfactory for a nozzle that is held stationary over the facility because of the small area covered. The full open position gives the extreme fog effect, which has small drops and a small area of coverage. This causes high intensities and high sensitivity to the wind. An intermediate opening gives a greater area of coverage and a more uniform pattern of input. The major disadvantages of both extremes are absent, giving the most satisfactory stationary distribution.

The distributions of rainfall provided by the nozzles were superimposed to determine the pattern of input that would result from a set of nozzles located on a single tower and directed in different directions. Several patterns were tried, with the superposition being done manually. It was clear that there is considerable non-uniformity in the distribution over relatively small distances and the pattern is not very satisfactory. In the real system there would be a certain amount of randomizing due to the wind and the interaction of drops from different nozzles,

so the actual distribution should be more uniform than is indicated by these tests. However, the basic characteristics of the pattern will persist in the actual system, giving high intensities with considerable local variation. In addition, the best orientation for the nozzles change as the wind pattern changes.

Because of the unsatisfactory nature of the distribution that was expected from the stationary placement of the nozzles, a rotating head was designed to be mounted on the top of a tower or pipe. Four or five nozzles can be mounted on the head, and, as the assembly rotates, each of the nozzles sprays over the entire 360-degrees of the compass. The result provides radial symmetry in the absence of wind effects. The rotating head is driven by the reaction of the jets issuing from the nozzles. The directions of the jet can be adjusted, so the amount of reaction can be controlled and the spray can be directed at some angle between horizontal and vertical. The rotating head has been described in the previous report and will not be presented in more detail here. A pilot system was constructed and operated satisfactorily, under moderate wind conditions, but the high intensities and the sensitivity to wind led to further study of alternative systems.

Irrigation Gun System

The tower system described above also had the disadvantage that it required the installation of permanent towers on the interior of the facility. This restricts the movement of large machines used to change the shape of the catchment. Therefore, one of the criteria given extra weight in the additional studies was to leave the catchment as free from obstruction as possible. The system based on large irrigation guns was particularly attractive from this standpoint. These guns have been used

in irrigation systems to give a very uniform input over large areas. The catchment could be left entirely free of towers. Four of the guns were obtained and a pilot system was tested on the facility.

The testing indicated several problems that had not been anticipated in the preliminary study of the system. The first problem was the intermittent nature of the jet because of the reaction arm used to drive the sprinklers. Part of this was anticipated, so a motor drive was designed for the system. However, the reaction arms were left on the nozzles to give a more uniform distribution of input. It was found that the reaction arms caused a definite jump in the position of the nozzle as can be seen in Figure 7, where the jet on the far side has two jets, or parts of jets, separated by a discrete increment. The near jet shows a related problem, namely, the intermittent input that occurs in the immediate vicinity of the nozzles. There is input only when the reaction arm has just hit the jet, as is the case with the near nozzle. The reaction causes a long delay before the arm again hits the jet. Thus, the areal average may be uniform over long periods of time but there is considerable short-term variation in the distribution. This can be partially overcome by replacing the reaction arm with a stationary deflector in the jet. This causes a more uniform distribution, but it also cuts down the distance to which the jet can reach.

A second problem with the large guns was the interference occurring between jets from different nozzles. The jets reach beyond the center of the facility and collide with those on the other side. This causes localized areas of high intensity. The deflector in the jet could only partially overcome this effect. The nozzles on one side of the facility

here at Colorado State University is based on the use of small diameter aluminum irrigation pipe supported slightly above the ground and having the nozzles raised to height of 10 feet by the smaller steel pipes. The aluminum pipe is supported by a small bipod at the riser for the nozzle. Thus, a minimum of structural support is required and the pipe is above ground so it does not influence the surface flow. The details of the system will be presented in a later section of this chapter.

A number of nozzles were given a preliminary screening to find some that could satisfy the needs of the facility. (The nozzles that were used by Shachori and Seginer were no longer available.) Several sprinklers of the type used in lawn sprinkler systems were found to be worthy of further testing. The individual nozzles were first tested in the laboratory to determine the distributions of intensities that are given. Some of the nozzles being tested provided circular patterns and one nozzle gave a square pattern. A series of tests were run at different pressures to determine the intensity patterns. Then the testing was shifted to the outdoors to include the effects of wind. The test facility is shown in Figure 8, set up on the outdoor facility for one of the nozzle tests. The results of three tests are shown in Figures 9, 10 and 11. The nozzle was operated for a measured length of time, usually 15 or 20 minutes, and the volume of water collected in each of the cans was measured.

Computer Simulation

A computer program was written to simulate the operation of the system of nozzles over a part of the facility. The program reads in the data from the test run and converts the measured volumes to intensities in inches per hour. The locations of the nozzles are read in terms of

coordinates on a master grid. The distribution of the input is then determined as a function of the relative position with respect to a nozzle. This is handled in one of two ways, depending on whether or not radial symmetry is assumed. If radial symmetry is assumed, then the location of each measurement is computed as a radial distance from the nozzle. The measurements within one grid interval, centered on a grid point along a radius, are then used to determine the average value of the input at that distance from the nozzle. For example, looking at nozzle 415, there are eight measurements that are between 5 feet and 7 feet from the nozzle. The average volume is 23 ml. The corresponding intensity, 0.15 in/hr, would then be assigned to the 6-foot radius if a 2-foot grid increment is being used. The other measurements would be treated in a similar manner. If radially symmetry is not assumed, the observed data are used to fill in the complete grid by a process of interpolation. One quadrant of the distribution is given more completely. For example, the second quadrant is filled in on 4-foot increments for the square nozzle of figure. The second quadrant would then be filled into 2-foot increments to correspond to the step size on the axes. Then the second quadrant data is used with the observations in the other quadrants to complete the entire grid about the nozzle.

For each nozzle, the positions of the locations of data points on the relative grid about the nozzle are converted to the corresponding location on the master grid, and the intensity contribution for the nozzle is added to the intensity matrix of the master grid. When all nozzles have been thus considered, the effect of the set of nozzles is contained in the master grid intensity matrix. The average intensity over a section in the center of the overlap area is computed and the coefficient of

variation of the intensities in that section is computed. These items are printed out along with the master grid intensity matrix. A summary of the averages and coefficients of variation for the last simulations before the grid system was designed is presented in Table 1.

The criterion for acceptance of a distribution pattern had been set at a coefficient of variation of 10% for the spatial uniformity. An examination of the table of simulated patterns indicates that all of the circular patterns could meet this criterion for all but the lowest intensities. The performance of the nozzles is better at a pressure of about 28 psi than at lower pressures. The square-pattern nozzle, which must operate at the lower pressure, was found to be unsatisfactory. The nozzle that was selected for the prototype system is the #78. The system was installed on the upper conic section of the facility during the summer of 1969. The distribution that actually resulted on the facility is shown for one test in Figure 12. The location of the cans used for the test are shown on the figure and can also be seen in Figure 13, which shows the facility in operation. In addition to the grid of cans in the upper part of the facility, a number of cans were located at random positions elsewhere on the facility. The average intensity and the coefficient of variation were computed for both sets of cans. For the grid, the average was 2.76 in/hr and the coefficient of variation was 0.049. For the randomly spaced cans, the values are 2.76 and 0.053, respectively. The averages and the coefficients of variation of several tests are listed in Table 2. The results show the same trends as the computer simulations, except for the run at 1.22 inches per hour, which has an anomalous coefficient of variation. This run will have to be examined in more detail to determine the cause of

Table 1 SUMMARY OF COMPUTER SIMULATIONS OF INTENSITY PATTERNS

Nozzle	Pressure psi	Spacing ft.	No. sets operations	P in/hr.	C. V.
Square Pattern	20	40	1	0.390	0.288
			2	0.783	0.185
			3	1.172	0.175
			4	1.560	0.154
415C	20	48	1	0.160	0.311
			2	0.323	0.195
			3	0.484	0.185
			4	0.647	0.165
415C	24	48	1	0.138	0.260
			2	0.276	0.150
			3	0.415	0.130
			4	0.553	0.103
415C	28	48	1	0.341	0.111
			2	0.672	0.0985
			3	1.013	0.0779
			4	1.343	0.0761
415C	28	40	1	0.473	0.137
			2	0.952	0.0713
			3	1.433	0.0662
			4	1.910	0.0561
			5	2.388	0.0590
			6	2.868	0.0546
			7	3.348	0.0548
			8	3.830	0.0525
415C	28	35	1	0.634	0.104
			2	1.274	0.0504
			3	1.907	0.0439
			4	2.546	0.0294
75	20	40	1	0.368	0.210
			2	0.738	0.127
			3	1.106	0.113
			4	1.476	0.0838
75	24	40	1	0.426	0.199
			2	0.853	0.104
			3	1.279	0.102
			4	1.706	0.0738
75	27	40	1	0.414	0.0909
			2	0.827	0.0618
			3	1.238	0.0466
			4	1.652	0.0366
			5	2.066	0.0365
			6	2.482	0.0333
			7	2.895	0.0304
			8	3.311	0.0276

Table 1 - Continued

Nozzle	Pressure psi	Spacing ft	No. sets Operations	P in/hr	C.V.
75	27	35	1	0.547	0.171
			2	1.102	0.100
			3	1.649	0.0576
			4	2.203	0.0235
78	19-20	40	1	0.412	0.224
			2	0.824	0.147
			3	1.235	0.132
			4	1.648	0.101
78	24	40	1	0.473	0.186
			2	0.944	0.125
			3	1.417	0.112
			4	1.888	0.0868
78	28	40	1	0.442	0.146
			2	0.890	0.0902
			3	1.337	0.0838
			4	1.790	0.0685
			5	2.234	0.0680
			6	2.671	0.0630
			7	3.142	0.0626
			8	3.565	0.0558
78	28	35	1	0.707	0.124
			2	1.419	0.0824
			3	2.132	0.0546
			4	2.852	0.0402
78	28	30	1	0.933	0.149
			2	1.870	o.104
			3	2.841	0.0739
			4	3.818	0.0558

Table 2 PARAMETERS OF RAINFALL DISTRIBUTION OF PROTOTYPE GRID SYSTEM

Average (in./hr.)	Coefficient of Variation
0.64	0.199
1.19	0.089
1.22	0.131
1.26	0.073
2.76	0.049
4.93	0.037

the high values. A large number of runs have been made, but the data for the other tests have not yet been analysed completely.

Drop Size Study

The distribution of drop sizes provided by the artificial rainfall system will be of significance in later studies of erosion processes. Therefore, a study of the drop sizes at various distances from the nozzle was made for the two nozzles that were considered best from the intensity distribution study.

The article by J. Otis Laws and Donald A. Parsons (6) was used as a guide in determining the drop-size distribution for the number 75C and 78C nozzles. The procedure used was the flour technique whereby drops of rain are allowed to impinge into sifted flour thus creating pellets. Under the system developed by Laws and Parsons and followed in the analysis under discussion, the flour pellets were left undisturbed for 24 hours before being placed in an oven for an hour for hardening and further dehydration. The particles were then sieved, using a stack of standard U.S. sieves in the appropriate size range. Following sieving, the pellets retained on each were counted and weighed on an analytical balance to the nearest one ten-thousandth of a gram. Using this information and a calibration curve (Figure 2 in Laws and Parsons), the diameter of the drop retained on each of the sieves was obtained for each sample location.

In selecting raindrop samples from the 75C and 78C nozzles, 9-inch pie pans were used. A sample was taken along a radius in 2.5 foot increments starting at the nozzle. The pie pans were filled with sifted flour, covered, hand carried, and placed on top of a gallon can about 6 inches above the ground to avoid splash from raindrops hitting the ground. The covers were taken off for a period of 4 to 10 seconds to allow the drops to impinge into the flour. As stated above, the pie pans were stored for 24 hours before being placed in a drying oven for an hour at 250^{O}F. They were then sieved. On the larger sieves all pellets were counted but on the smaller sieves, where the number of drops was much more numerous, only 50 pellets were counted and weighed. However, the total mass on each sieve was determined so that the percentage of total rainfall falling as a given drop size could be determined.

Following the collection and weighing as described above, the data was initially processed in the manner outlined in Table 2 of Laws and Parsons. The 9100 A.H.P. Computer was used in the data reduction. One program is used to determine $mp = M_{p/n}$ = mass of the average pellet. Using this value a mass ratio "R" is determined from Figure 2 in Laws and Parsons and this value is entered into the program so the mass of all drops $M = RM_p$ may be determined. This program also determines the diameter of the average drop using the formula $d = \sqrt{\bar{6}/\pi}^{(m)}$. A second program was developed to find the percent of rain that fell as a given drop size at each location.

At this point in the data reduction, the data was processed to get it into a form that would be suitable for input data into the CDC 6400 digital computer programs developed previously for overlapping rainfall intensities from a given nozzle pattern.

The data collected in the above analysis was summarized as shown in Table 3.

After collecting the data in one table, the weighted mean-drop size at each location was determined by multiplying the average drop diameter by the corresponding percent which indicated the fraction of rain that fell as the given drop size. Another program for the 9100 A.H.P. computer was used for this determination.

The mean drop size at 2.5 foot intervals from the nozzle and the intensity at the given points are shown in Table 4. This table indicates the deficiency in the 75C and 78C nozzles in providing a high percentage of large drops. The drop size increases as the distance from the nozzle increases but the intensity decreases with distance from the nozzle. Hence, there is only a small percentage of the total rain that falls as large drops.

Table 3 Nozzle #75. Drop-size Analysis. August 8, 1969 C. Brent Cluff

.in from :zle	SIEVES																				Mean Diam.
	Drop Size mm	5 %	Drop Size mm	6 %	Drop Size mm	7 %	Drop Size mm	8 %	Drop Size mm	10 %	Drop Size mm	14 %	Drop Size mm	20 %	Drop Size mm	28 %	Drop Size mm	35 %	
0											1.37	.4	1.00	4.4	.80	34.6	.58	60.6	.68
2.5												0	.97	9.0	.73	34.4	.52	56.6	.63
5.0												0	.99	14.9	.75	58.6	.47	26.5	.71
7.5											.84	.1	1.00	8.0	.81	42.7	.56	48.5	.70
10.0											1.37	5.3	1.07	43.9	.82	47.8	.60	2.9	.95
12.5											1.41	19.7	1.09	74.5	.86	5.1	.60	0.7	1.13
15.0									2.24	4.2	1.64	80.6	1.21	9.9	.80	2.9	.60	2.4	1.57
17.5							2.72	2.7	2.34	29.5	2.00	63.3	1.16	1.5	.78	1.5	.50	1.4	2.07
20.0									2.37	35.5	2.00	55.1	1.14	2.1	.75	3.8	.57	3.5	2.02
22.5							2.87	19.5	2.43	55.3	1.98	18.2	1.14	1.6	.75	3.6	.56	2.7	2.31
25.0			3.60	12.0	3.34	38.0	2.82	28.7	2.51	4.1	1.43	3.0	1.04	5.9	.82	4.1	.56	4.2	2.77
27.5	0		3.94	43.1	3.59	27.9	3.15	3.1	0	0	1.53	10.8	1.05	3.6	.78	6.0	.60	5.3	3.07
30.0	0		4.14	59.1	3.41	20.0	2.91	9.4	2.51	2.0	1.97	3.6	1.03	3.1	.77	3.5	.53	4.1	3.37
	WT Meandrop) Size)		4.00		3.43		2.86		2.38		1.79		1.10		.82		.55		

Table 4 MEAN DROP SIZE DISTRIBUTION

Dist. From Nozzle	75C		78C	
	Intensity in/hr.	Mean Drop size-mm	Intensity in/hr.	Mean Drop Size-mm
0	.325	.68	.497	.66
2.5	.325	.63	.497	.66
5.0	.353	.71	.434	.67
7.5	.373	.70	.455	.51
10.0	.378	.95	.468	.90
12.5	.373	1.13	.460	1.16
15.0	.330	1.57	.403	1.09
17.5	.289	2.07	.358	1.45
20.0	.259	2.02	.285	1.62
22.5	.185	2.31	.209	1.83
25.0	.095	2.77	.152	2.18
27.5	.061	3.07	.093	2.42
30.0	.009	3.37	.097	2.78
32.5			.069	2.68

The 9100 A.H.P. Computer was used to determine the weighted drop size retained on each sieve size. The percentage that fell at each location was used a weighting factor to determine the mean drop size at each sieve. The percent of rain that fell as a particular drop size at each location was used to weight the respective diameters in the determination of a weighted mean for each sieve size because it was noted the the accuracy of the diameter determination was a function of the given percent.

The next step in the procedure was to determine the quantity of rain in inches per hour that fell as a particular drop size at each location. In order to do this the intensity at each location determined from a previous test was tabulated in column 2 of Table 6. These intensities were then proportioned into the different drop sizes using the percentages determined in the drop size analysis.

Table 6 Nozzle #75. Drop-size Analysis. August 8, 1969 C. Brent Cluff

Pos. in ft. from nozzle	Intensity in in/hr.	Drop Size (mm) 4.00 %	4.00 in/hr.**	3.43 %	3.43 in/hr.	2.86 %	2.86 in/hr.	2.38 %	2.38 in/hr.	1.79 %	1.79 in/hr.	1.10 %	1.10 in/hr.	.82 %	.82 in/hr	. %	. in/
0	.325*									.4	.001	4.4	.014	34.6	.112	60.6	
2.5	.325									0	0	9.0	.029	34.4	.118	56.6	
5.0	.353									0	0	14.9	.053	58.6	.207	26.5	
7.5	.373									.1	0	8.0	.029	42.7	.159	48.5	
10.0	.378									5.3	.020	43.9	.166	47.8	.181	2.9	
12.5	.373									19.7	.074	74.5	.278	5.1	.019	.7	
15.0	.330							4.2	.014	80.6	.266	9.9	.033	2.9	.010	2.4	
17.5	.289					2.7	.008	29.5	.085	63.3	.183	1.5	.004	1.5	.004	1.4	
20.0	.257							35.5	.091	55.1	.251	2.1	.005	3.8	.010	3.5	
22.5	.185.					19.5	.036	55.3	.1023	18.2	.034	1.6	.003	2.6	.005	2.7	
25.0	.095	12.0	.011	39.0	.036	28.7	.027	4.1	.004	3.0	.003	5.9	.006	4.1	.004	4.2	
27.5	.061	43.1	.026	27.9	.017	3.1	.002	0	0	10.8	.007	3.6	.002	6.0	.004	5.3	
30.0	.009	54.1	.005	20.0	.002	9.4	.001	2.0	0	3.6	0	3.1	0	3.5	0	4.1	

* Rate in inches/hr. of rain falling in given drop size.

**#75 nozzle May 30 at 27 psi, average using circular overlap program.

The intensities of a given drop size at every sample location were used as input data to determine the effect of overlapping on drop-size distribution for the nozzle patterns found to be best for uniformity in the rainfall intensity analysis. It is to be noted that the nozzle patterns selected may not be the optima for drop-size distribution, but are close to the optima for uniformity of rainfall intensity.

The overlap program printed out the amount of rain falling in inches per hour of each drop size at grid points within a sample area. By combining the results of all drop size overlaps, the drop-size distribution at any point within the sample grid can easily be determined.

As an example of how the overlap output can be used, the drop-size distribution at two different locations was made. The drop-size distributions of 78C nozzle at two arbitrarily selected locations, (13,11) and (23,13), for the basic and maximum intensity nozzle patterns are given in Table 5.

Table 5 EXAMPLES OF POINT DISTRIBUTIONS OF DROP SIZES

Drop Size (mm)	Location 13, 11				Location 23, 13			
	Basic		Maximum		Basic		Maximum	
	Intensity in/hr	%	Intensity in/hr	%	Intensity in/hr	%	Intensity in/hr	%
.55	0.01	1.9	.31	7.0	.22	44	.50	10.9
.68	.04	7.7	.64	14.5	.20	40	.56	12.2
1.04	.25	48	1.30	29.5	.04	8	1.21	26.4
1.64	.13	25	1.27	28.8	0.0	0	1.54	33.6
2.36	0.0	0	.20	4.5	0.0	0	.17	3.7
2.77	.05	9.6	.39	8.8	0.02	4	.37	8.1
3.29	.04	7.7	.26	5.9	0.02	4	.21	4.6
3.71	0.0	0	.04	0.9	0.0	0	.02	.4
Total	.52	100.0	4.41	100.0	.50		4.58	100.0

For the basic pattern there is a considerable difference in the drop-size distribution although the intensities are the same.

For the maximum intensity pattern both the intensities and drop-size distributions are essentially the same even though the sample points are 25 feet apart. This indicates the value of the multi-nozzle approach for increasing the uniformity of the distribution patterns.

The mean drop-size distributions over the sample area for both the 75C and 78C nozzles, with a comparison with natural rainfall, are given in Table 7.

Table 7 COMPARISON WITH NATURAL RAINFALL (Ref. 5)

Natural Rain			75C		78C	
Drop Size	Intensities		Drop Size	%	Drop Size	%
mm	0.5" hr	2.00"/hr	mm		mm	
0.0-0.5	0.5	0.2	.47-.66	7.1	.47-.59	8.1
0.5-1.0	5.4	2.3	.73-.83	14.2	.65-.82	15.6
1.0-1.5	14.1	6.4	.97-1.21	18.0	.93-1.17	22.7
1.5-2.0	18.7	10.4	1.37-1.98	35.5	1.32-1.86	37.5
2.0-2.5	21.5	13.9	2.24-2.51	14.6	2.16-2.59	4.6
2.5-3.0	16.3	15.3	2.72-3.15	4.4	2.49-2.87	7.1
3.0-3.5	12.1	14.4	3.34-3.59	3.3	3.17-3.34	3.9
3.5-4.0	7.0	12.4	3.60-4.14	2.9	3.71	.5
4.0-4.5	2.9	9.5				
4.5-5.0	1.5	6.5				
5.0-5.5		4.1				
5.5-6.0		2.4				
6.0-6.5		1.2				
6.5-7.0		1.0				
Total	100.0	100.0		100.0		100

Although the above chart is based on the basic pattern, additional patterns will have essentially the same mean drop size over the sample area because the basic pattern is superimposed. Thus, the mean drop-size distribution over a given area will be essentially the same for all intensities for the simulator. However, for natural storms the drop size increases as the intensity increases. The two nozzles are seen to have a higher percentage of drops smaller than 2 mm than natural rainfall. If larger drops are required for later studies, it will be necessary to seek nozzles with different characteristics or to modify some of the existing nozzles in the higher intensity patterns.

DESCRIPTION OF THE CURRENT SYSTEM

The current rainfall input system is shown in operation for the upper conic section of the facility in Figure 13. It is based on nozzle 78, with each nozzle located on a riser above the aluminum supply main. The riser section is about 10 feet high and is pictured in Figure 14. The entire riser is shown in Figure 14a, where it can be seen that the 3/4-inch riser is guyed to the adjacent risers by a wire. The wire is anchored at the ends of the aluminum supply line. Figure 14b shows the detail at the bottom of the riser. The elements that make up the riser are identified in the schematic of Figure 15. The sprinkler head is mounted at the top of the riser. A 7-foot section of 3/4-inch steel pipe joins the sprinkler to the tire pressure tap. The pressure tap allows a rapid check of pressures at a number of risers in a very short time, using a pressure gage that has been equipped to fit the tire pressure tap. The pressure regulator maintains the pressure for the sprinkler at a constant value, so all sprinklers will have the same pressure. The pressure is currently set at 28 psi. The hydraulic valve below the pressure regulator turns the sprinkler on and off. Each nozzle is fitted with a control valve, and a series of valves

Figure 13. Operation of Grid System on Upper Conic Area

Figure 14(a). Typical Riser for Sprinkler

Figure 14(b). Detail at Base of Riser

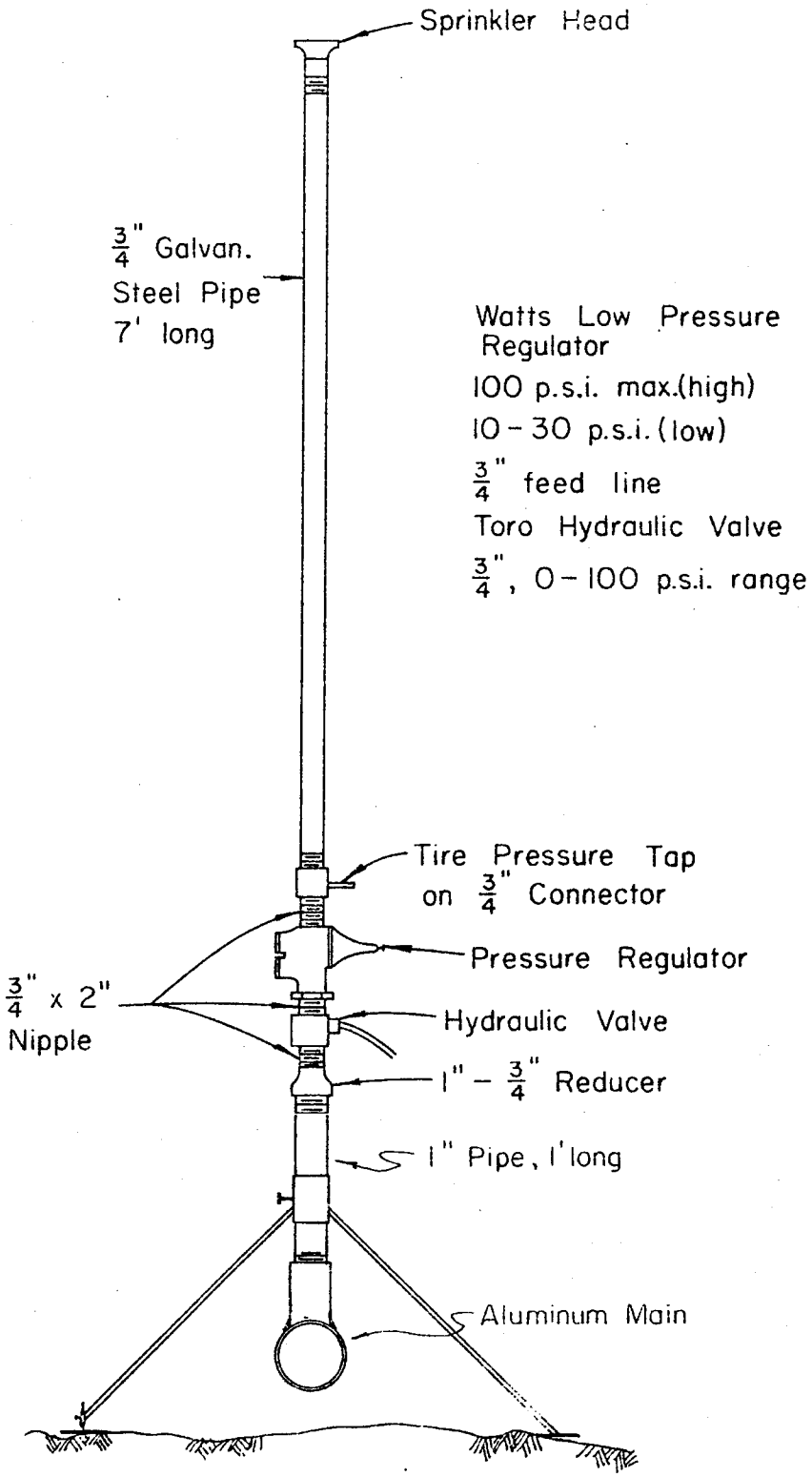

Figure 15 Schematic of Sprinkler Riser for Grid System

is connected to one pressure manifold to provide simultaneous operation of a set of sprinklers.

The control system is illustrated in Figure 16, where several risers are shown on a 2-inch aluminum supply line. A small plastic pipe joins a set of risers to the pressure manifold. In this figure only the first and last risers are connected to the pressure manifold that is shown. The other risers are connected to other manifolds. The supply to the pressure manifolds is controlled by electric control valves that are connected to a switching panel in the instrument trailer. There are four different sets of sprinklers in the system at the present time. These are shown in the overlay Figure 17. The colored overlays represent the pressure manifolds for the hydraulic control valves. The arrangement can, of course, be changed by changing the connections of the sprinkler risers to the pressure manifolds, but the system shown in Figure 17 will be used for the current studies. The four intensities available are approximately 0.5 inch/hour (red), 0.5 inch/hour (yellow), 1 inch/hour (green) and 2 inch/hour (blue). By adding the sets as illustrated with the overlay, the four intensities listed on the figure can be obtained. Starting with the red set, there is an intensity of 0.54 inch/hour. By adding the yellow set, it is increased to 1.11 inch/hour, and with the green and blue sets added in turn it becomes 2.31 and 4.24 inches per hour, respectively. By changing the switching patterns it is also possible to obtain the intensities of about 1.5, 2.5, 3, and 3.5 inch/hour. The actual location of the risers on the pipe system is shown by black dots on the solid black lines of the base figure. The black lines represent the 2-inch aluminum supply lines. They are connected to the larger aluminum supply manifolds along the east side of the facility. The slashed lines on these aluminum pipes indicate the locations of the quick coupling joints. Because of these joints, the system can be set up or taken down rapidly. The supply

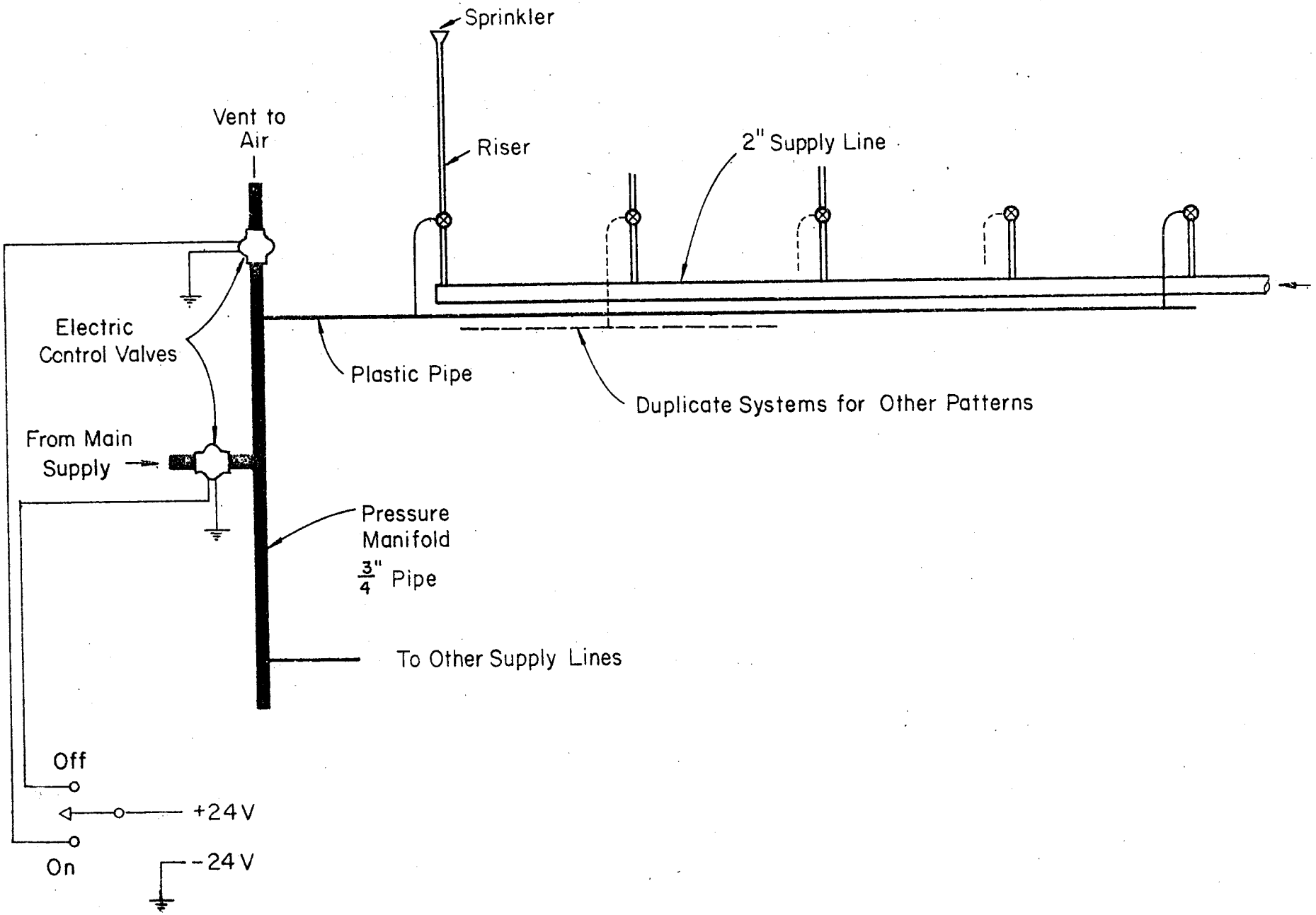

Figure 16 Schematic of Hydraulic Control System for Sprinklers

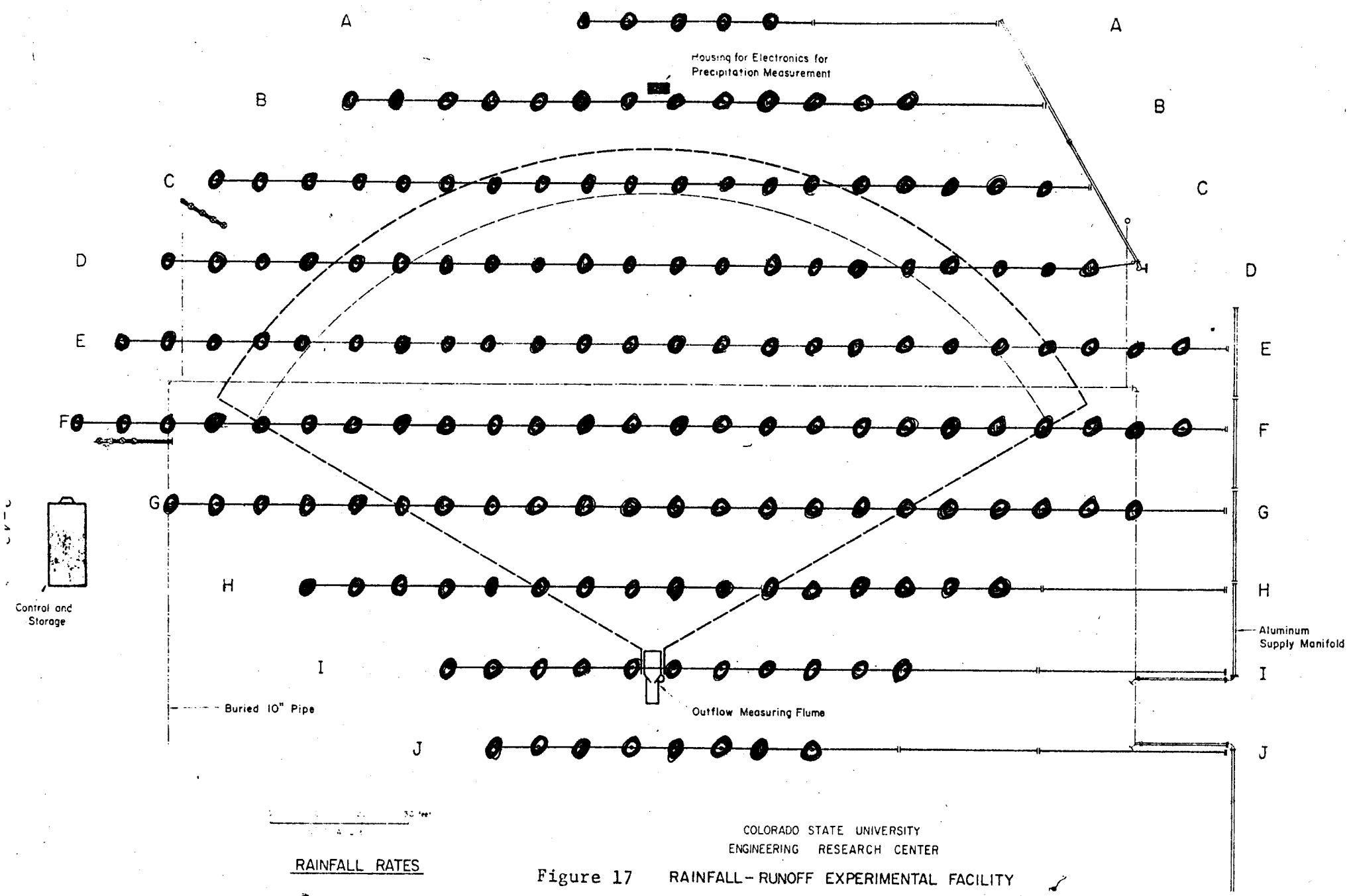

COLORADO STATE UNIVERSITY
ENGINEERING RESEARCH CENTER

Figure 17 RAINFALL-RUNOFF EXPERIMENTAL FACILITY

SITE MAP – UPPER PORTION
CONTROL MANIFOLD

manifolds are connected to the 10-inch supply main the surrounds the facility. Only part of the 10-inch line shows in the figure of the upper section.

This rainfall system has been operated during the fall of 1969. It can be programmed to generate pulses of varying durations for any of the intensities available. By increasing the capacity of the switching circuit it is possible to create varying distributions in space as well. This is, however, not planned at this time. A summary of the runs that have been made on the facility this fall will be given in Chapter 5.

Chapter 3. MEASUREMENT OF RAINFALL AND RUNOFF

REQUIREMENTS OF INSTRUMENTS

In a system with complete control over the input in both time and space variations, there is little need for the measurement of rainfall. This is the condition for the laboratory models which have individual droplet formation by small tubes or other similar systems. The experimental facility, on the other hand, utilizes the measurement of rainfall as the prime means of determining the input over the catchment. There is a reasonable degree of uniformity and reproducibility provided by the artificial rainfall system described in the previous chapter, but there are also variations due to the natural atmospheric conditions that vary in a random fashion over the facility. The wind patterns over the outdoor facility will cause small variations that need to be recorded. Therefore, the selection of a measurement system for the rainfall was a very important part of the design of the instrumentation for the facility. The runoff measurement is the dependent variable in nearly all hydrologic studies and is important in all physical modeling systems, even those inside laboratories.

The objective in both rainfall and runoff measurement is a nearly continuous record of the variation of the respective variable as a function of time. In addition, the rainfall must be determined at a number of locations across the catchment. Because of the large quantity of data that is collected in a relatively short time on the facility, computer analysis is essential. Therefore, automatic recording of the data in a form suitable for input to the computer is also very important.

PRELIMINARY STUDIES

In the preliminary studies of raingage systems, several types of

automatic recording gages were considered. The need to record data from a number of locations on the catchment using only one analog-to-digital converter placed an additional constraint on the system. It is impossible to record the data from each location continuously, so it is necessary to arrange for a recording from the various locations in a sequential manner. This makes it more difficult to use gages that record on an intensity basis, because extremely high or low values may occur at the measuring point during the short interval of time data are being recorded. For gages of the volume type, that is, those that measure the volume of precipitation that has accumulated to a given time, there is an averaging of the extreme points, so the sequential sampling procedure is not a serious problem if the period between readings is small.

The most common recording raingages are the weighing type and the tipping bucket type. The tipping bucket gage provides a signal that is already in an electrical form when the bucket tips. However, this is an intensity form of measurement, and it would be necessary to remain at a given gage for a short time to record the number of times the bucket tips during the known time interval. This increases greatly the time between measurements at each gage. The weighing type raingage can be modified to generate an electrical signal by replacing the weighing mechanism with a pressure transducer. But the weighing gage is not very sensitive at low small volumes of input that may occur in tests of short duration at the lower intensities. Alternatives were sought that would be more sensitive at low volumes.

The Bell Telephone Laboratory (7) has a raingage that records the intensity of rainfall by measuring the depth of water running down an

inclined plane between two plates. The two plates form a capacitor, and the changing depth of water changes the capacitance between the plates. This suffers from the disadvantage of sampling point intensities if it is used for the facility. However, the idea of using a capacitance gage to measure rainfall led to the consideration of a gage that was developed by Dr. Eric Plate for the measurement of waves in a flume. Dr. Plate's gage was developed in the Fluid Mechanics Laboratory to measure the waves generated by wind in the water-and-wind tunnel.

CAPACITANCE RAINGAGE

The capacitance gage can be used to measure the depth of water in the raingage. The greater sensitivity for lower volumes of rainfall is obtained in the same manner as in the standard non-recording gage, by using a smaller tube inside the large can. The depth in the smaller tube is magnified by a factor of 10. The operation of these instruments is outlined as follows. Referring to Figure 19 a probe is installed vertically in a precipitation measuring can, such that the height of water directly causes a change in the capacitance to ground. This probe is essentially an insulated rod, with water as one capacitor "plate", and the rod as the other. This capacitor probe is connected by a shielded cable approximately 100 feet long to a converter, which converts the capacitance to a voltage by means of an electronic circuit and amplifier. There is one converter for each probe in the present system, although a switching device could reduce the number of converters as desired. Voltage from the converters is recorded either on magnetic tape or punched cards as shown in Figure 18. The details of the recording system have been presented in the previous report on the facility (4).

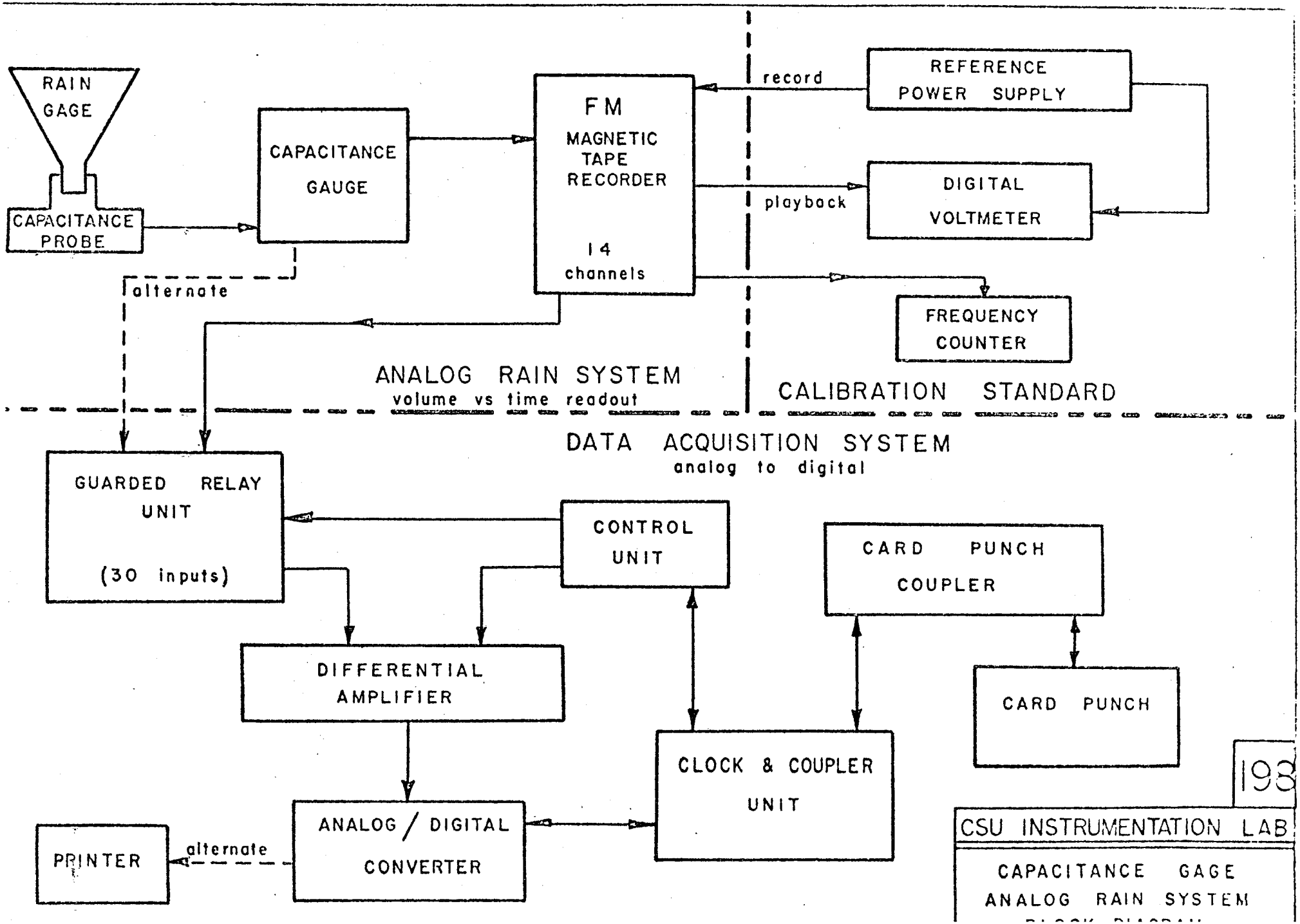
RAIN GAGE
CAPACITANCE PROBE
CAPACITANCE GAUGE
alternate
FM MAGNETIC TAPE RECORDER
14 channels
record
playback
REFERENCE POWER SUPPLY
DIGITAL VOLTMETER
FREQUENCY COUNTER
ANALOG RAIN SYSTEM
volume vs time readout
CALIBRATION STANDARD
DATA ACQUISITION SYSTEM
analog to digital
GUARDED RELAY UNIT
(30 inputs)
CONTROL UNIT
CARD PUNCH COUPLER
CARD PUNCH
DIFFERENTIAL AMPLIFIER
CLOCK & COUPLER UNIT
ANALOG / DIGITAL CONVERTER
alternate
PRINTER
198
CSU INSTRUMENTATION LAB
CAPACITANCE GAGE
ANALOG RAIN SYSTEM

As shown in Figure 19, the measuring unit consists of an outer aluminum measuring can 7.6 inches inner diameter and 6.5 inches high, and a smaller concentric plastic cylinder 2.5 inches inside diameter. The inner can overflows when full into the outer can. Rain enters the smaller inner can through a funnel-shaped cover. Probes measure water rise in both inner and outer cans. The capacitance probes in the cans originally consisted of a lacquer-coated copper wire running the depth of the can, plus a bare wire to make contact with the water. These probes were copied from the system developed by Dr. Plate.

The raingages were tested in the electronics laboratory and found to work very well. They produced consistent records of high sensitivity and precision. However, when they were installed in the field, the results were not satisfactory. After a series of tests, the electronics laboratory concluded that the cause of the problem must be a temperature sensitivity. The testing program was turned over to a graduate research assistant working for the Agricultural Research Service and assigned to the facility.

TEMPERATURE SENSITIVITY STUDIES

Using 120 feet of cable like that installed in the field setup and a randomly selected can and converter, tests were conducted in the laboratory making measurements at various water and can temperatures. It was quickly noted that for any test, starting from a dry can, a severe initial drift in voltage output occurred for several minutes after water was added. Tests of an empty can at temperatures from less than 40^0 to 75^0F, however, indicated negligible effect of can temperature. Tests with water temperature varying from 33^0 to 75^0F showed only a small temperature effect, as presented in Figure 20. These results were taken after allowing the initial drift mentioned above to subside.

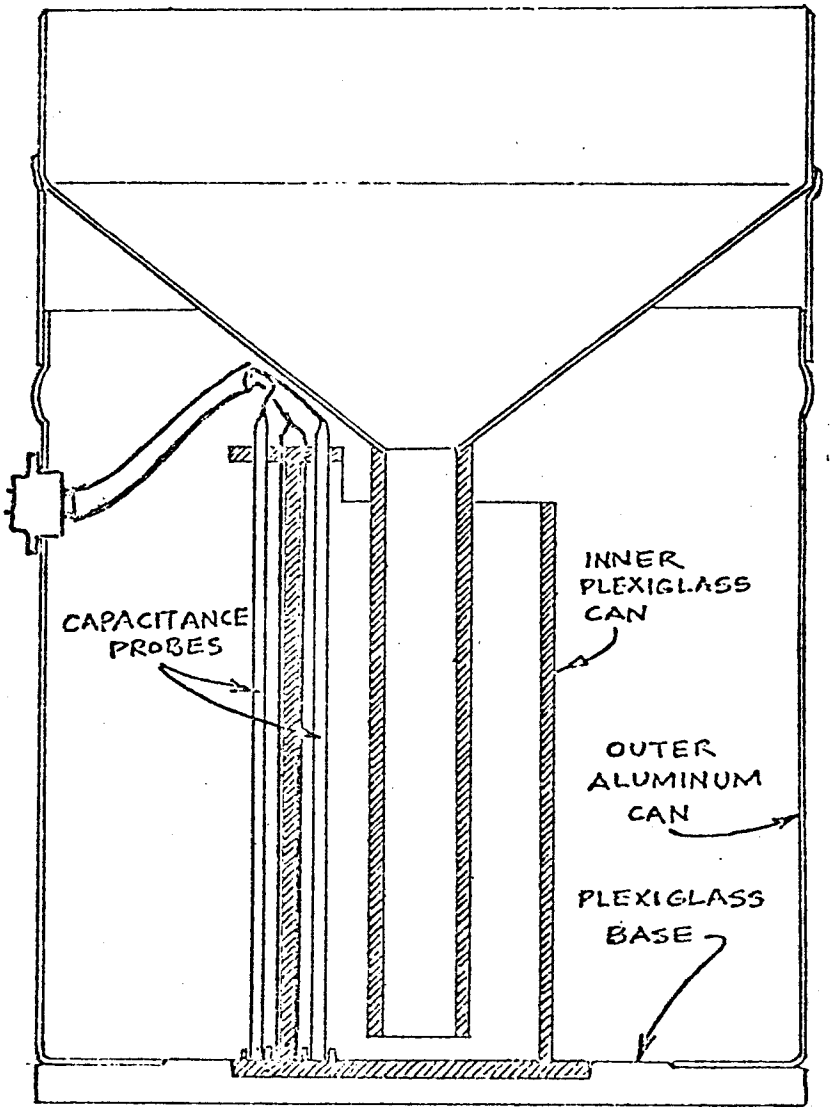

Figure 19 Section Through Electronic Raingage

Further measurement of the nature of this drift indicated it was in some way connected with the initial dryness of the can, and that it continued even when water was temporarily removed from the can. Figure 21 shows the results of one such test.

The conclusion drawn was that the wire coating was affected enough by contact with water to alter its dielectric strength some 20 percent.

IMPROVEMENTS MADE

It was decided that a probe with capacitance comparable to the old probes was required, since the electronics were designed for a certain capacitance range, but that a uniform coating inert to water should be found. Since capacitance is proportional to plate area and inversely proportional to "plate" separation, a larger diameter probe could be used with a somewhat thicker insulation. From suggestions of Dr. Plate, it was decided to try a larger rod or tube. After a trial with thicker materials, a high tolerance 0.009 inch thick KYNAR heat shrink tubing was chosen as quite suitable as a watertight dielectric coating. Brass tubing was used as the probe, the bottom was sealed with epoxy after the shrink-fit tubing was shrunk on, and a lead soldered to the top end. Different sizes of tubing were tried, and each had different sensitivity to water height. A 1/8" O.D. tube was chosen as being most suitable for the inner can, and a 5/32" probe used in the outer can. Allowable sensitivity is limited in this case by the converter, since too high capacitance will "saturate" the amplifier, and dv/dc will approach zero.

Each can and new probe was calibrated by careful titration, and the results analyzed by least squares regression. All gages were slightly nonlinear, but all data fit on the same normalized curve to within 0.9998

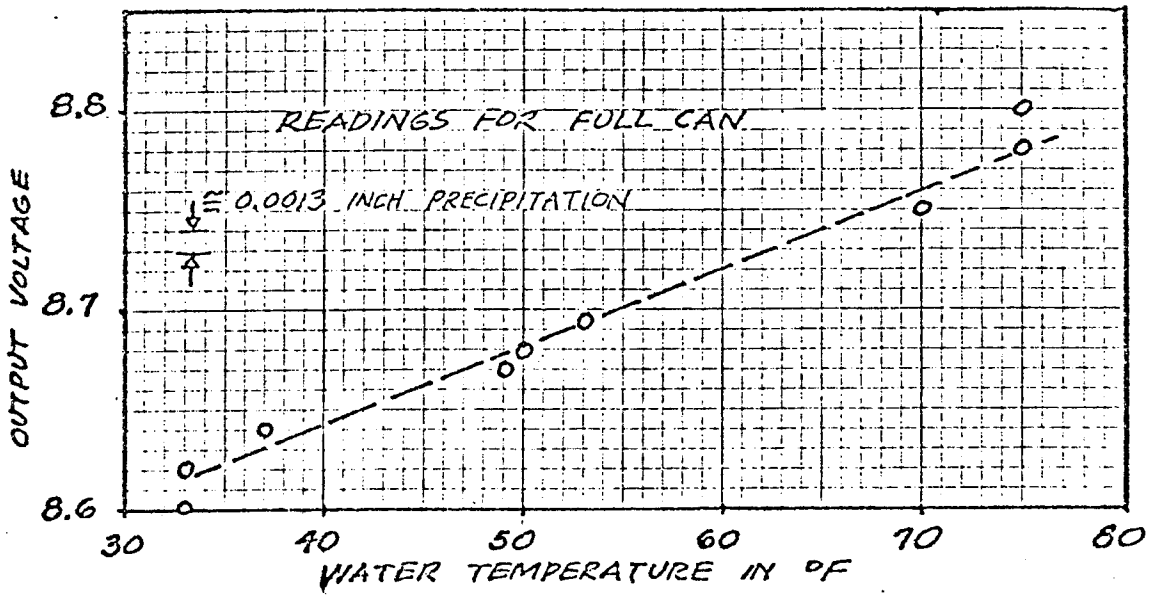

Figure 20 Sensitivity to Water Temperature

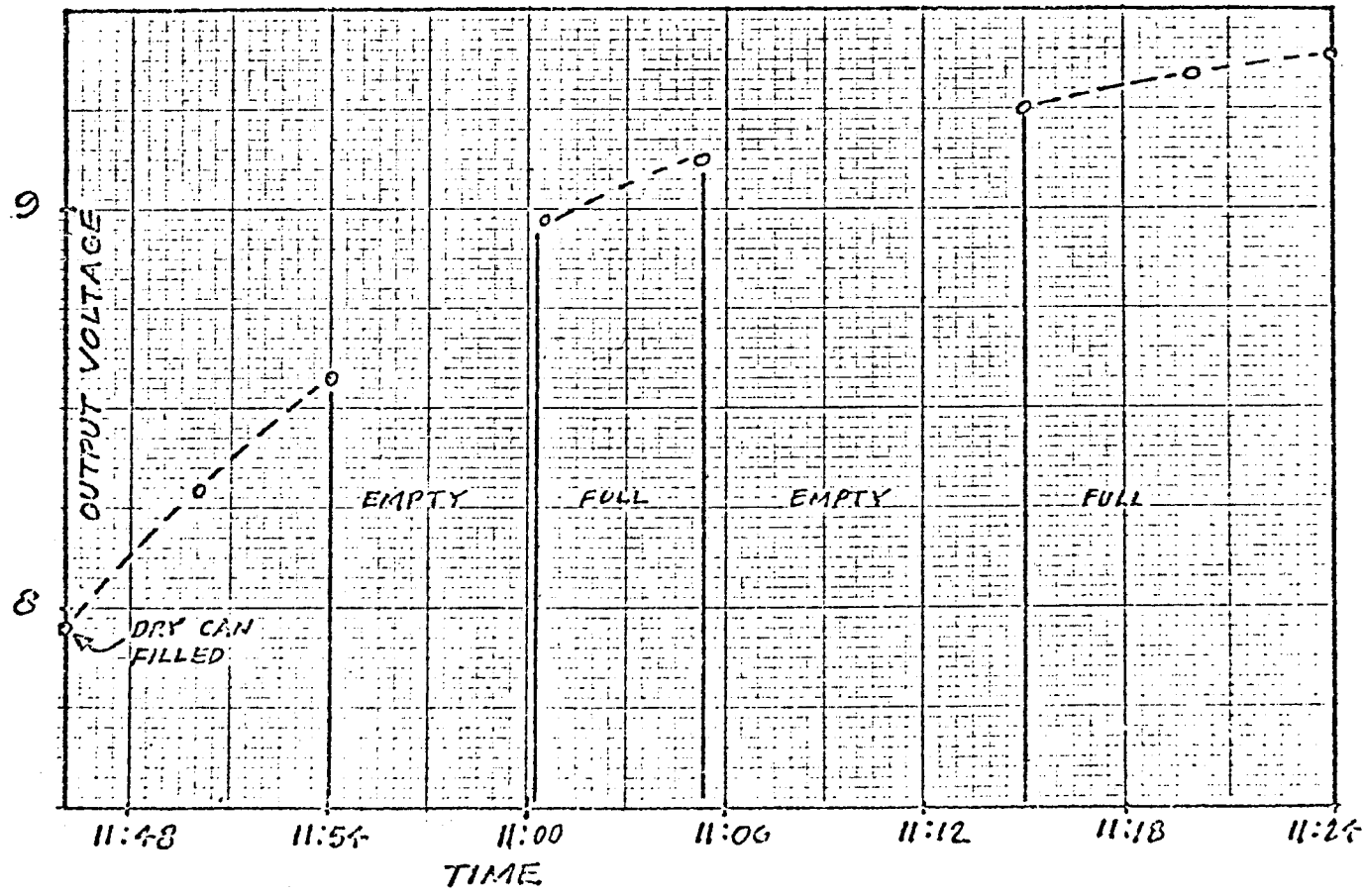

Figure 21 Typical Drift of Enameled Wire Probes

multiple correlation coefficient, and a standard error of estimate of 0.0029 inches of precipitation. No drift on wetting was noted.

Six of the modified raingages were operated during the fall series of tests on the facility. The complete data have not been analyzed, but the data collection system appears to be functioning satisfactorily. There is one problem that has occurred in the field tests with the modified gages. The capacitance gage does not always give a reproducible zero. The gages must be warmed up for several hours before a series of tests is run. When the zero depth reading has shifted from that used in a previous set of tests, it is necessary to provide a new calibration. This is not a major problem because the calibration curves all fit the same type curve when they are normalized. This is an inconvenience, but not a major fault. The warm-up problem is also a minor one because the system can be left on for several days at a time without damaging the components.

The raingages sense the depth of water accumulated as a capacitance measurement. The measurement of the capacitance is not made at the gage but is made at one of the bunkers located at the edge of the facility as shown in Figure 22. The length of lead wire from the gage to the bunker is the same for all gages. Since only the upper conic section of the facility is in operation, only bunker A, at the top of the area is being used at this time. The power supply to the bunkers and the readout lines have been installed to all of the bunkers.

ADDITIONAL RAINGAGES

In addition to the capacitance raingages, which transmit readings to the A-D converter for punched card format, there is one weighing bucket raingage on the facility that produces a chart record. This raingage was provided by the Agricultural Research Service and has been modified to use a synchronous motor drive that provides a chart rotation

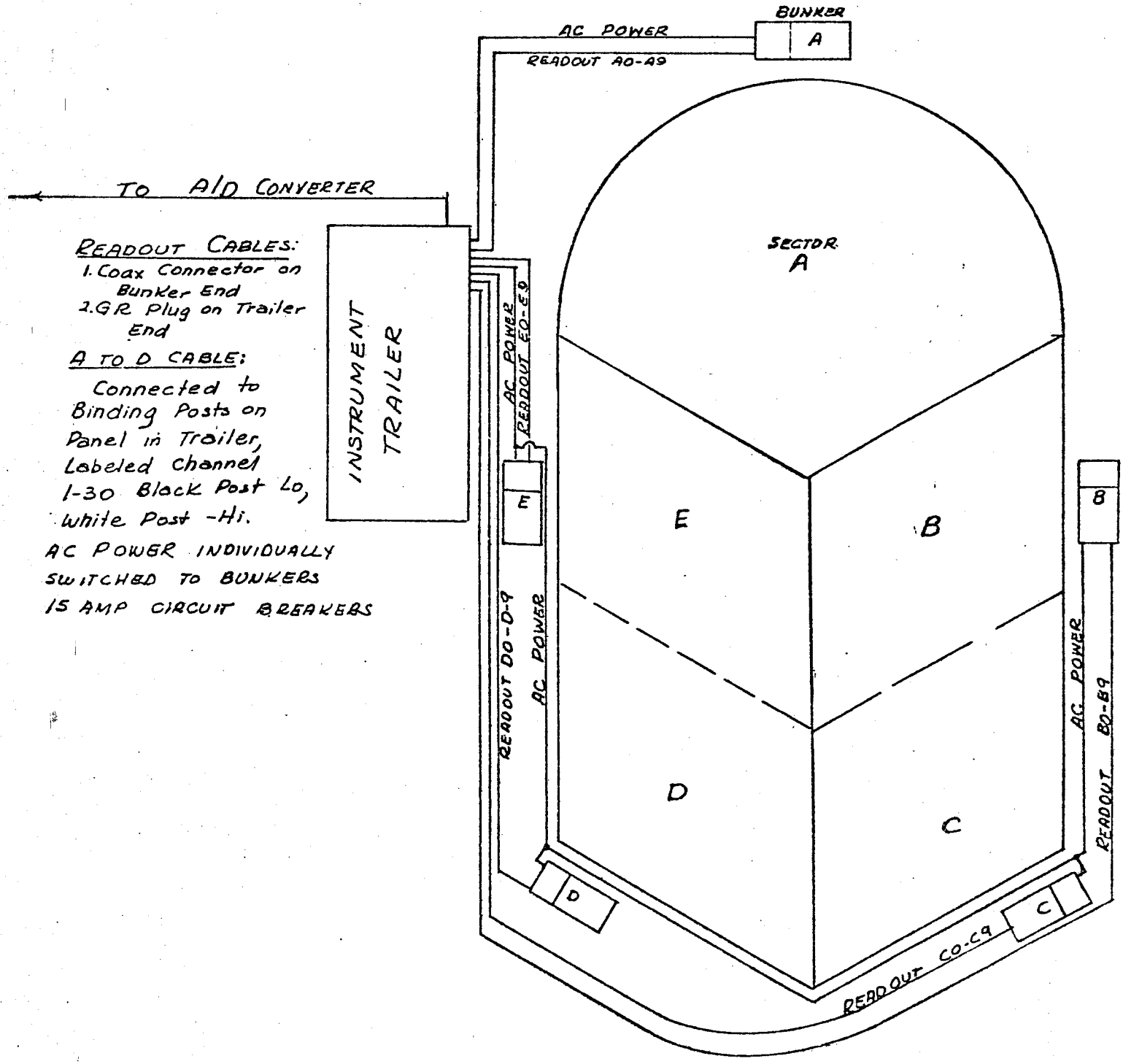

Figure 22 Schematic of Automatic Data Recording System for the Experimental Facility

in 15 minutes, instead of the normal 6 hours. This gage has two uses. First, it serves as a check on the operation of the capacitance gages. It can be moved to locations near the capacitance gages to provide additional calibration data. Second, the chart gives a visual trace of the rainfall pattern that can be checked to see that the performance of the input system was along the lines that were intended.

A large number of cans will also be used in the early tests on the facility to determine in more detail the actual distribution of rainfall in space that is provided by this system. The results of the early tests have already been mentioned in Chapter 2. After the characteristics of the input distribution have been defined, less use will be made of the non-recording cans.

The data for the weighing bucket raingage and for the non-recording cans must be converted to the form used for computer input. The data for the cans must be punched by hand. The chart record from the weighing bucket gage is digitized by using an AutoTrol digitizer. This converts the record to a series of x and y coordinates as a tracer is moved along the pen trace. The data must be adjusted for the curvature of the chart grid lines, but this is a simple matter on the computer.

RUNOFF MEASUREMENTS

The measurement of runoff from the experimental facility uses the H-flume developed by the Agricultural Research Service. The design and construction of the flumes for the facility has been adequately described in the previous report (4). The measurement of stage is now being done by two methods -- a chart recording float gage and a capacitance gage.

Figure 23(a). Chart Recorder at H-Flume

Figure 23(b). Capacitance Gage at H-Flume

When the difficulty with the raingage capacitance probes developed, the use of the capacitance probe in the flume was shelved because the conditions in the flume would be even more variable than in the raingages. The runoff in the flumes will contain a more variable quantity of dissolved and suspended material, especially in later stages of use of the facility. Therefore, the float gage was made the prime recording system. There are only two flumes for the facility, so the conversion of the data to digital format by the AutoTrol is not too difficult. At the present time, of course, only the upper flume is in operation.

The chart recorder at the flume was also supplied by the ARS and was modified to use the synchronous motor drive for a faster revolution. The successful modification of the capacitance probe for the raingages led to the installation of a longer capacitance probe at the flume. The two systems are pictured in Figure 23. The chart recorder in Figure 23a shows a recession occurring. The capacitance probe in Figure 23b requires a smaller stilling well and has a faster response than the chart gage. The two systems will both be operated for some time before a decision is made about which will ultimately be the preferred system. The direct recording of the capacitance gages is an advantage that is offset by the value of the visual record immediately available from the chart.

ANALYSIS OF DATA

The rainfall and runoff data will be analyzed jointly to determine the input to the facility. The recording and non-recording raingages will be used to determine the volume of input. The volume of runoff will also we used as a reference for the total quantity of input to the catchment. The time distribution of rainfall will be well described by the recording raingages. There are

six capacitance raingages and one weighing gage for a total of seven observations over an area of 1/3 acre. Additional data for each run can be added when the data from the non-recording cans is added to the computer input.

Chapter 4. GEOMETRY AND SURFACE TREATMENT

The selection of the geometry for the experimental facility was described in the earlier report (4). It was based on a study of sixty-one small watersheds drawn from the Research Data Assembly Program for Small Watershed Floods (8). The general shape of the facility was decided as a compromise between the best-fit shape for the natural watersheds in the study and the existing configuration of the area in which the facility was to be located. In addition, it was decided to use simple geometric shapes to make up the facility, so description of the areas would be readily provided to the computer. The result is the shape made up of three segments, each 1/3-acre in size. The two lower segments are planes that intersect to form an arrowhead shape, and the upper area is a sector of a cone. This shape gives the general characteristics of natural watersheds in idealized form.

A decision was made early in the project design to use an impervious surface in the initial operation of the facility. This provides a significant simplification of the watershed processes, and will be more suitable for the first studies. After the system has been in operation for a period of time, the infiltration process will be included. A variety of methods were considered for making the surface impermeable, including treatment of the soil with soil cement, the use of plastic or rubberized sheeting to cover the ground and the placement of asphalt or concrete surfaces.

SOIL CEMENT STUDIES

A series of tests were run to determine the characteristics of the soil cement treatment. It was found that the soils existing at the facility site were

not suited to soil cement treatment. An example of this is shown in Figure 24. In the upper part of the figure the natural soil is shown before and after water has been run across it. This series of tests was run in a flume in the ERC laboratories. The natural soil shows the effects of erosion, which was being tested at the time, but the soil remains in a continuous mass. At the bottom of the figure the soil has been treated with soil cement. It is clear that the cracking which takes place when the soil is dried causes a permeability that will vary with time when water is added to the system. This is of course completely unsatisfactory.

Both soil cement and lime were tested for use on the facility. The reduction in permeability for these is indicated in Figure 25. The only region in which the soil cement had a significant effect of lessening the saturated permeability of the soil is in the range where cracking is the most serious. The lime treatment also requires a fairly high dosage to provide any reduction in permeability. There is also a marked variation in the soil characteristics at certain points on the facility because of an outcrop of shale. The shale is a problem to work with in all conditions, wet or dry.

The use of soil cement treatments were rejected as an alternative for the development of the impermeable surface on the facility.

OTHER METHODS CONSIDERED

The second method considered for the treatment of the soil was the use of liquids, such as paraffin-base materials. Some samples of the materials were obtained and a few tests were made on small area within the facility. However, these liquids were very expensive, and before the tests were completed, the availability of less expensive alternatives led to the discontinuance of the testing.

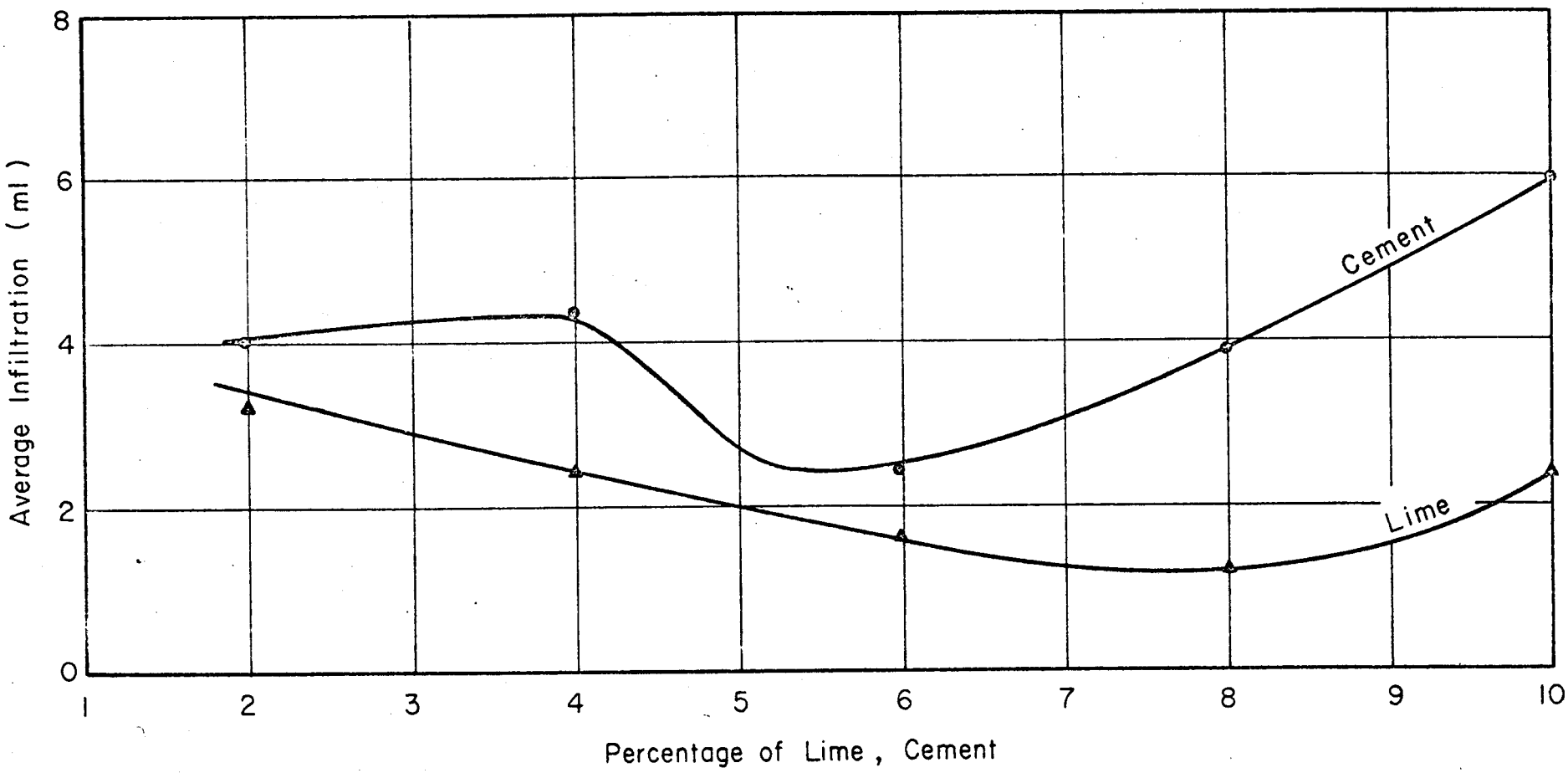

Figure 25 Effect of Lime and Soil Cement on Infiltration Capacity

The use of asphalt or concrete surfaces was considered as a possible last-resort solution. The cost of these approaches would be high and the surfaces are rigid. One of the objectives in the use of the facility is to test the response of the system under a variety of conditions of slope, drainage network, etc., and the use of the rigid surface would preclude this to a great extent. Therefore, these methods were never given detailed study.

Plastic sheeting has been used as a covering material in a variety of ways in outdoor applications. The lining of canals and reservoirs are examples of uses that are somewhat similar to the use on the facility. However, in the previous uses of plastic, the material was covered by a layer of soil or other material to weight is down or the use was such that the effect of wind lifting the plastic would be unimportant. For the experimental facility application there will be times when it is desired to use the facility with no soil cover of any type. The shifting of the surface as wind causes waves on the plastic is also unacceptable. Therefore, plastic sheeting, although a potential material when covered by a thin layer of soil, was rejected for the present.

RUBBERIZED CLOTH SHEETING

Butyl sheet with cloth reinforcing was considered as an alternative for the facility at a early date. The material is very expensive, and was therefore rejected. However, when some of third material was found to be available in government surplus, it became a feasible method. The butyl material is better than the plastic material because it is stronger and wears longer, and also because it is heavier. The material is affected by the wind when it is first installed, but is quickly stabilized by the action of the soil moisture adhering to the underside enough to keep it down. The

weight of the material is sufficient, together with the moisture effect, to provide stability.

The material available in surplus was not sufficient to cover the facility, so more was purchased. However, the upper conic section and most of the lower area could be covered at a reasonable cost. A survey of government surplus material is continually made in case additional material becomes available.

The butyl material is placed in strips extending completely across the catchment, and the ends are buried in a small trench to prevent the wind from getting under the material to lift it from contact with the ground. The material has been in place for over a year and shows some wear in a few locations. When water seeps through the material, it may collect at a joint and form a small ridge that affects the flow on the surface. Therefore, the worn areas are patched by painting with a rubber-based liquid or, if the area is more extensive or more seriously worn, by cutting out the worn area and replacing it. Patches can be made fairly easily, and joints can be covered with a light plastic sheet glued to the rubber to make a watertight joint without overlapping the thicker rubber material.

DEFINITION OF BOUNDARIES

The boundary of the facility is sharply defined by using a wood section covered with a sheet of plastic. The plastic is bonded to the rubber covering the area, and the wood prevents water from overtopping the boundary. This method has also been used to form temporary boundaries for changing the area contributing runoff to the flume. Ponding on the contributing area can also be created in this way.

Chapter 5. USES OF THE FACILITY

INITIAL RUNS

The initial series of tests run on the experimental facility are currently being analyzed. A set of 68 runs were made in the fall to test the facility and to provide data for testing a kinematic model of overland flow on a converging section. This model was developed under the direction of Dr. Woolhiser of the Agricultural Research Service and will be presented by him elsewhere.

The variations that were made in this series of tests illustrates some of the potential of the facility. The first tests were on the bare facility, with the intensity of rainfall as the variable. The intensity was maintained constant until an equilibrium flow was achieved in some cases. In other runs, the duration was less than the time to equilibrium and in some runs the intensity was changed during the course of the run. In later tests the area contributing runoff to the flume was changed by erecting temporary boundaries to separate a 30^0 sector from the remaining 90^0 sector and to create shorter radii of 72 feet and 36 feet. The results of these experimental tests are being compared with the computer model output to determine the ability of the model to reproduce the variations that are caused by the respective parameters.

In the final series of tests, a very coarse gravel was used to provide roughness and detention effects on the facility. This is illustrated in Figure 26, where a uniform spread is shown in part (a) and a section without gravel spread were used on the facility at different times. Only the 30^0 sector was used for this series of tests because the spreading was done entirely by hand and a number of test runs were desired before the cold weather set in. A number of different patterns were used in the placement of gravel for the runs. The uniform spread and the lower bare section

Figure 26(a). Gravel Spread for Uniformly Distributed Roughness

Figure 26(b). Roughness on Upper Section with Bare Section Below

have been shown. In addition, alternating strips of gravel and bare surface each 10 feet wide were used, a checkerboard pattern of sections with gravel cover was tested and finally a uniform gravel was laid out with a tree arrangement cleared to represent a stream network. The initial results indicate that the total quantity of gravel on the system is the most important parameter and the pattern makes little difference except when the flow can define a route to the flume by-passing the gravel completely. A more detailed analysis will yield more definite conclusion on the effect of the gravel in specific patterns.

FUTURE STUDIES USING THE FACILITY

The experimental facility will be useful in a number of different studies of hydrologic and related phenomena. Two projects have already been funded that will utilize the facility.

The first project is a study of the pollution characteristics of waste piles from oil shale development. As a part of this study, several piles of oil shale wastes will be arranged in the form of lysimeters on the facility. The artificial rainfall will be provided and the runoff, both surface and subsurface, will be collected and chemically analyzed. The effects of varying periods without rain can be determined with the facility. It is not currently known whether drying and weathering effects will increase the pollutant outflow from the system. This project is being conducted by the Sanitary Engineering group of the Civil Engineering Department.

The second project was funded to the Geology Department in cooperation with personnel from the experimental facility project. It is a study of the geomorphic development of stream networks. Under this project several containers about 10 feet by 40 feet in size will be filled with material that can be easily eroded. The development of the stream networks will be

observed and recorded photographically. The process that requires many decades and centuries in nature will be studied in a few weeks.

Both of these projects will be utilizing the experimental facility in the coming spring and summer. The possibility of conflicting needs for the projects using the facility have already become clear. The operation of the facility will have to be carefully managed to allow effective use for a diverse set of projects. This will be even more important as additional projects in the areas of water quality and geomorphology, for example, are funded to use the facility.

Each project that uses the facility is expected to provide some permanent contribution to the development of the facility. Thus, no single project or agency will have to provide the entire funds for developing the facility while little is gained in terms of research results. Now that the value of the facility is being shown, a number of proposals are being made to use it. Each of the projects using the facility and benefiting from the investment that has already been made will be investing in the further development of the area and versatility of the experimental facility.

THE KINEMATIC CASCADE AS A HYDROLOGIC MODEL

by

David F. Kibler

and

David A. Woolhiser

HYDROLOGY PAPERS
COLORADO STATE UNIVERSITY
FORT COLLINS, COLORADO 80521

March 1970

No. 39

ACKNOWLEDGMENTS

A substantial part of this paper is based upon the Ph.D. dissertation "A Kinematic Overland Flow Model and its Optimization" by David F. Kibler. The work was supported by the Colorado State University Experiment Station and by the Northern Plains Branch, Agricultural Research Service, USDA. Experimental data were obtained from the Colorado State University Experimental Rainfall-Runoff Facility which has been supported in part by grant B-030-COLO by the United States Department of the Interior, Office of Water Resources Research as authorized under the Water Resources Research Act of 1964. The research project also received support from Agricultural Research Service and the Colorado State University Experiment Station under Projects 114 and 124.

TABLE OF CONTENTS

LIST OF FIGURES AND TABLES

ABSTRACT

A kinematic cascade is defined as a sequence of n discrete overland flow planes or channel segments in which the kinematic wave equations are used to describe the unsteady flow. Each plane or channel is characterized by a length, l_k, width, w_k, and a roughness-slope factor, α_k. Outflow from the $k^{\underline{th}}$ plane, along with the parameters for planes k and $k + 1$, establishes the upstream boundary condition for plane $k + 1$. Nondimensional equations are presented for the $k^{\underline{th}}$ element in a kinematic cascade. Properties of the solutions for a kinematic cascade with pulsed lateral inputs are examined. Cascade solutions are compared with characteristic-analytic solutions and with experimental data for flow over a linearly converging section.

THE KINEMATIC CASCADE AS A HYDROLOGIC MODEL*

by

David F. Kibler** and David A. Woolhiser***

Chapter I

INTRODUCTION

Scope and Objectives of the Study

The basic premise underlying the "reductionist" approach to hydrologic modeling is that the complex geometry and topography of natural catchments can be replaced by large numbers of simple elements such as overland flow planes and channels. In its most elementary form, the surface runoff process is thus reduced to the hydraulic problem of unsteady, spatially-varied flow over a uniform plane or channel. The simple plane or channel thus represents a single element in a distributed hydrologic model of the catchment.

In general, a distributed watershed model should possess the following characteristics:

1. The model should be based on sound physical reasoning.

2. The parameters should have direct physical significance.

3. The model should be numerically accurate; i.e., the approximation introduced by finite difference schemes should not influence parameter estimation in any significant way.

4. The model should be subject to experimental verification.

5. The structure of the model should not be so complicated as to require extremely difficult programming logic.

The kinematic cascade is a distributed hydrologic model that exhibits many of these desirable properties and has, therefore, been selected for further analysis in this investigation. The broad objective of this study is to examine certain mathematical properties of the selected model and to describe its application to the problem of watershed transformation and simulation.

The kinematic cascade is defined in this study as a sequence of n discrete overland flow planes or channel segments in which the kinematic wave equations are used to describe the unsteady flow. An n-plane cascade receiving lateral inflow and discharging into a channel segment is shown in Figure 1. Discharge leaving the downstream boundary enters at the upstream boundary of the next plane and establishes the upstream boundary condition for flow on that plane. Discharge leaving the downstream boundary of the last plane is then fed laterally into a channel of known dimensions where it is conveyed via a cascade of channels to some downstream gauging point.

Previous investigators using the kinematic wave technique for simulating watershed response either have relied on severe geometrical simplification or have not examined the approximation errors of their finite difference schemes. Errors caused either by geometric oversimplification or by the finite-difference scheme can affect optimized model parameters in a manner which casts doubt on their physical significance.

Thus, the specific purpose of this study is to evaluate errors introduced by various computational algorithms and by transformation of watershed slope. The dimensionless equations describing kinematic flow over a cascade of planes will first be developed. Solutions to these equations, obtained by the method of characteristics, will then serve as standards in subsequent comparisons with solutions obtained by three rectangular grid methods. The effects of kinematic shock waves, which are produced by exact integration of the characteristic equations for certain cascade configurations, will then be analyzed. A method for tracing the propagation path and a discussion of hydrograph distortions caused by shock propagation are presented. Finally, the effects of transforming the slope of an overland flow surface will be examined by means of outflow hydrograph comparisons. This discussion is prefaced by a brief

* Contribution from the Colorado Agricultural Experiment Station and the Northern Plains Branch, Soil and Water Conservation Research Division, Agricultural Research Service, USDA, Fort Collins, Colorado.

** Associate Engineer, Water Resources Engineers, Incorporated, Walnut Creek, California. Formerly Graduate Student, Colorado State University, Fort Collins.

***Research Hydraulic Engineer, USDA, Fort Collins, Colorado.

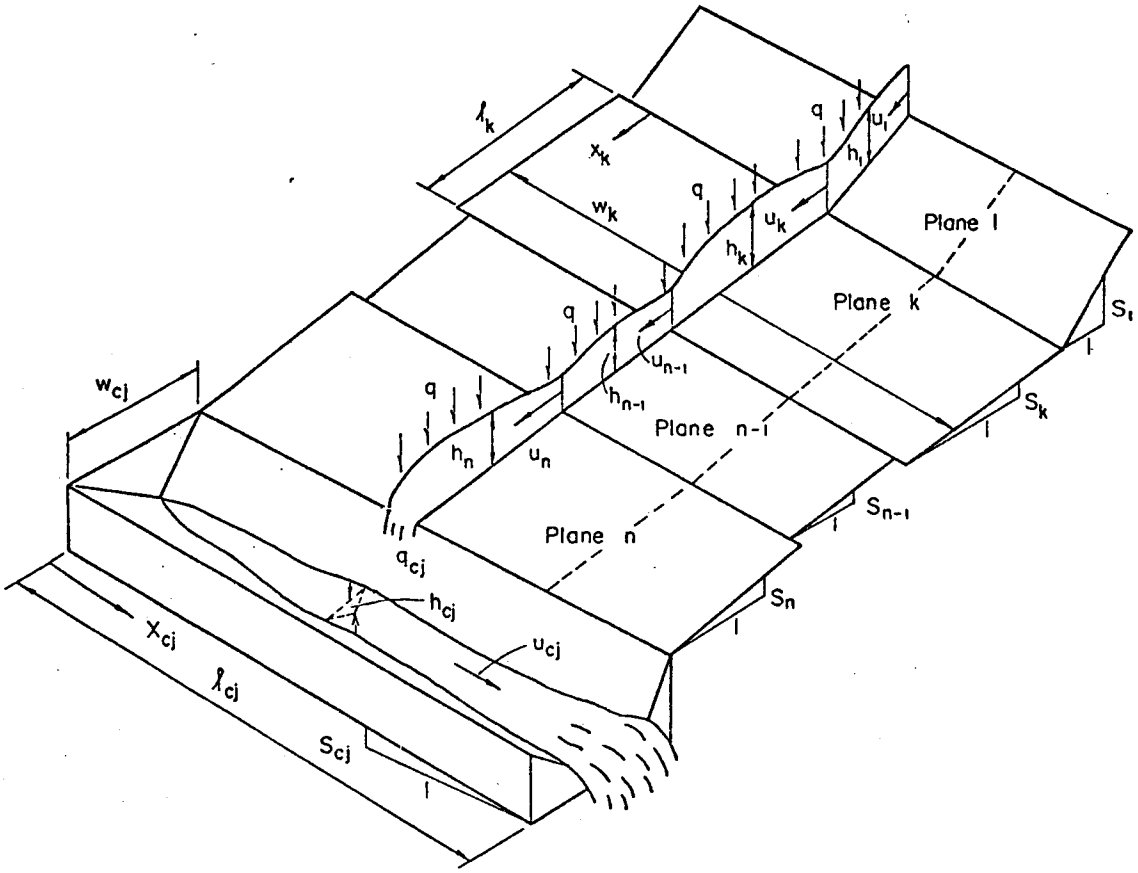

Figure 1. Cascade of n planes discharging into the j^{th} channel section.

review of work leading to the formulation of the kinematic cascade as a hydrologic model.

Background of the Kinematic Cascade

The concept of the kinematic cascade was first introduced by Brakensiek (1967a) who transformed an upland watershed into a cascade of planes discharging into a single channel. His transformation technique was based on preservation of the hypsometric curve and the contour length-elevation curve for the watershed. Brakensiek has also written on basic application of the kinematic flood-routing method and has described the properties of the kinematic technique within the context of hydraulic and hydrologic flood-routing procedures (1966, 1967b).

The theory of kinematic flow, which forms the mathematical basis for this hydrologic model, was first set forth by Lighthill and Whitham (1955) in a paper dealing with flood movement in rivers. The authors used the term "kinematic" to describe those waves whose properties are given by the equation of continuity and a stage-discharge relation, such as the Chézy or Manning friction formula. This is in contrast to dynamic or long gravity waves whose motion is governed by both the continuity and momentum or shallow-water equations. Accordingly, kinematic waves possess only one velocity and one system of characteristics along which flow is to be computed. The resulting first-order differential equations for the kinematic wave are in marked contrast to the hyperbolic system associated with the shallow-water equations. The latter possess two families of characteristics and can be solved only by resort to finite-difference methods.

In a paper on the celerity of subsiding flood waves, Henderson (1963) described the conditions under which flow in a prismatic channel (without lateral inflow) could be classified as kinematic. The criterion developed for kinematic flow was that the partial derivative terms appearing in the equation of motion must be negligible in comparison with the bed slope; i.e., the flow must be essentially uniform. It was thus concluded that flood waves will be kinematic in rivers with slopes that are steep, but flatter than those found in torrential mountain streams. Woolhiser and Liggett (1967) also examined the hydraulic conditions required by the kinematic flow assumption and concluded that much of the experimental work on overland flow has been carried out under essentially kinematic conditions.

Iwagaki (1955) used the kinematic assumption implicitly in his analysis of unsteady flow in steep channels. However, the kinematic wave technique was first applied to flow over a sloping plane by Henderson and Wooding (1964). In a series of three papers, Wooding (1965a, 1965b, 1965c) discussed the application of kinematic wave theory to the overland and channel components of runoff from a hypothetical V-shaped watershed consisting of two rectangular planes and a straight channel. Investigation of the response of this elementary watershed system represents one of the first attempts to simulate catchment behavior using the kinematic wave technique.

The rising hydrograph of overland flow on a single plane has been analyzed by Woolhiser and Liggett (1967, op.cit.) using both the shallow-water equations and their kinematic approximation written in dimensionless form. Comparison of results obtained from the complete equations and from the kinematic wave solution disclosed that the degree of departure was related to the dimensionless parameter, k. This parameter is an index representing the magnitude of slope and friction effects--i.e., high values of k indicate that slope and friction dominate the flow and consequently that the kinematic hydrograph is a good approximation to that derived from the complete shallow-water equations. Because of the finding that the shape of the dimensionless hydrograph can be dependent on both k and the Froude number, it was concluded that there can be no unique dimensionless rising hydrograph of overland flow--in contrast to the contention of Izzard (1946). Morgali's (1968) analysis of experimental overland flow hydrographs by means of the kinematic equations is noted in this regard. Woolhiser (1969) has further discussed kinematic flow on an inverted cone-shaped surface having a specified degree of convergence at the apex. This basic watershed element is investigated later in the current study.

The reductionist approach to watershed simulation alluded to earlier in this paper was used by Huggins and Monke (1966) in developing a distributed watershed model. They employed a finite element or square grid technique for decomposing a complex watershed into elemental surface units. The kinematic wave technique was then applied sequentially in the downstream direction to route overland flow generated by each subarea and thereby obtain a complete hydrograph of watershed runoff. As in the kinematic cascade used by Brakensiek, the value of Mannings roughness was adjusted to minimize the discrepancy between observed and computed hydrographs.

Other work on which the present study is based is identified at appropriate points in the text. However, the literature on overland flow is replete with intensive analytical and experimental investigations and clearly, an exhaustive review is outside the scope of the present effort. For a summary of related work in the areas of numerical flood-routing methods, experimental overland flow, mathematical watershed models, and finite-difference solutions to the shallow-water equations reference is made to a publication by Kibler (1968).

Chapter II

KINEMATIC EQUATIONS FOR A CASCADE OF PLANES

The kinematic flow relations are based on the continuity and momentum equations, commonly referred to as the De Saint-Venant or shallow-water equations. These basic equations are derived in Appendix A. In the kinematic wave derivations which follow, the dependent quantities are the local velocity, u, in fps and the depth, h, in feet. The independent variables are the space-time coordinates, x in feet, and t in seconds, respectively.

Kinematic flow on planes and in channels arises whenever a balance between gravitational and frictional forces is achieved. The existence of such a balance implies that the derivatives of the energy and velocity terms in the momentum equation are negligible in comparison with gravity and friction effects. The momentum equation is thus reduced to the form:

$$S = S_f \tag{1}$$

where S and S_f are the bed slope and friction slope, respectively. The hydraulic conditions required by this assumption have been examined by Lighthill and Whitham (op.cit.), Henderson (op.cit.) and by Woolhiser and Liggett (op.cit.).

The continuity equation appears in the usual form for planes or wide rectangular channels

$$\frac{\partial h}{\partial t} + \frac{\partial uh}{\partial x} = q \tag{2}$$

where q is the lateral inflow (precipitation less infiltration) in cfs/ft^2.

In this study a parametric form of the Chézy friction relation is used to represent equation (1) as follows:

$$u = \alpha h^{N-1} \tag{3}$$

where α and N are parameters related to channel (or plane) roughness and geometry. For a wide channel or plane, α and N have values

$$\alpha = C\sqrt{S} \quad ; \quad N = 3/2 \tag{4}$$

where C is the Chézy roughness coefficient.

Dimensionless Equations for $k^{\underline{th}}$ Plane

The characteristic equations can be expressed in dimensionless form by defining normalizing quantities for the $k^{\underline{th}}$ overland flow plane.

Let Q_k = maximum or steady-state discharge per foot of width from the downstream boundary of the $k^{\underline{th}}$ plane resulting from q_k, where q_k is the maximum rate of rainfall excess in cfs/sq.ft. units for the first through the $k^{\underline{th}}$ plane.

$$Q_k = Q_{k-1}\left(\frac{w_{k-1}}{w_k}\right) + q_k\, l_k \tag{5}$$

where l_k and w_k are the length and width, respectively, of the $k^{\underline{th}}$ plane.

In general Q_k is given by the summation

$$Q_k = \frac{1}{w_k} \sum_{i=1}^{k} q_i \cdot l_i \cdot w_i \tag{6}$$

Let L_k = normalizing length for the $k^{\underline{th}}$ plane

$$L_k = \sum_{i=1}^{k} l_i \tag{7}$$

where l_i is the length in feet of plane i.

Let H_k = normal depth in feet corresponding to Q_k at the downstream boundary of the $k^{\underline{th}}$ plane.

$$H_k = \left(\frac{Q_k}{\alpha_k}\right)^{\frac{1}{N}} \tag{8}$$

where α_k and N are Chézy parameters of the $k^{\underline{th}}$ plane.

Let V_k = normal velocity in fps corresponding to Q_k at the downstream boundary of the $k^{\underline{th}}$ plane.

$$V_k = \alpha_k H_k^{N-1} = \alpha_k \left(\frac{Q_k}{\alpha_k}\right)^{\frac{N-1}{N}} \tag{9}$$

Let T_k = normalizing time in seconds for the $k^{\underline{th}}$ plane

$$T_k = \frac{L_k}{V_k} \tag{10}$$

The normalizing quantities have been obtained with the assumption that the planes have equal lengths: $l_1 = l_2 = \ldots = l_n$.

Substituting the parametric friction relation in the continuity equation and using the normalizing quantities of equations (5) through (10), the dimensionless kinematic flow equation for the $k^{\underline{th}}$ plane is given by

$$\frac{\partial h_*}{\partial t_*} + \beta h_*^{N-1} \frac{\partial h_*}{\partial x_*} = q_* \qquad (11)$$

where the asterisk indicates the terms are dimensionless. The only terms in equation (11) previously undefined are q_* and β. The dimensionless lateral inflow is:

$$q_* = \frac{q}{I_k} \qquad (12)$$

where I_k is the normalizing lateral inflow given by

$$I_k = \frac{1}{T_k} \left(\frac{Q_k}{\alpha_k}\right)^{\frac{1}{N}} = \frac{Q_k}{L_k} \qquad (13)$$

and the parameter β is defined as

$$\beta = \frac{\alpha_k N T_k}{\sum_{i=1}^{n} l_i} \left(\frac{Q_k}{\alpha_k}\right)^{\frac{N-1}{N}} = \frac{N L_k}{\sum_{i=1}^{n} l_i} \qquad (14)$$

The dimensionless characteristic equations developed from equation (11) for the $k^{\underline{th}}$ plane in a cascade of n planes are:

$$\frac{dx_*}{dt_*} = \beta h_*^{N-1} \qquad (15)$$

$$\frac{dh_*}{dt_*} = q_* \qquad (16)$$

The asterisk has been dropped from the dimensionless equations for the remainder of this paper except where noted. Integration of equation (16) leads to

$$h = h_o + q(t - t_o) \qquad (17)$$

where h_o and t_o are initial values of depth and time, respectively. The equation of the characteristic curve, obtained by integration of equation (15) is:

$$t = t_o + \frac{1}{q} \left[\left[(x - x_o)\frac{N \cdot q}{\beta} + h_o^N\right]^{\frac{1}{N}} - h_o\right] \qquad (18)$$

When the lateral inflow rate, q, becomes zero, the hydrograph recession is described by the equations:

$$h = h_o \qquad (19)$$

$$x = x_o + \beta h_o^{N-1}(t - t_o) \qquad (20)$$

$$t = t_o + \frac{x - x_o}{\beta} h_o^{1-N} \qquad (21)$$

where x_o, t_o, and h_o are the values of x, t, and h at which the lateral inflow ceases.

The dimensionless velocity of flow on the $k^{\underline{th}}$ plane, as given by the Chézy formula, in terms of the dimensionless depth is:

$$u = h^{N-1} \qquad (22)$$

From equation (22) the dimensionless discharge per foot of width leaving the $k^{\underline{th}}$ plane is obtained as

$$Q = uh = h^N \qquad (23)$$

Equations (17) through (23) can now be used to compute the entire outflow hydrograph arising from known rates of rainfall excess, q, on the $k^{\underline{th}}$ plane.

The problem of hydrograph computation for the $k^{\underline{th}}$ plane is thus completely specified once the initial depths along plane k at time zero and the inflow hydrograph coming from plane $k-1$ are known. The initial and boundary conditions for the cascade are as follows:

$$\text{plane 1:} \quad h_1(x_1, 0) = 0$$

$$h_1(0, t_1) = 0$$

$$\text{plane k:} \quad h_k(x_k, 0) = 0$$

$$h_k(0, t_k) = f(h_{k-1}, t_{k-1}) \qquad (24)$$

That is, all planes in the cascade are considered dry at time $t = 0$; the inflow hydrograph coming from the previous plane in the cascade establishes the flow at the upstream boundary for $t > 0$. No flow enters at the upstream boundary of plane 1. Because of the difference in normalizing quantities used in defining the dimensionless flow variables for each plane, it is necessary to convert the depths and times associated with the inflow hydrograph at the upstream boundary to those of the current plane. The following recursion formulas have been developed for that purpose:

$$\frac{t_k}{t_{k-1}} = \frac{k-1}{k} \left[\frac{w_{k-1}}{w_k} \left(1 + \frac{w_k}{\sum_{i=1}^{k-1} w_i}\right)^{\frac{N-1}{N}} \left(\frac{\alpha_k}{\alpha_{k-1}}\right)\right]^{1/N} \qquad (25)$$

$$\frac{h_k}{h_{k-1}} = \left[\frac{\sum_{i=1}^{k-1} w_i}{\sum_{i=1}^{k} w_i}\right]^{1/N} \qquad (26)$$

where t_{k-1} and h_{k-1} are time and depth at the downstream boundary of plane k-1, and t_k and h_k are the corresponding time and depth at the upstream boundary of plane k . The use of these relationships allows all computations to be done in dimensionless quantities with a general program for plane k.

The dimensionless equations for a cascade of wide rectangular channels are analogous to those for planes and so will not be reproduced here.

Chapter III

KINEMATIC SHOCK-WAVE FORMATION

Several dimensionless rising hydrographs were computed for various two-plane cascades to obtain estimates of the influence of the parameters α (Chézy slope-roughness coefficient) and w (width of plane) on the outflow hydrograph. However, it soon became clear from the hydrograph computations that shock-wave formation occurred for certain α and w combinations and that these shock waves had a profound influence on the properties of the hydrograph. The discussion of this chapter is thus directed at the properties of shock waves in kinematic flow.

A shock wave is represented by the intersections of characteristics in the x - t plane and produces an abrupt increase in flow depth. The surge causes successive wavelets to travel with greater celerity so that earlier wavelets are eventually overtaken and a shock wave, representing the coalescence of wavelets, is formed. Since the discharge-depth relation at the point of intersection of two characteristics is no longer valid, it is necessary to terminate the characteristics at the intersection and fit in the path of the shock. The path of the shock wave in the x - t plane will be given by the locus of the intersection of pairs of characteristics. There are two main objectives in this section: (1) to establish when shock waves will form in terms of the α and w ratios between two successive planes in the cascade; and (2) to devise a technique for tracing the path of a shock wave in the x - t plane and determining the time at which it intersects the downstream boundary of a given plane.

The solution domains are shown for planes k and $k-1$ in Figure 2. The domain enclosed by the line $t = 0$, the downstream boundary and the characteristic originating at $t = 0$ at the upper boundary of the plane is indicated by the letter A. Within this zone the solution depends only on the initial conditions at $t = 0$ for that plane. If the initial conditions are uniform and the overland slope parameters are constant for each plane, characteristics originating along the x-axis at $t_k = 0$ cannot intersect. This is seen from the fact that in order for an intersection to occur, the slopes of the characteristics must bear the following relation at the point of intersection:

$$\left.\frac{dx}{dt}\right|_{\substack{\text{along upper}\\ \text{characteristic}}} > \left.\frac{dx}{dt}\right|_{\substack{\text{along lower}\\ \text{characteristic}}} \qquad (27)$$

Since $\frac{dx}{dt} = \beta h^{N-1}$ and $h = q_k t_k$ in domain A for plane k, the slope $\frac{dt}{dx}$ is constant at any given time t and hence the inequality in equation (27) can never be satisfied in this zone. It follows that a shock can never originate in domain A, although characteristics originating along the upstream boundary may intersect those in domain A. This argument holds for the case of changing q_k, the lateral inflow rate for plane k, since at a given time coordinate q_k will be a known constant and

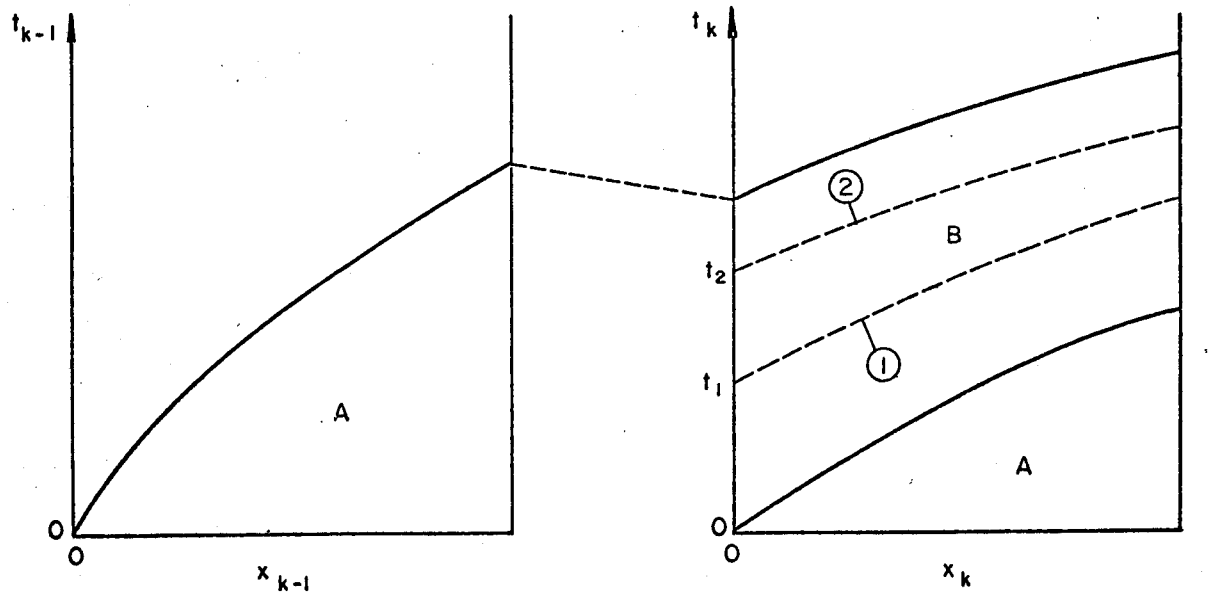

Figure 2. Solution domain for planes k and $k-1$.

hence the slope $\frac{dt}{dx}$ at that point in time is also a constant for all characteristics in A . It is concluded from this argument that a shock wave can never form on the uppermost plane in the cascade for initially dry conditions.

In the domain labeled B in Figure 2, the solution depends upon the upstream boundary condition of plane k which in turn is affected by the initial conditions for plane k - 1 . The necessary condition for an interesection of the characteristics 1 and 2 is:

$$\left.\frac{dx}{dt}\right|_2 > \left.\frac{dx}{dt}\right|_1 \qquad (28)$$

where the derivatives are the inverse slopes of the characteristics originating at t_2 and t_1 , respectively. From equations (15) and (25) we obtain the condition at the intersection

$$\beta h_2(x,t)^{N-1} > \beta h_1(x,t)^{N-1}$$

or

$$h_2(x,t) > h_1(x,t) \qquad (29)$$

By integrating the characteristic equations we obtain

$$\left.\begin{aligned} h_2(x,t) &= h_2 + q_k(t-t_2) \\ h_1(x,t) &= h_1 + q_k(t-t_1) \end{aligned}\right\} \qquad (30)$$

where h_1 , and h_2 are the depths of flow at times t_1 , and t_2 , respectively. Substituting equation (30) into inequality (29) leads to:

$$h_2 - h_1 > q_k(t_2 - t_1) \qquad (31)$$

For uniform stepped lateral inflow the depth in zone A for plane k-1 is:

$$h_{k-1} = q_{k-1}\, t_{k-1} \qquad (32)$$

By converting t_{k-1} and h_{k-1} to t_k and h_k using equations (25) and (26) and substituting these relationships into inequality (31), we obtain the following after algebraic manipulation:

$$\frac{w_{k-1}}{w_k}\,\frac{\alpha_{k-1}}{\alpha_k} = P_s > 1 \qquad (33)$$

Equation (33) defines the shock parameter, P_s , and establishes that shock formation will occur on plane k whenever P_s exceeds unity for the condition of a spatially uniform stepped time-distribution of rainfall excess. Note that while equation (33) is valid for time varying lateral inflow, it does not hold when the inflow changes with distance.

Hence, the inequality of (33) is the general shock-wave criterion, denoted by P_s , for zone B of any plane k . If it is satisfied, then an intersection of any characteristic emanating from the upstream boundary in zone B and a characteristic originating along (x,o) occurs somewhere in the (extended) x - t plane, though not necessarily within the boundaries of the $k^{\underline{th}}$ plane for a sufficiently small interval, $t_2 - t_1$, on the t_k axis. It has been shown that for initially dry conditions and a time-varying, spatially uniform rainfall excess, shock waves cannot originate in zone A of any plane, including plane k = 1 . However, shocks originating in other regions can be propagated into zone A . Further, it is clear that zone B is the critical one from the standpoint of shock-wave formation and propagation in other planes of the cascade. Sequential application of the general rule stated in equation (33) to the k - 2 preceding planes permits one to determine the number of shocks crossing the $k^{\underline{th}}$ plane in the cascade.

Shock-Wave Propagation - Tracing the Shock Path

In an early paper dealing with kinematic flood waves, Lighthill and Whitham (op. cit.) outlined a technique for obtaining the path of a shock wave in the x - t domain. Their semigraphical method is based on continuity of flow and the rate at which flow passes a kinematic wavelet having a given velocity. The procedure described in this chapter is based on the geometry of characteristics which intersect on the shock path and the continuity of flow across the shock front. Figure 3 shows the general features of a shock-wave path as defined by the locus of successive pairs of intersecting characteristics. In particular, two intersecting characteristics, labeled A and B , originate at x_i , t_i , and x_u , t_u , respectively, and carry initial depths h_i and h_u at those points. The space-time coordinates at the point of intersection are x_s and t_s , respectively, as shown for the characteristics labeled A and B in Figure 3.

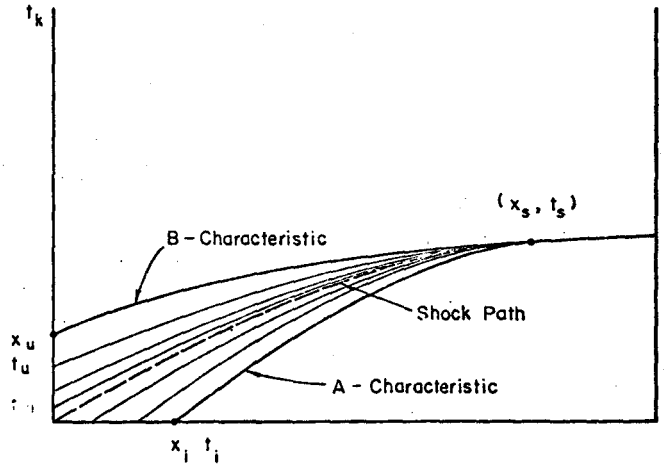

Figure 3. Shock-wave path given by locus of intersecting characteristics.

From the equations for the characteristic ground curves, the following system of equations can be developed for the A and B characteristics:

The B characteristic is defined by:

$$t_b = t_u + \frac{1}{q}\left[\left[(x_b - x_u)\frac{N \cdot q}{\beta} + h_u^N\right]^{1/N} - h_u\right] \quad (34)$$

where x_b and t_b are coordinates along the B-characteristic curve; N and β are parameters defined previously; q is the rate of lateral inflow; t_u and h_u are the initial values of time and depth, respectively, for the B characteristic.

The A characteristic is defined by:

$$t_a = t_i + \frac{1}{q}\left[\left[(x_a - x_i)\frac{N \cdot q}{\beta} + h_i^N\right]^{1/N} - h_i\right] \quad (35)$$

Equations (34) and (35) along with an expression for the local velocity of the shock wave

$$V_s = \frac{\beta}{N}\frac{h_b^N - h_a^N}{h_b - h_a} \quad (36)$$

are sufficient to obtain the shock path by a numerical procedure.

Iterative Scheme for Locating the Shock Path

The procedure is as follows. The x axis is divided in increments Δ_s as shown in Figure 4. The shock path originates at the point (0,0) and its velocity is first approximated by expression (36). The time of arrival of the shock at s_2 can then be obtained and equations (34) and (35) can be solved for t_u and x_i. The depths h_b and h_a at s_2 can then be computed and are substituted back into the expression for shock velocity. This iterative procedure is continued until t_2 is stabilized at s_2. Then the shock path is projected to the next coordinate s_3 by using the stabilized flow depths at s_2 in equation (36) and the process is repeated. This procedure is terminated when the downstream boundary is reached. The discharges Q_a and Q_b existing on the shock path at the time of its arrival at the downstream boundary are then inserted in the outflow hydrograph. When all shock paths traversing the $k^{\underline{th}}$ plane have been projected to the downstream boundary, the values of x_i and t_u (or t_i and t_u), corresponding to the intersection at this boundary of each shock path, can be used in filling with characteristics that portion of the x - t plane unaffected by shock-wave propagation. A complete outflow hydrograph, showing the effects of shock formation, can thus be obtained.

Shock-Path Intersections

If a first-order or simple shock wave is defined as the locus of intersecting A and B characteristics, then second-order shocks would be those resulting from the convergence and intersection of adjacent shock paths. While higher order shock waves could conceivably be produced by the mathematical model representing the cascade, attention is focused on the simple or first-order case.

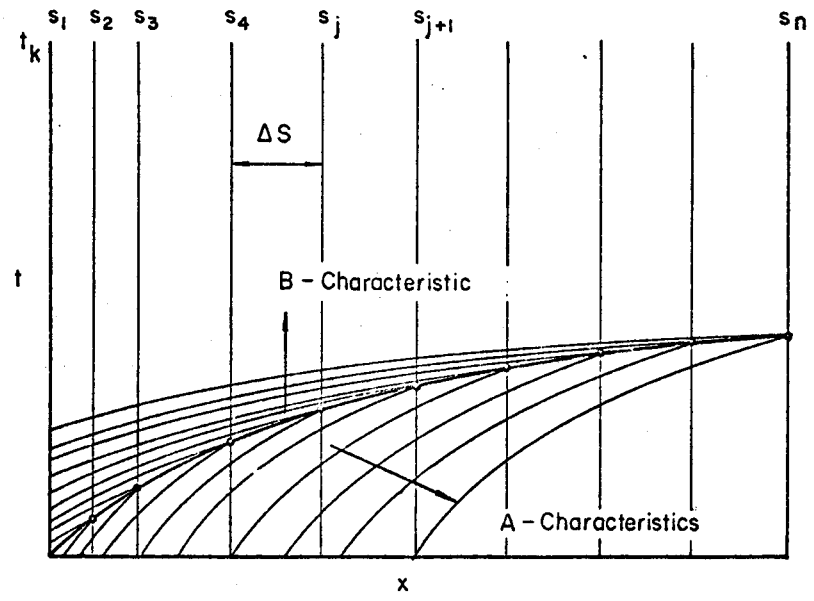

Figure 4. Scheme for describing complete locus of shock-path by use of Δs increments.

Chapter IV

RESULTS OF KINEMATIC SHOCK FORMATION

Tracing the Shock Path

To illustrate certain aspects of the method described in the last chapter, a three-plane kinematic cascade was defined in such a way that shock formation occurred at the origins of planes 2 and 3. The uniform lateral inflow was a pulse of rainfall excess having intensity 0.75 in./hr. and duration 30 minutes. The planes described below are listed in order of highest elevation. All three planes are equal with respect to length, width, and roughness. Only the overland slope is different as indicated by variations in the α parameter.

Table 1. Description of Three-plane Cascade

Plane No.	$\alpha = C\sqrt{S_o}$	Length-ft.	Width-ft.	P_s
1	10.0	400	400	-
2	5.0	400	400	2.0
3	2.5	400	400	2.0

The shock paths crossing planes 2 and 3 are presented in Figure 5. The shock-path computations, involving integrations along the intersecting characteristics, were carried out by means of the dimensionless kinematic flow equations. Only those characteristics which intersect on the shock path at the downstream boundaries of planes 2 and 3 are shown.

Several features of the shock paths presented in Figure 5 are noteworthy. The first is that shock 2-A travels faster than either shock 3-B (a continuation of shock 2-A) or 3-A even though the shock-parameter, P_s, is equal on both planes. This indicates the dependence of absolute shock speed on the overland slope of plane 3, since (assuming constant roughness) the slope of plane 2 is four times that of plane 3. The apparent discontinuity in shock path 2-A is thus attributed to a sudden decrease in velocity upon the shock's arrival at the upstream boundary of plane 3.

Another interesting aspect of the shock paths illustrated in Figure 5 is the constant velocity of propagation achieved over the lower portions of each plane. This can be observed from the linearity of shock 3-B over the entire length of plane 3. Such a

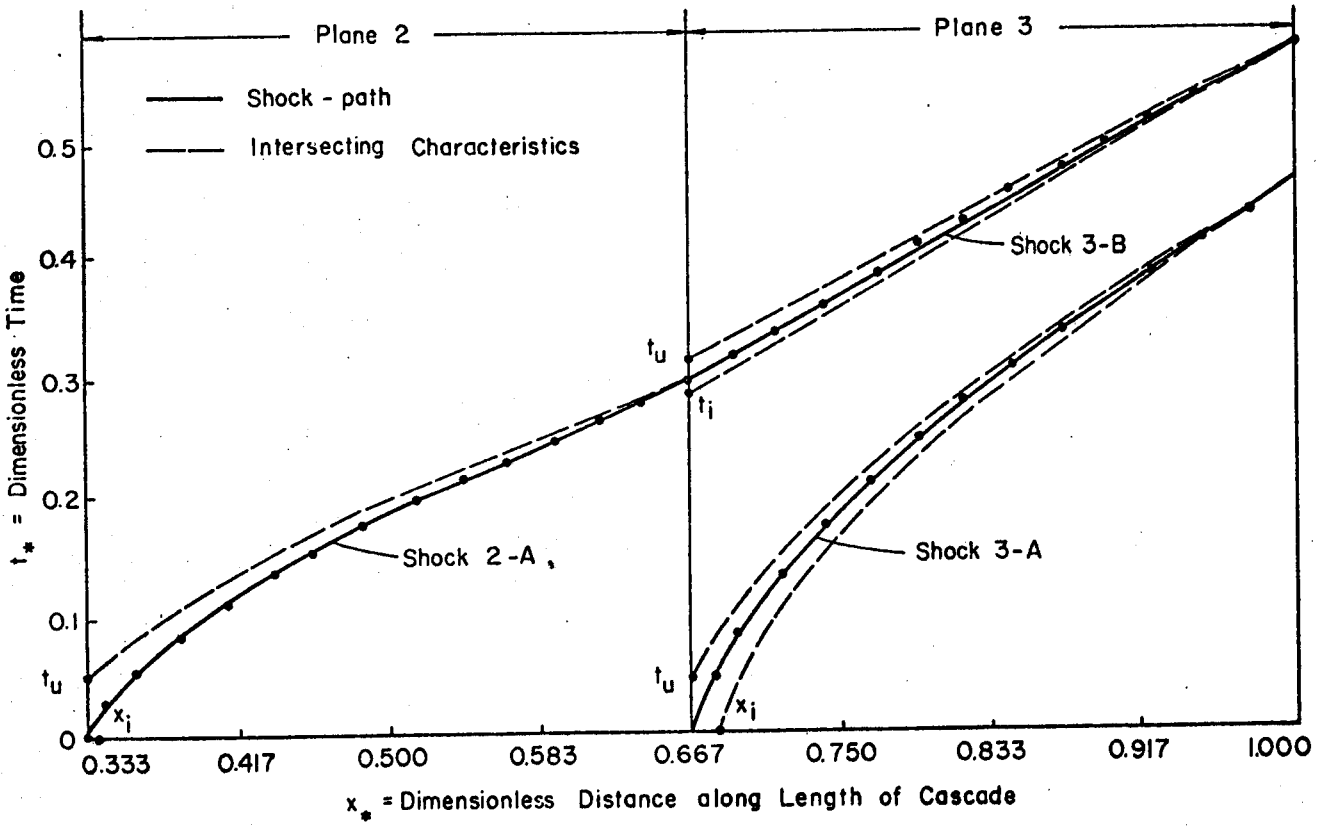

Figure 5. Shock-paths on planes 2 and 3 for the cascade of Table 1.

condition, once detected, could be used to project the shock path across greater distances and thereby increase the speed of the iterative procedure described in the last section.

The outflow hydrograph for plane 3, showing the surges in discharge associated with shocks 3-A and 3-B, is presented in Figure 6. The outflow hydrograph obtained when shocks 3-A and 3-B are ignored is shown for purposes of comparison by means of a dashed line in Figure 6. This hydrograph was obtained by eliminating from the computations those characteristics passing through disturbed regions of the $x_* - t_*$ plane created by the shock. It therefore represents an approximate solution over the two intervals, shown in Figure 6, which are affected by the arrival of kinematic shock waves.

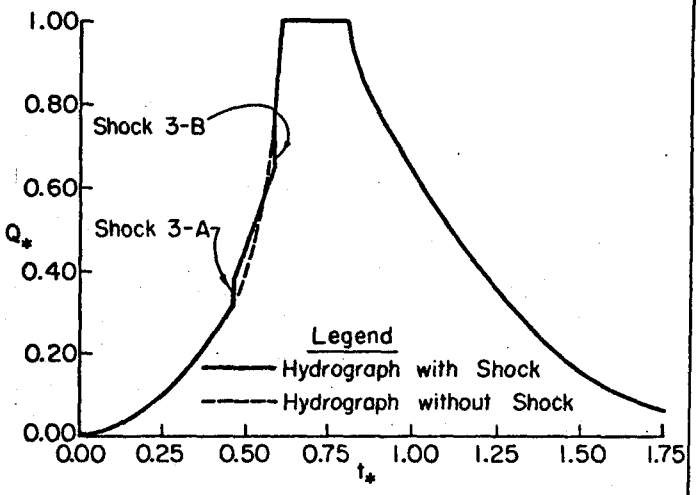

Figure 6. Dimensionless hydrograph for cascade of Table 1 showing effect of 2 shocks on plane 3.

Shock Paths for Various 2-plane Cascades

In order to examine the effect of the shock parameter, P_s, on the shock path, a number of 2-plane cascades were defined as indicated in Table 2. The lengths and widths of the upper planes were held constant while the slopes, as represented by the α parameter, were varied between the limits: $1.25 < \alpha < 10.0$. The lower plane was maintained at a constant length, width and slope for all cascades. The Chézy C factor was assumed constant for all planes. The resulting ratios of overland slopes for the upper and lower planes in each cascade are also listed in Table 2. Lateral inflow was given as a uniform pulse having intensity 0.75 in./hr. and duration 30 minutes.

The family of shock paths observed on plane 2 of the cascades described in Table 2 is presented in Figure 7. The influence of the shock parameter, P_s, is clearly evident from the decreasing passage time of shocks associated with high P_s values. This result indicates the dependence of shock velocity on P_s when the slope of the lower plane is held constant.

The same shocks would occur if the slopes for each plane were the same but if the Chézy C were varied so that α remained as shown in Table 2.

Table 2. Description of upper and lower planes in 2-plane cascades.

Cascade No.	α-slope	Length ft.	Width ft.	P_s	S_1/S_2
(upper planes)					
1	1.25	100	400	1.25	1.56
2	1.50	100	400	1.50	2.25
3	1.75	100	400	1.75	3.06
4	2.00	100	400	2.00	4.00
5	2.50	100	400	2.50	6.25
6	3.00	100	400	3.00	9.00
7	4.00	100	400	4.00	16.00
8	5.00	100	400	5.00	25.00
9	6.00	100	400	6.00	36.00
10	7.00	100	400	7.00	49.00
11	8.00	100	400	8.00	64.00
12	9.00	100	400	9.00	81.00
13	10.00	100	400	10.00	100.00
(lower planes)	1.00	100	400	-	-

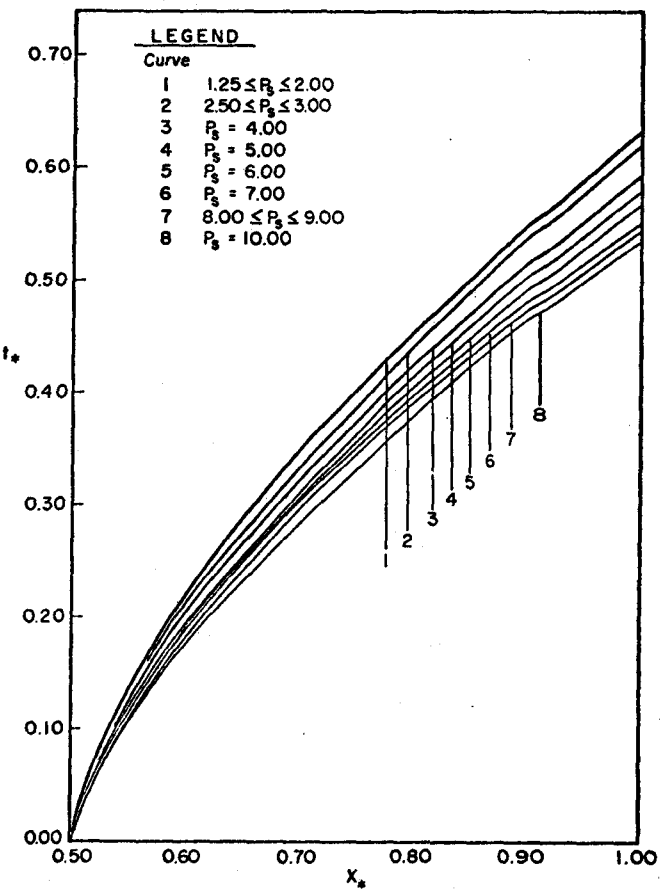

Figure 7. Shock-paths in dimensionless $x_* - t_*$ plane for various P_s values and cascades of Table 2.

In order to more fully investigate the effect of changing P_s on the shock path, another series of 2-plane cascades was defined. According to this definition, the upper plane was held constant with $\alpha = 10.0$, length = 400 feet, and width = 400 feet. The lengths and widths of each lower plane were set at 400 feet, while the overland slope was varied in the range $1.00 < \alpha < 8.00$. The shock parameter was thus given values over the interval $1.25 < P_s < 10.00$ as in the previous set of cascades.

The resulting shock paths possessed the general features presented in Figure 7, except that they varied with P_s in reverse order. That is, the shock paths associated with higher values of P_s arrived at the downstream boundary of plane 2 later than those having a smaller value of P_s. This inverted relation between P_s and time of arrival is a result of the shock traveling across an overland plane of small slope compared with the second plane having the same P_s in the previous set of cascades described in Table 2.

Outflow Hydrographs for Various 2-plane Cascades

The outflow hydrographs observed at the downstream boundary of the second plane for the cascades of Table 2 are presented in Figure 8. It is observed that the hydrographs for all cascades coincide over the regions that are outside the influence of the shock front. The effect of P_s is evident from the varying position of the vertical portion of the rising limb representing the surge in flow created by shock formation. Previous results have shown that both the strength and velocity of the shock will increase directly as P_s for the cascades of Table 2. This relationship is clearly observable in the outflow hydrographs of Figure 8.

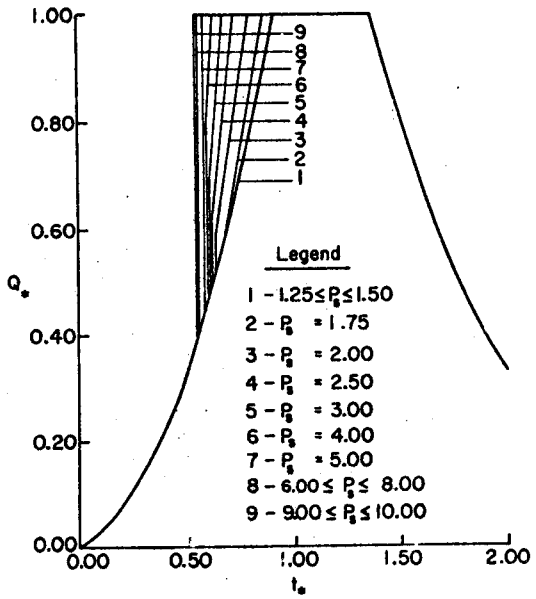

Figure 8. Dimensionless outflow hydrographs for various P_s values and cascades of Table 2.

The dimensionless shock paths and rising hydrographs presented in Figures 7 and 8, respectively, are perfectly general for cascades of 2 planes, having equal lengths, widths, and roughness, in which the lower plane is fixed with respect to overland slope. The equilibrium and recession portions will vary according to the equilibrium time of the lower plane, which in turn is a function of the length, width, and slope of both planes. Since the discussion of this section has centered on the effect of shocks on the rising limb, further dimensionless results are not presented.

Kinematic Shocks in Partial Equilibrium Hydrographs

When lateral inflow ceases before steady-state conditions are established, outflow from the lower plane peaks at a rate less than that of the lateral inflow pulse. Because characteristics become straight lines and carry constant depths after lateral inflow ceases, it is anticipated that the depths across the shock and consequently the shock path itself will differ from the full equilibrium case.

In order to determine the effect of shock formation on partial equilibrium hydrographs, the 3-plane cascade of Table 1 was run for a lateral inflow pulse of intensity 0.75 in./hr. and durations 15, 20 and 25 minutes. Since the 3-plane cascade reaches equilibrium in approximately 22 minutes for this lateral inflow rate, the first two cases will produce partial equilibrium hydrographs while the third will produce full equilibrium.

The resulting 3-plane hydrographs are shown in Figure 9 in which shocks A and B are indicated by heavy vertical lines. Several features of Figure 9 are of interest. The first is that, although the depths across shocks A and B decrease with decreasing pulse length, the speed of each shock remains approximately constant. Hence the shock path is not significantly affected by cessation of lateral inflow.

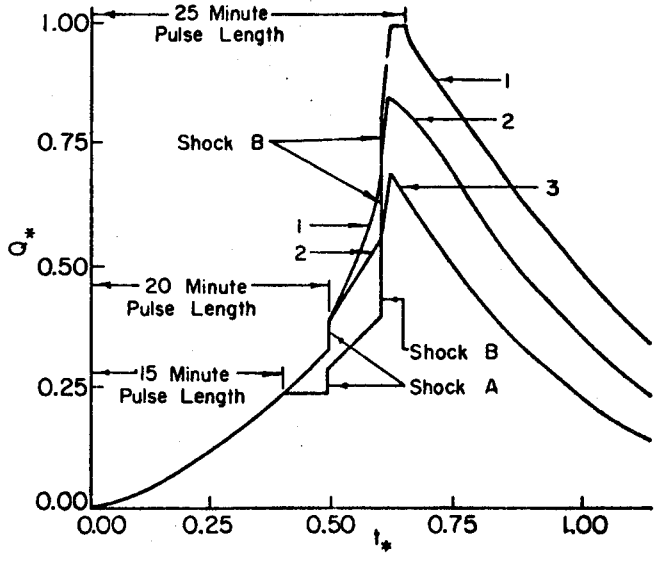

Figure 9. Dimensionless partial equilibrium hydrographs for the 3-plane cascade of Table 1 with 2 shocks on plane 3.

A simple computation reveals that the shock strength, as measured by the ratio h_B/h_A, is roughly constant for shock A and shock B occurring in the hydrograph of Figure 9. This result is in agreement with the motion of a shock wave whose speed is independent of lateral inflow cessation.

Another interesting aspect of Figure 9 is that portion of the hydrograph which connects the two shocks. It is evident that this connecting portion becomes flatter as the pulse duration is decreased. If the pattern observed in hydrograph 3 were continued, it is expected that eventually the linkage between successive shocks would become horizontal. The resulting partial equilibrium hydrograph would then exhibit a stair-step structure in the region affected by the arrival of successive shock waves. This feature, observed in hydrograph 3, is a consequence of shocks arriving at the downstream boundary after lateral inflow has stopped.

Iwagaki (1955) performed some laboratory experiments involving unsteady, open-channel flow with lateral inflow. One set of experiments was run in a flume 24 meters long, where the uppermost 8-meter section had a slope of 0.020, the middle section slope was 0.015 and the lower section slope was 0.010. Under conditions of uniform lateral inflow the kinematic model would predict three shocks. Iwagaki, however, adjusted the lateral inflow supply so that the middle section had a lower rate of lateral inflow than the upper and lower section. The hydrographs he obtained are reproduced in Figure 10. These hydrographs can be qualitatively compared with the partial equilibrium hydrographs in Figure 9. Obviously the physical manifestation of a kinematic shock is a rapid rise in the outflow rate as the shock reaches the downstream boundary. Furthermore, it appears that the kinematic representation of a shock will lead to errors in a very small region of the outflow hydrograph.

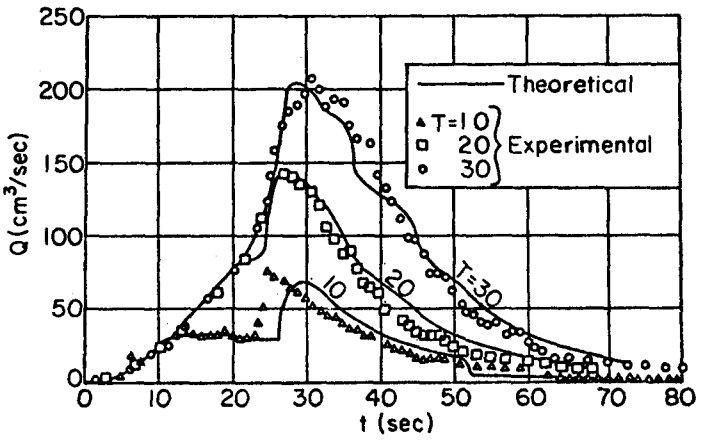

Figure 10. Theoretical and experimental overland flow hydrographs showing physical manifestation of kinematic shock waves (after Iwagaki, 1955).

Difference Solutions to the Kinematic Equation Using Rectangular Grids

In investigating the properties of the kinematic cascade it seemed desirable to use the method of characteristics and a characteristic net to minimize errors. The possibility of large discontinuities in the solution at kinematic shock waves also seemed an important consideration in the choice of a numerical method. For practical cases, however, rectangular grid schemes are much easier to work with. Accordingly, we compared solutions from three rectangular grid schemes with solutions obtained by the method of characteristics. The three rectangular grid methods used were: (1) the upstream differencing method; (2) the single-step Lax-Wendroff scheme (Houghton and Kasahara, 1968) and (3) the four-point implicit scheme used by Brakensiek (1967a). The finite difference formulation, the order of approximation and the linear stability criterion for each of these schemes is shown in Table 3. The derivation of the single-step Lax-Wendroff method and stability calculations for the three methods are included in the Appendix. For a definition sketch of the notation in Table 3, see Figure 11.

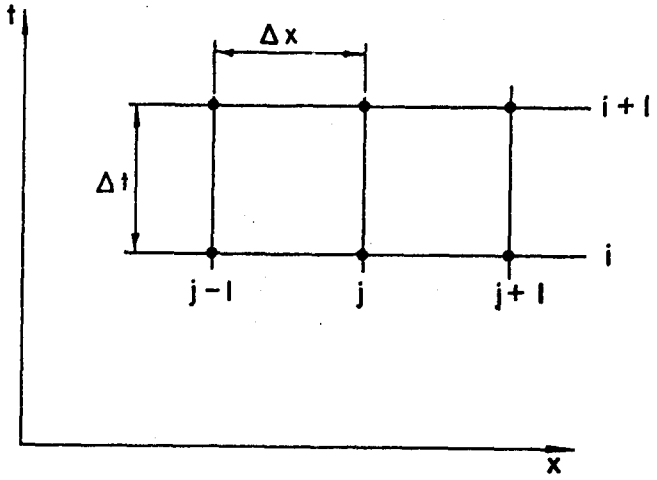

Figure 11. Notation for finite-difference schemes.

Dimensionless hydrographs computed by the above three methods and by the method of characteristics are shown in Figure 12. The input pulse duration was equal to the time to equilibrium of the 2-plane cascade. The smoothing effect of the rectangular schemes is clearly shown and the second-order Lax-Wendroff method does give the best approximation. In general, the peak response is delayed and reduced by as much as 20% for the first-order schemes. Differences of this magnitude seem to be sufficiently great to warrant further examination.

We have not experienced any instabilities in the difference schemes attributable to the shocks, but this is a possibility. In Brakensiek's method the equation for h_j^{i+1} is nonlinear and must be solved by an iterative procedure. With strong shocks and small Δt increments there was no positive solution for this equation for the first Δx increment on the second plane. However, Brakensiek's method has the important advantage of unconditional stability which may result in more rapid calculations because fewer steps are required. This advantage may be partially or completely offset by the iterative procedure required.

Table 3. Rectangular Grid Finite-Difference Schemes

Method	Finite Difference Equation	Order of Approximation	Linear Stability Criterion
Single-Step Lax-Wendroff	$h_j^{i+1} = h_j^i - \Delta t \frac{k}{n}\left[\frac{\left(h_{j+1}^{iN} - h_{j-1}^{iN}\right)}{2\Delta x} - \frac{1}{2}\left(q_{j+1}^i + q_{j-1}^i\right)\right] + \frac{\Delta t^2}{4n\Delta x}\frac{Nk}{}\left\{\left(h_{j+1}^{iN-1} + h_j^{iN-1}\right)\left[\frac{k}{n}\frac{\left(h_{j+1}^{iN} - h_j^{iN}\right)}{\Delta x} - \frac{1}{2}\left(q_{j+1}^i + q_j^i\right)\right] - \left(h_j^{iN-1} + h_{j-1}^{iN-1}\right)\left[\frac{k}{n}\frac{\left(h_j^{iN} - h_{j-1}^{iN}\right)}{\Delta x} - \frac{1}{2}\left(q_j^i + q_{j-1}^i\right)\right] + \frac{2n\Delta x}{Nk\Delta t}\left(q_j^{i+1} - q_j^i\right)\right\}$	$O(\Delta x)^2$	$\frac{\Delta t}{\Delta x} \le \frac{n}{Nk\bar{h}^{N-1}}$
Upstream Differencing	$h_j^{i+1} = h_j^i - \frac{Nk}{n}\frac{\Delta t}{\Delta x}\left(h_j^{iN} - h_{j-1}^{iN}\right) + q_j^i \Delta t$	$O(\Delta x)$	$\frac{\Delta t}{\Delta x} \le \frac{n}{2.75kNh^{N-1}}$
Brakensiek's Four Point Implicit	$\frac{h_j^{i+1} - h_j^i + h_{j-1}^{i+1} - h_j^i}{2\Delta t} + \frac{k}{n\Delta x}\left(h_j^{i+1N} - h_{j-1}^{i+1N}\right) - \frac{1}{4}\left(q_{j-1}^{i+1} + q_j^{i+1} + q_{j-1}^i + q_j^i\right) = 0$	$O(\Delta x)$	Unconditionally stable

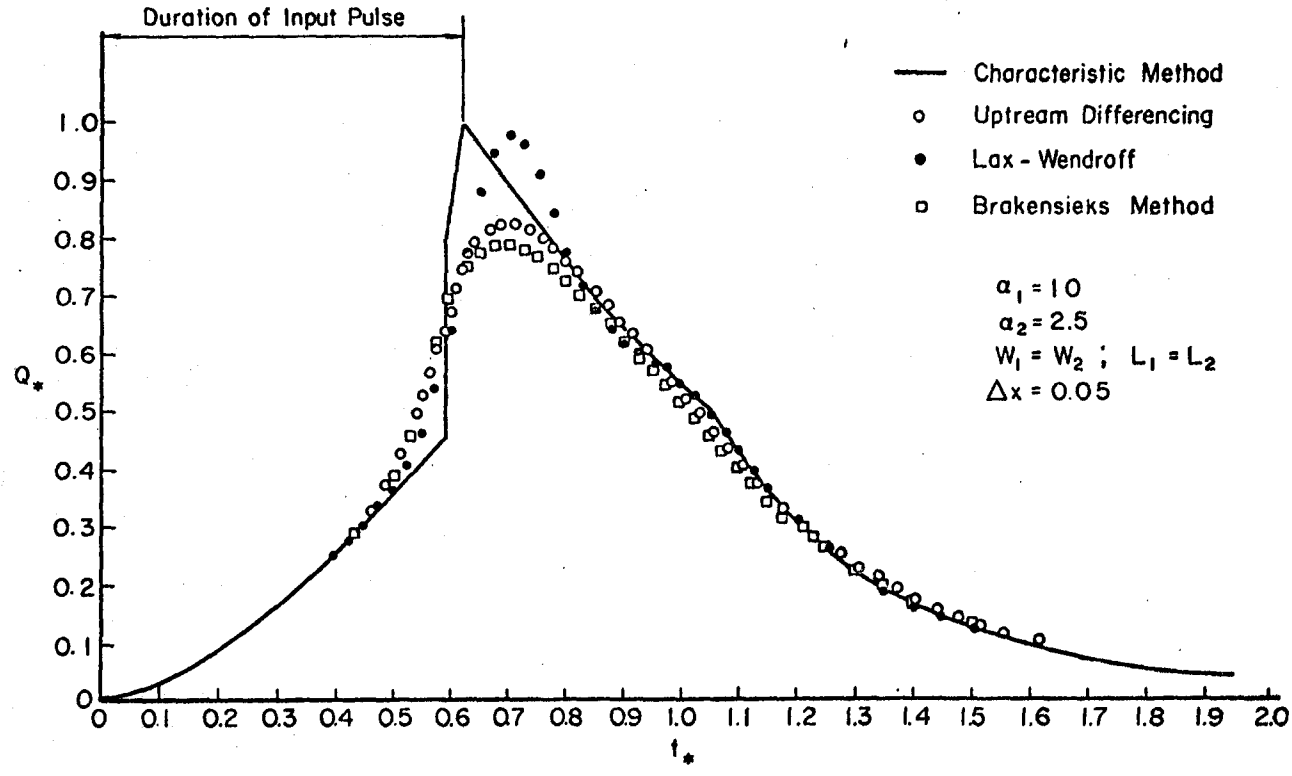

Figure 12. Comparison of finite-difference methods.

Chapter V

APPLICATIONS OF THE KINEMATIC CASCADE TO COMPLEX WATERSHED GEOMETRIES

In any practical application, use of the kinematic cascade to simulate surface runoff from complex watersheds will introduce certain errors of approximation. These errors are associated with the manner in which the cascade is adapted to actual watershed configuration. For example, a converging overland surface will be replaced by a series of rectangular planes with decreasing widths, while a complex continuous overland slope will be represented by a series of discrete planes with individually uniform slopes. It is evident that by making the individual plane lengths small enough (i.e., increasing the number of planes in the cascade) we can minimize the errors of approximation associated with the kinematic cascade transformation.

Comparison with Exact Solutions for a Converging Surface

One test of the kinematic cascade is to determine how well cascade solutions conform to those exact solutions obtained for selected watershed shapes. Woolhiser (1969) has obtained such exact solutions for kinematic flow on a converging surface, as shown in Figure 13. The purpose of this chapter is to compare kinematic cascade solutions with kinematic solutions for overland flow on a converging watershed surface.

For the geometry of the converging section shown in Figure 13, the continuity equation has been written by Veal (1966) as:

$$\frac{\partial h}{\partial t} + \frac{\partial uh}{\partial x} = q + \frac{uh}{(L_o - x)} \qquad (37)$$

The momentum equation is given by the friction relation of equation (3). Woolhiser (1969) has derived the characteristic equation, based on equations (3) and (37), and has put them in dimensionless form. He introduced a parameter r which defines the degree of convergence exhibited by the section--a small value of r indicates high flow convergence, while as r approaches unity, the convergence of flow tends toward that of a plane rectangular surface.

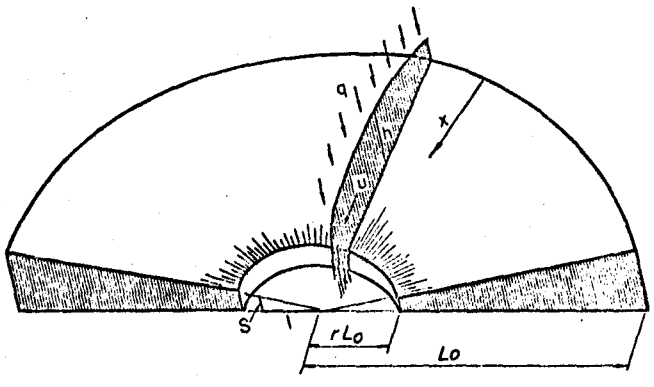

Figure 13. Geometry of converging section.

The test case selected had the following parameters:

L_0 = 100 ft.; r = 0.1 ; Chézy C = 100;

S = 0.05 ; N = 3/2

The rainfall excess was 1 in./hr. applied for 90 seconds.

In approximating the above converging section with a kinematic cascade we have a choice of the total number of planes, defined by n, and the size of the Δx increment for rectangular grid schemes. The total number of grid points in the x-direction is $1/\Delta x + 1$. Hydrographs were computed for cascade configurations ranging from one plane to ten planes of equal length, with a maximum of 21 grid points in the x direction. The width of the $i^{\underline{th}}$ plane of an n-plane cascade was calculated by the following area-preserving relation

$$w_i = \frac{\theta \pi L_0}{360} \cdot \left[2 + \left(\frac{1-r}{n}\right)\left(1-2i\right) \right] \qquad (38)$$

$$i = 1, 2 - - - n$$

where θ is the angle subtended by the converging section.

Hydrograph calculations were carried out by using the second-order Lax-Wendroff scheme for the interior of each plane, while the upstream differencing method was used at the downstream boundary. The results of these computations are shown in Figures 14(a), (b), (c), and (d). The parameter B in Figure 14 is equal to the number of Δx increments in each plane. Therefore, nB is the number of increments in the cascade and is related to the number of computations performed. The information in Figure 14 is summarized in Figure 15 where an error index is shown as a function of nB, with n as a parameter. The error index is defined as the sum of the difference between the characteristic-analytic solution and the finite difference solution at the time to equilibrium and at the time that lateral inflow ceases. This is admittedly a rather crude index and it is not recommended for general use. However, it is adequate for this special case.

An examination of Figures 14 and 15 shows that the error index decreases as nB increases for any n, but that very little accuracy is gained by increasing nB from 15 to 20. The error index decreases as n goes from 1 to 3, but for this case there appears to be a decrease in accuracy as n is increased from 3 to 4. This probably occurs because as the number of planes is increased, the first-order differencing scheme for the lower boundary is used

more frequently and eventually decreases the overall accuracy of this solution. Shocks present in the cascade solutions have been smoothed by the finite-differending method used to obtain outflow hydrographs. Although this is by no means an exhaustive test, it appears that the kinematic cascade is very effective in handling lateral convergence and that three planes with Δx increments of 0.0667 L_o will give satisfactory results for linearly converging flow with r = 0.10.

Effect of Changing Overland Slope on Cascade Hydrographs

A second set of computations was performed to examine the effect of varying overland slopes on hydrograph shape. The slopes of each 3-plane cascade are shown in Table 4.

Table 4. Cascade Slopes

Run No.	Slope of Plane		
	S_1	S_2	S_3
1	.0197	.05	.08
2	.08	.05	.0197
3	.025	.10	.025
4	.065	.02	.065
5	.05	.05	.05

Each plane of the 3-plane cascades was 36.67 ft. long, 1 foot wide, and has a Chézy coefficient C = 100. The total relief for each cascade was 5.5 ft. A rainfall excess of 1.00 in./hr. was applied for 100 seconds which is the time of equilibrium of a single plane 110 ft. long with 5 percent slope.

The results of the computations are shown in Figure 16. The general shape of the rising hydrograph is the same as the shape of the overland slope. The time to peak is not greatly affected by the shape of the overland-slope profile for this near-equilibrium situation, but it would be significantly affected for partial equilibrium cases. There is a maximum difference of 10 percent in the peak rates, with the constant slope cascade having the highest peak and the complex slopes (runs 3 and 4) having the lowest peak rate. The Lax-Wendroff scheme was used for all computations, so the same type of errors as evidenced in Figure 11 are present. Shocks should theoretically occur in cases 2, 3, and 4. The finite-difference scheme smooths these shocks and probably attenuates the peaks. It is apparent from this example that, for surfaces with the same length and relief, shape of the overland-slope profile is a significant factor in determining the shape of the rising hydrograph of outflow from the kinematic cascade.

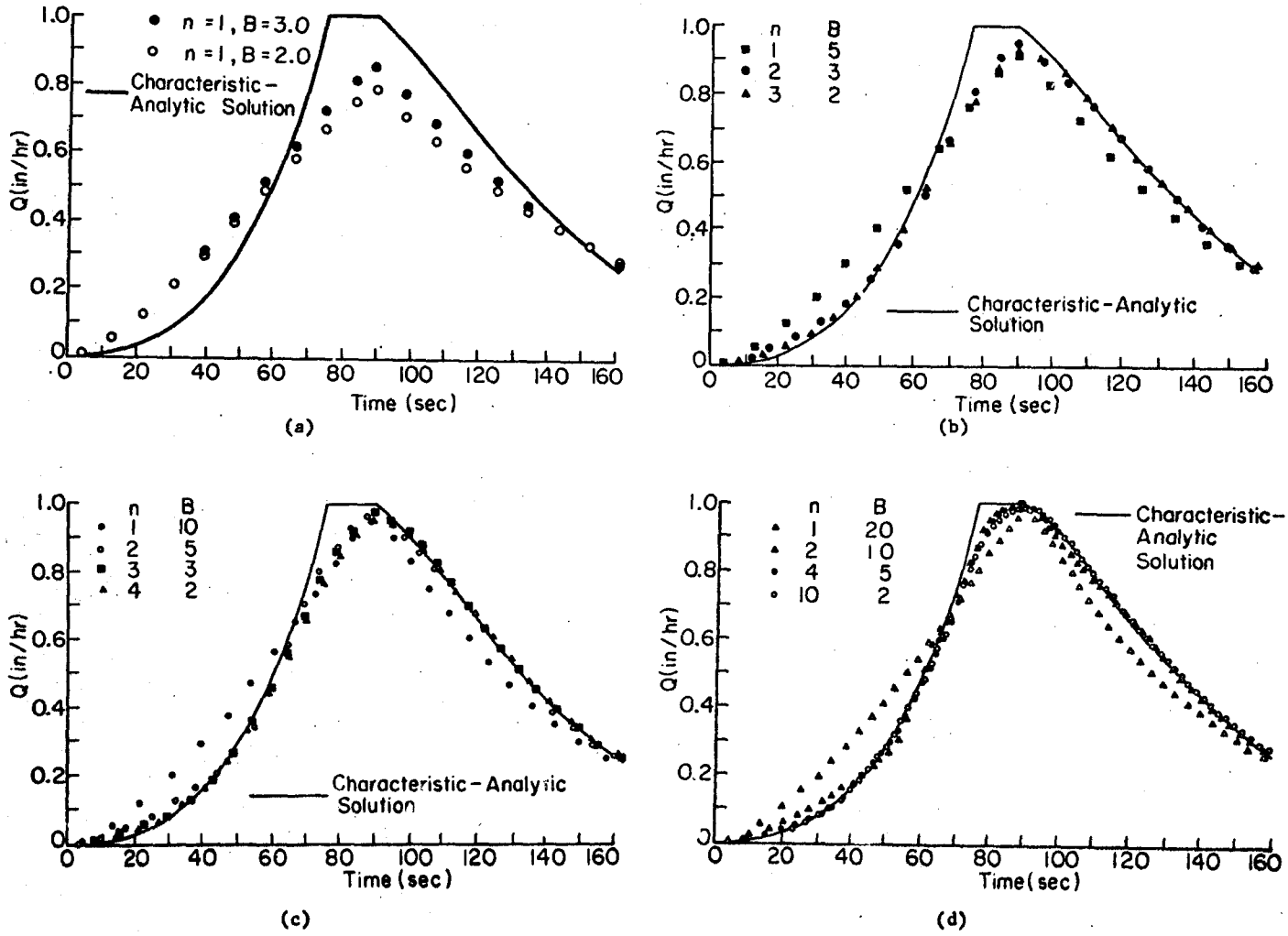

Figure 14. Kinematic cascade results compared with characteristic-analytic solution converging section r = 0.10 L_o = 100

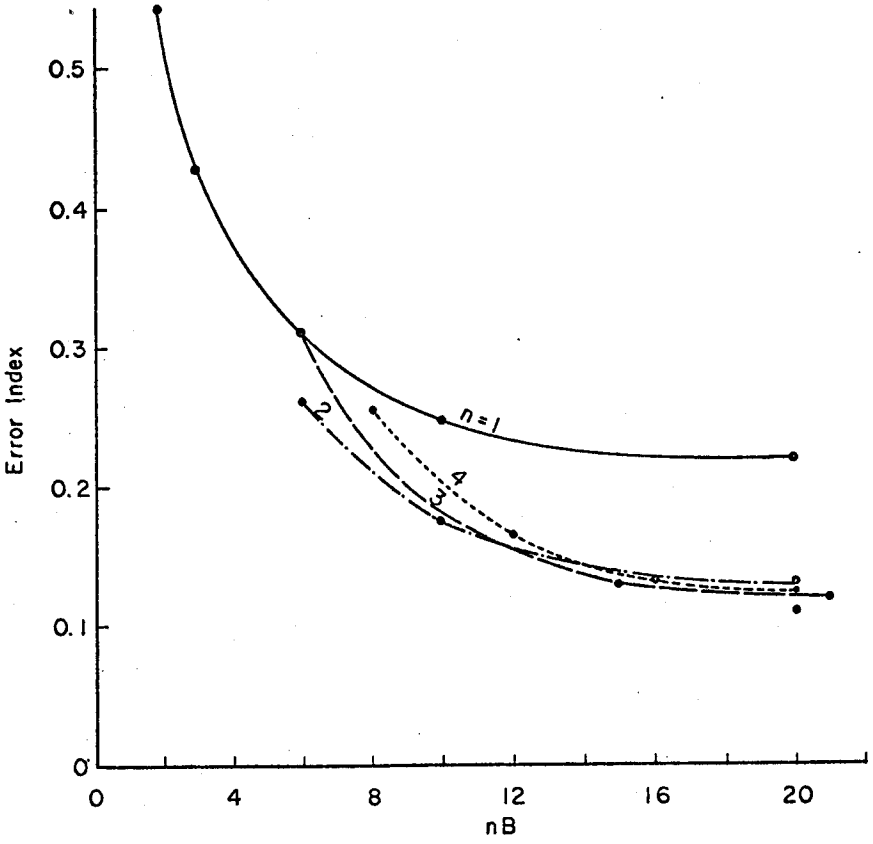

Figure 15. Effect of number of Δx increments on error index.

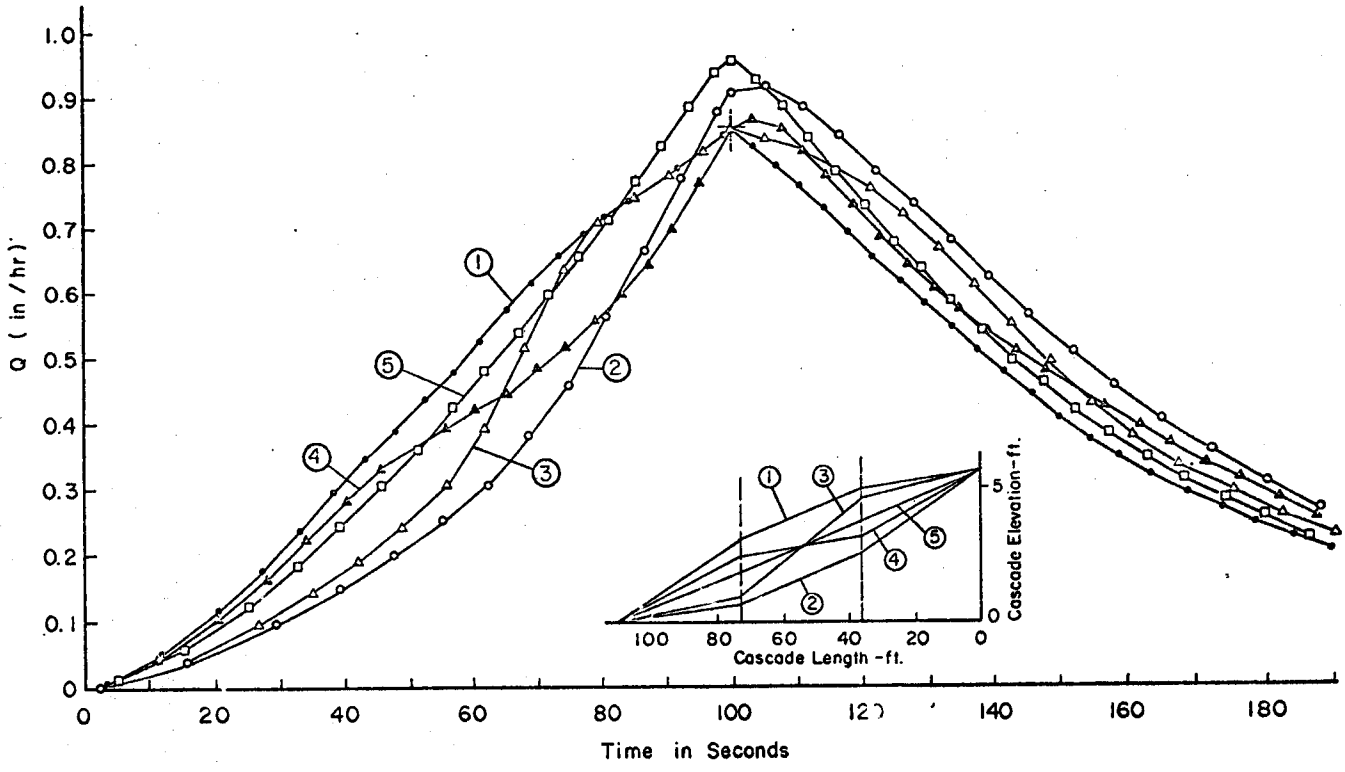

Figure 16. Effect of slope-shape on hydrographs.

Chapter VI

COMPARISON WITH EXPERIMENTAL DATA

Experimental data have been obtained for the case of converging overland flow at the Colorado State University Experimental Rainfall-Runoff Facility (Dickinson, Holland and Smith, 1967). The geometry of the upper basin of the facility is identical to the section of a cone shown in Figure 13. A 120^{o} sector with $L_o = 110$ ft. and $r = 0.0106$ was covered with butyl rubber. Lateral inflow was applied through a grid of sprinklers capable of applying water at four intensities: 0.5, 1.04, 2.39, and 4.22 inches per hour. At the lowest intensity, nozzles are located on the corners of 40-foot equilateral triangles. To obtain the higher intensities, additional nozzles are activated. The rainfall pattern is quite uniform, with coefficients of variation from 18% for 0.5 in./hr. to less than 3% for 4.22 inches per hour.

Runoff rates were measured with a 1.5-ft. H flume equipped with a FW-1 stage recorder that has been modified to attain a complete drum revolution in 30 minutes. Time on the analog chart can be read to 5 seconds.

Experimental runs were performed at each of four intensities. Each run consisted of two parts: an equilibrium run to establish the steady-state input rate, and a partial equilibrium run.

The Chezy C was estimated from the equilibrium run data in the following manner. Woolhiser (1969) presented the following dimensionless equations for recession from equilibrium for flow on a converging surface.

$$Q_* = x_o \frac{\left[2 - (1 - r)\, x_o\right]}{(1+r)} \qquad (39)$$

$$t_*' = \left(\frac{1+r}{r}\right)^{\frac{N-1}{N}} \frac{\left\{\left[1-(1-r)x_o\right]^{\frac{2N-1}{N}} - (r)^{\frac{2N-1}{N}}\right\}}{(2N-1)\,(1-r)\left\{x_o\left[2-(1-r)\,x_o\right]\right\}^{\frac{N-1}{N}}} \qquad (40)$$

Where Q_* is the dimensionless discharge, r is the convergence parameter, x_o is the origin of the characteristic, t_*' is the time after lateral inflow stops until a characteristic originating at x_o, t_o intersects the downstream boundary $x = 1$, and N is the exponent as defined in equation (3). The dimensionless recession hydrograph can be obtained by substituting values of x_o $(0<x_o<1)$ into equations (39) and (40). This hydrograph is shown in Figure 17.

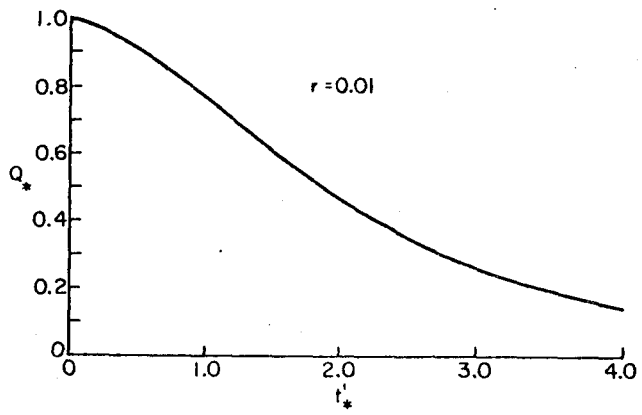

Figure 17. Dimensionless recession hydrograph.

If we assume that the kinematic model with a constant C is adequate for the converging section, we can estimate the normalizing time T_o from the experimental recession from equilibrium and the dimensionless recession curve. On Figure 17 $t_*' = 1$ when $Q_* = 0.76$, $t_*' = 2$ when $Q_* = 0.46$ and $t_*' = 3$ when $Q_* = 0.26$. Let the time after lateral inflow is stopped until the appropriate dimensionless outflow is reached be t_{Q_*}. Then an estimate of T_o is given by

$$T_o = \frac{1}{3}\left[t_{.76} + \frac{1}{2}\,(t_{0.46}) + \frac{1}{3}\,(t_{0.26})\right] \qquad (41)$$

Now T_o is defined as the time required to traverse the distance $L_o(1-r)$ at a velocity of V_o where V_o is the normal steady state velocity at the downstream boundary. From equation (3)

$$V_o = \alpha^{1/N} Q_o^{\frac{N-1}{N}} = \frac{L_o(1-r)}{T_o} \qquad (42)$$

Recalling that $\alpha = C\sqrt{S}$ for the Chezy formulation and $N = 3/2$ we obtain

$$C = \left[\frac{L_o(1-r)}{T_o}\right]^{3/2} \frac{1}{\sqrt{S}\, Q_o} \qquad (43)$$

The converging section was approximated with a five-plane cascade with dimensions as shown in Figure 18. The Lax-Wendroff method was used in the numerical calculations and five partial equilibrium cases were simulated. The characteristic method was also used for comparison. Results of the simulations for two partial equilibrium runs are shown in Figure 19 (a) and (b). In both cases the computed peak rates were higher than the observed peaks, but this was not the general case. In two of the five cases simulated, computed peak rates were less than the observed rate. In general, the observed hydrographs rise more slowly during the initial stages than do the computed hydrographs. Although analysis has not proceeded far enough to explain this discrepancy, it could be accounted for by any one or a combination of the following:

(1) Flow is initially laminar

(2) A stilling-well lag

(3) Interception losses occur so that only part of the area contributes initially.

The timing of the peaks agrees very well and the recession hydrograph is accurately simulated by the kinematic cascade.

Additional analyses of experimental data will be required before definitive conclusions can be reached but it appears that the kinematic cascade adequately simulates linearly converging overland flow over a butyl surface. By induction we might assume that the cascade could simulate more complicated converging flow situations.

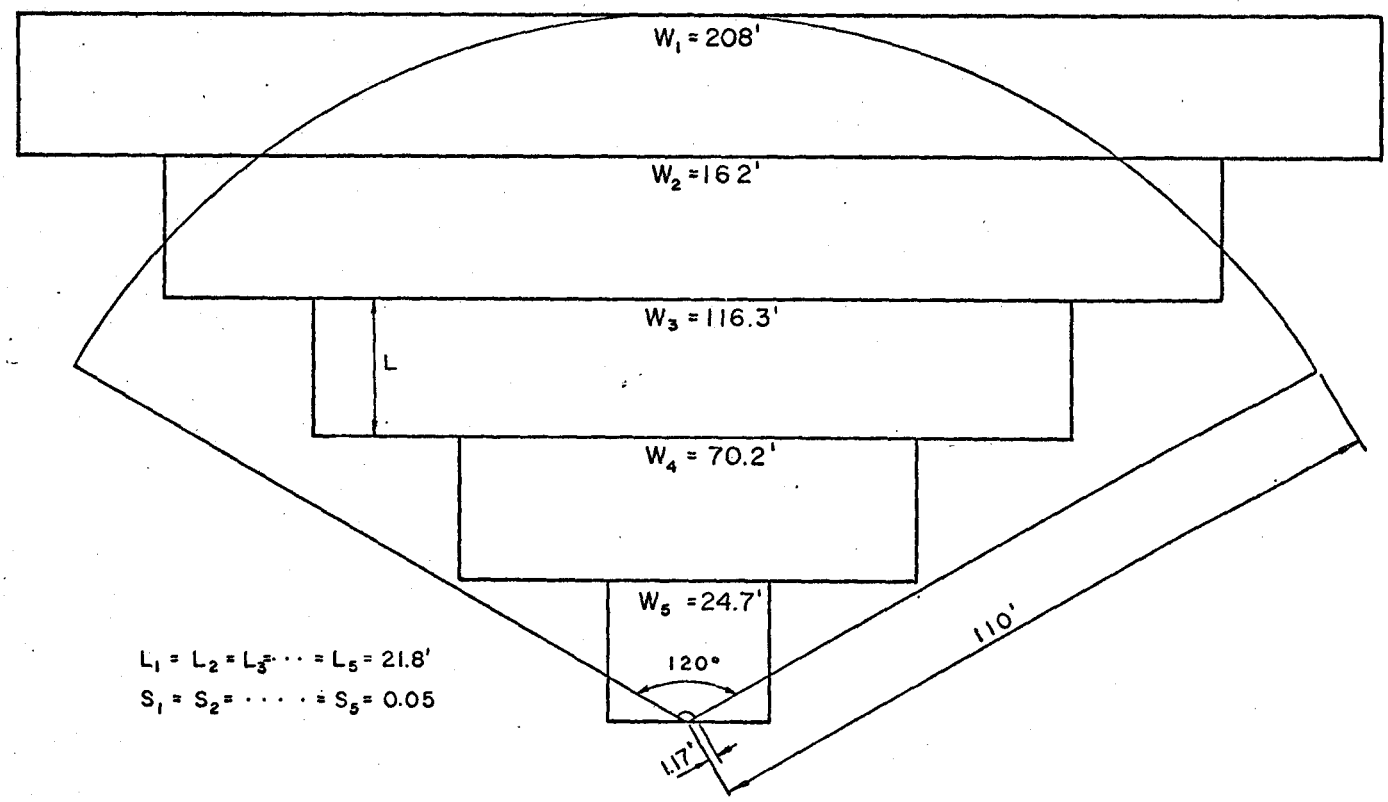

Figure 18. Cascade approximation of converging section.

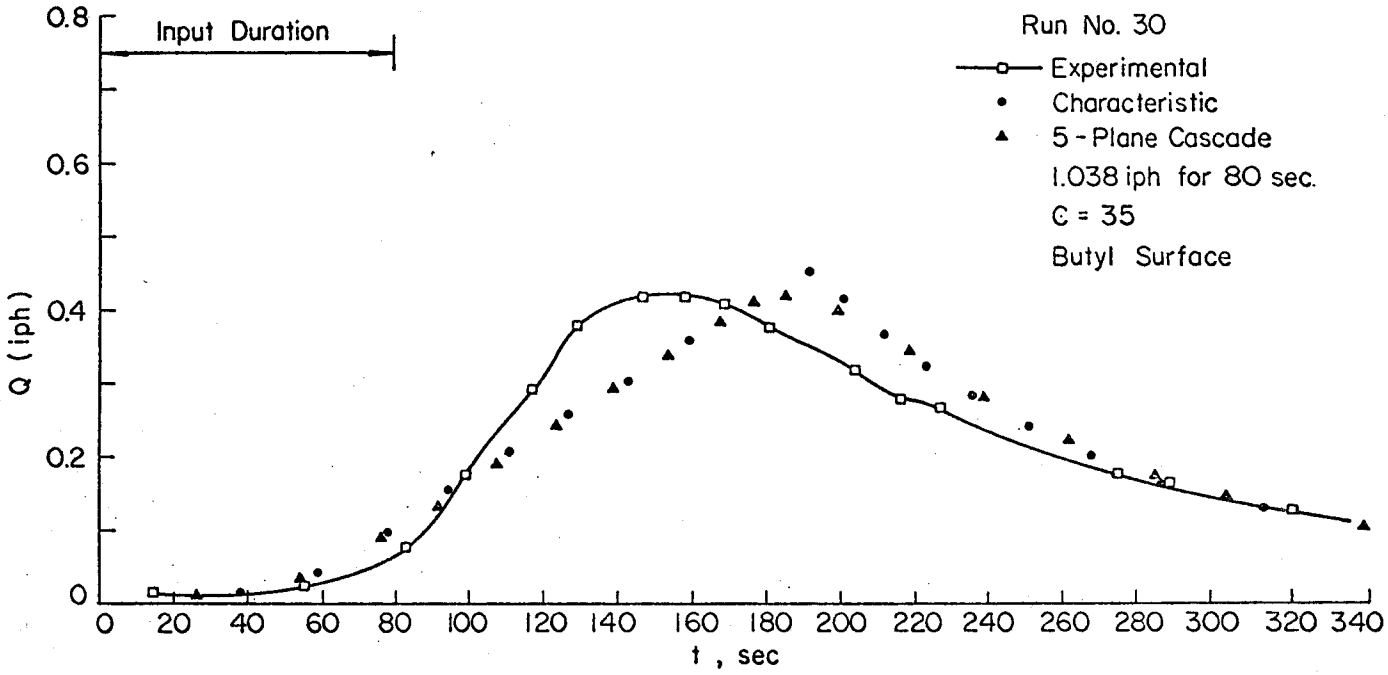

(a)

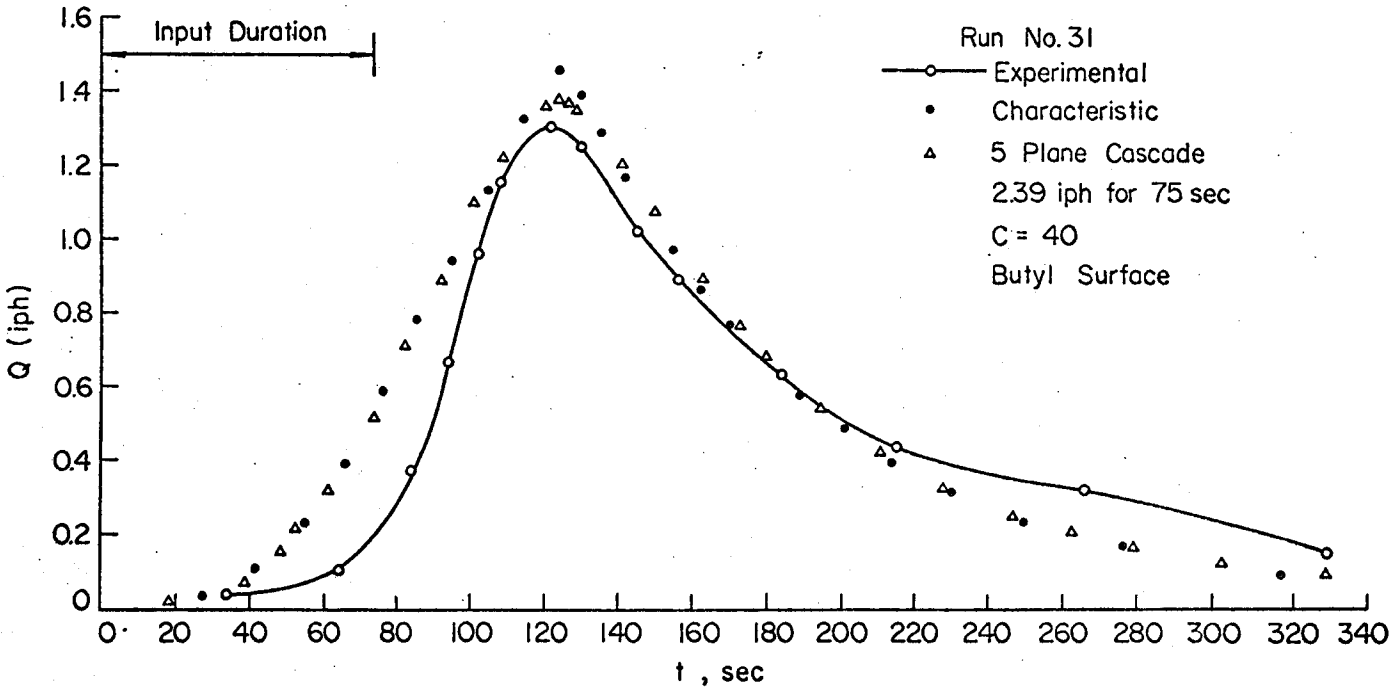

(b)

Figure 19. Comparison of kinematic cascade results with experimental data.

Chapter VII

SUMMARY AND CONCLUSIONS

It was hypothesized that the kinematic cascade is an appropriate mathematical model for describing the dynamic behavior of surface runoff. The mathematical properties of the kinematic cascade were first investigated. Solutions obtained by the method of characteristics were used as standards of comparison in examining other finite-difference schemes. The application of the kinematic cascade to complex watersheds was investigated by comparing cascade solutions to exact solutions and to experimental observations for flow on a linearly converging surface.

The following conclusions may be drawn from this study.

Mathematical Properties of Kinematic Cascade

From the results obtained for both full and partial equilibrium flow conditions, it is evident that the abrupt increase in discharge produced by the shock can be severe, particularly for high P_s values. The results of the 2-plane cascade tests demonstrate that the velocity of the shock, and therefore its path in the x-t plane, is dependent on the parameters P_s and α_2 which are computed from the physical specification for a given plane in the cascade. The shock-parameter, P_s, has been shown to be most closely related to the strength of the shock and therefore influences its celerity or relative velocity. The slope-parameter, α_2, on the other hand, governs the velocity of the flow immediately downstream of the shock. Hence, the absolute propagation speed of the kinematic shock is related to the two interdependent parameters, α_2 and P_s.

While the shock-wave phenomenon may arise under certain highly selective physical circumstances, it is looked upon in this study as a property of the mathematical equations used to explore the overland flow problem rather than as an observable feature of this hydrodynamic process. Nevertheless, the tendencies toward shock formation inherent in the kinematic wave approximation to the shallow-water equations have been ignored in recent investigations using this approach.

Solutions of the kinematic equations in the presence of shocks were obtained by three rectangular difference schemes to evaluate errors of approximation attributable to various finite-difference methods. The three methods studied were the upstream-differencing method, the single-step Lax-Wendroff scheme, and the four-point implicit scheme used by Brakensiek. Of these three methods, the Lax-Wendroff scheme yielded the best approximation to the exact solution obtained by the method of characteristics. The smoothing effect of all rectangular methods in the shock-affected region of the hydrograph was clearly visible and, in general, the hydrograph peak was reduced and delayed by as much as 20 percent for the first-order schemes. The significance of these errors requires further study.

Applications of the Kinematic Cascade to Complex Watersheds

In order to investigate the lumped errors associated with both the finite-difference scheme and the kinematic transformation of a watershed surface, kinematic cascade hydrographs were compared with the exact solutions obtained for flow on a linearly converging surface. Results of this application indicate that the kinematic cascade effectively reduces geometric complexity and accurately simulates overland flow derived from rather complex watershed surfaces. Investigation of the effects of changing overland slope on the outflow from the kinematic cascade revealed a strong correlation between the general shape of the rising hydrograph and the profile of overland slope for the cascade.

Although additional analysis of experimental data will be required before definitive conclusions can be reached, it appears that the kinematic cascade accurately simulates linearly converging flow on an impervious butyl surface.

BIBLIOGRAPHY

1. Brakensiek, D. L., Hydrodynamics of Overland Flow and Nonprismatic Channels. Trans. ASAE, Vol. 9, No. 1, pp. 119-122, 1966.

2. Brakensiek, D. L., A Simulated Watershed Flow System for Hydrograph Prediction: A Kinematic Application. Paper No. 3, Proc. of the Int'l Hydrology Symposium, Fort Collins, Colorado, 1967a

3. Brakensiek, D. L., Kinematic Flood Routing. Trans. ASAE, Vol. 10, No. 3, pp. 340-343, 1967b.

4. Dickinson, W. T., Holland, M. E., and Smith, G. L., An Experimental Rainfall-Runoff Facility. Hydrology Paper No. 25, Colorado State University, Fort Collins, Colorado, 81 pp., 1967.

5. Henderson, F. M., Flood Waves in Prismatic Channels. Jour. Hydraulics Div. Amer. Soc. Civ. Engineers, Hy. 4, 1963.

6. Henderson, F. M., and Wooding, R. A., Overland Flow and Groundwater Flow from a Steady Rainfall of Finite Duration. Jour. Geophysical Research, Vol. 69, No. 8, pp. 1531-1540, 1964.

7. Houghton, David D., and Kasahara, Akira, Nonlinear Shallow Fluid Flow Over an Isolated Ridge. Communication on Pure and Applied Mathematics, Vol. XXI, 1968.

8. Huggins, L. F., and Monke, E. J., A Mathematical Model for Simulating the Hydrologic Response of a Watershed. Paper presented at December 1966 meeting of ASAE, Chicago, Illinois.

9. Iwagaki, Y., Fundamental Studies on Runoff Analysis by Characteristics. Disaster Prevention Research Institute Bulletin No. 10, Kyoto University, Kyoto, Japan, 1955.

10. Izzard, C. F., Hydraulics of Runoff from Developed Surfaces. Proc. Highway Research Board, Vol. 26, pp. 129-146, 1946.

11. Kibler, D. F., A Kinematic Overland Flow Model and its Optimization. Ph.D. Thesis, Colorado State University, Fort Collins, 1968.

12. Liggett, J. A., General Solution for Open Channel Profiles, Proc. ASCE, HY 6, November 1961.

13. Lighthill, M. J., and Whitham, C. B., On Kinematic Waves. I. Flood Movement in Long Rivers. Proc. of the Royal Society of London, Series A, Vol. 229, 1955.

14. Morgali, J. R., Laminar and Turbulent Overland Flow. Paper presented at the 49th Annual Meeting American Geophysical Union, Washington, D. C., 1968.

15. Veal, D. G., A Computer Solution of Converging, Subcritical Overland Flow. M.S. Thesis, Cornell University, 1966.

16. Wooding, R. A., A Hydraulic Model for the Catchment-stream Problem. (a) I. Kinematic Wave Theory. (b) II. Numerical Solutions. (c) III. Comparison with Runoff Observations. Jour. of Hydrology, Vol. 3, 1965.

17. Woolhiser, D. A., Overland Flow on a Converging Surface. Trans. ASAE, Vol. 12, No. 4, pp. 460-462, 1969.

18. Woolhiser, D. A., and Liggett, J. A., Unsteady, One-dimensional Flow over a Plane--the Rising Hydrograph. Water Resources Research, Vol. 3, No. 3, pp. 753-771, 1967.

APPENDIX A

Derivation of the Shallow-water Equations

Introduction

The flow of surface water over a uniform plane or in a channel is classified as spatially varied and unsteady. Accordingly, the basic equations of the kinematic model designed to simulate the surface runoff process are derived from the principles of conservation of mass and momentum. The derivations presented in this section follow the development in standard hydraulic references treating spatially varied unsteady flow. The dependent quantities are the local velocity, u, in fps and depth, h, in feet. The independent variables are the space-time coordinates, x in feet and t in seconds, respectively.

Continuity Equation

The sketch of Figure A.1 illustrates the variables used in deriving the continuity equation for a plane or channel element of arbitrary cross-section having one-dimensional flow. The continuity equation written over a time increment dt for the element of fluid shown in Figure A.1 is:

$$(A.u + q.dx)\,dt - (A + \frac{\partial A}{\partial x}dx)\,(u + \frac{\partial u}{\partial x}dx)\,dt =$$

(inflow) (outflow)

$$\frac{\partial A}{\partial t}\,dt.dx \qquad (A\text{-}1)$$

(change in storage)

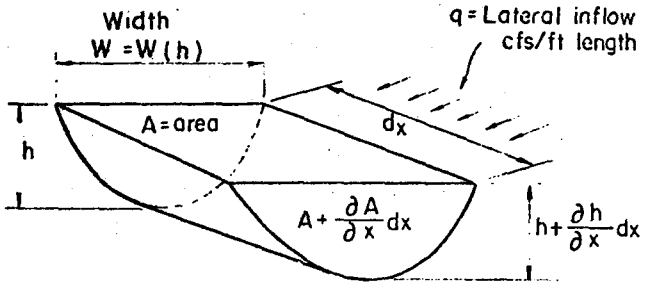

Figure A.1 Definition sketch for continuity equation.

Cancelling the product $A \cdot u$, dividing by $dx \cdot dt$, and neglecting the higher order products, equation (A-1) becomes:

$$\frac{\partial A}{\partial t} + A\frac{\partial u}{\partial x} + u\frac{\partial A}{\partial x} = q \qquad (A\text{-}2)$$

For channels of triangular or rectangular cross-section, the area can be expressed in the form:

$$A = bh^m \qquad (A\text{-}3)$$

The constants b and m are equal to the width, W, and 1, respectively, for a rectangular section, and equal to the side slope, Z, and 2, respectively, for a triangular section. Substitution of (A-3) in equation (A-2) yields the following relation:

$$b \cdot m \cdot h^{m-1}\frac{\partial h}{\partial t} + b \cdot h^m \frac{\partial u}{\partial x} + b \cdot m \cdot h^{m-1} u\frac{\partial h}{\partial x} = q \qquad (A\text{-}4)$$

In the case of a wide plane or channel, equation (A-4) can be written as:

$$\frac{\partial h}{\partial t} + u\frac{\partial h}{\partial x} + h\frac{\partial u}{\partial x} = q \qquad (A\text{-}5)$$

Equation (A-5) is the one-dimensional continuity equation for surface flow over a wide plane or channel.

Momentum Equation

An element of fluid receiving lateral inflow in cfs/sq.ft. is shown in Figure A.2. Newton's second

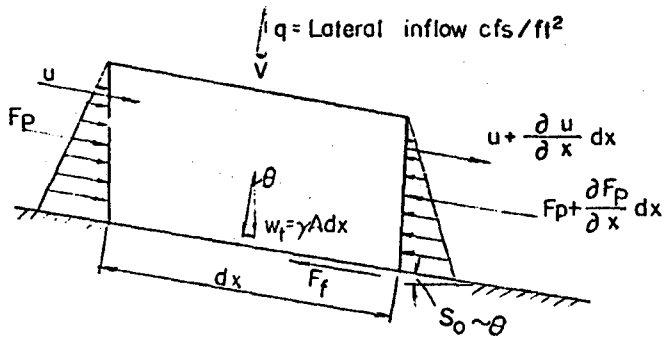

Figure A.2 Forces acting on fluid element used in deriving the momentum equation.

law is written for the forces acting in the x-direction, where x is measured downstream. The lateral inflow has a velocity component, v, in the x-direction. The basic equation to be satisfied is:

$$\Sigma F_x = m_s\frac{du}{dt} + m_l\frac{dv}{dt} \qquad (A\text{-}6)$$

where m_s and m_l are the masses of water in the main stream and lateral inflow, respectively.

Forces acting in the x-direction on the element are the following:

(1) The weight component acting in the downstream direction.

$$W_t \cdot \sin\theta = \gamma A \sin\theta \, dx \approx \gamma A \, S_o \, dx$$

where γ is the unit weight of water and S_o the bed slope;

(2) The hydrostatic force acting to the right of the centroid of area

$$F = \gamma \bar{h} A,$$

where $\bar{h}$ is the distance from the water surface to the centroid of area A;

(3) The hydrostatic force acting to the left at the centroid of area

$$F_p + \frac{\partial F_p}{\partial x} dx = \gamma \bar{h} A + \frac{\partial F_p}{\partial x} dx$$

Liggett (1961) has shown that the hydrostatic pressure differential, $\frac{\partial F_p}{\partial x} dx$, is given by

$$\frac{\partial F_p}{\partial x} dx = -\gamma A \frac{\partial h}{\partial x} dx; \text{ and}$$

(4) The friction force retarding the flow

$$F_f = -\gamma A \, S_f \, dx$$

where S_f is the slope of the energy line.

Hence the basic equation (A-6) may be written as

$$\Sigma F_x = \gamma A \, S_o \, dx - \gamma A \, S_f \, dx - \gamma A \frac{\partial h}{\partial x} dx \qquad (A\text{-}7)$$

The momentum changes on the RHS of equation (A-6) may be evaluated as

$$m_s \frac{du}{dt} = \frac{1}{g} \gamma A dx \frac{du}{dt}$$

$$= \frac{1}{g} \gamma A \, dx \left(\frac{\partial u}{\partial t} + \frac{\partial u}{\partial x} \cdot \frac{dx}{dt}\right)$$

$$= \frac{1}{g} \gamma A \, dx \left(\frac{\partial u}{\partial t} + u \frac{\partial u}{\partial x}\right) \qquad (A\text{-}8)$$

$$m_l \frac{dv}{dt} = \frac{1}{g} \gamma q \, dx \, dt \, \frac{(u-v)}{dt}$$

$$= \frac{1}{g} \gamma \, q \, (u-v) \, dx \qquad (A\text{-}9)$$

where g is acceleration due to gravity and $\frac{du}{dt}$ is interpreted as the total derivative of a particle along its stream path.

Combining equations (A-6), (A-7), (A-8) and (A-9) yields the momentum expression:

$$\gamma A \, S_o \, dx - \gamma A \, S_f \, dx - \gamma A \frac{\partial h}{\partial x} dx = \frac{1}{g} \gamma A \, dx \left(\frac{\partial u}{\partial t} + u \frac{\partial u}{\partial x}\right)$$

$$+ \frac{1}{g} \gamma q \, (u-v) \, dx \qquad (A\text{-}10)$$

Dividing (A-10) by $\frac{1}{g} \gamma A \, dx$ and re-arranging:

$$\frac{\partial u}{\partial t} + u \frac{\partial u}{\partial x} + g \frac{\partial h}{\partial x} = g(S_o - S_f) - \frac{q}{A}(u-v) \qquad (A\text{-}11)$$

For the case of one-dimensional flow in a wide channel or over a plane surface, equation (A-11) can be written:

$$\frac{\partial u}{\partial t} + u \frac{\partial u}{\partial x} + g \frac{\partial h}{\partial x} = g(S_o - S_f) - \frac{q}{h}(u-v) \qquad (A\text{-}12)$$

Equations (A-5) and (A-12) are the one-dimensional unsteady spatially varied flow equations applicable to wide channels and overland flow planes. The assumptions made during their derivation are the following:

(1) The flow is gradually varied so that vertical components of velocity and acceleration are negligible in comparison with the components along the direction of flow.

(2) The pressure on the vertical surfaces of the flow element is hydrostatic.

(3) The energy and momentum coefficients, used as corrections to nonuniform velocity distributions, are equal to one.

(4) The channel slope, S_o, is small and is approximately equal to $\sin\theta \approx \theta$.

(5) Frictional resistance in unsteady flow is the same as that for the corresponding depth in uniform flow so that the friction slope, S_f, can be obtained by either the Manning or Chézy friction relations.

Reference is made to publications by Gilcrest (1950), Chow (1959) and Yevjevich (1961) for more extensive treatment of the spatially varied unsteady flow equations.

APPENDIX B

Derivation of Lax-Wendroff Scheme

The dimensionless equation for kinematic flow is

$$\frac{\partial h}{\partial t} + \beta h^{N-1} \frac{\partial h}{\partial x} = q \qquad \text{(B-1)}$$

where $\beta = Nk/n$

This equation can be written in the conservation form:

$$\frac{\partial h}{\partial t} + \frac{\partial}{\partial x}\left(\frac{k}{n} h^N\right) - q = 0 \qquad \text{(B-2)}$$

Expanding $h(x,t+\Delta t)$ in a Taylors Series we obtain:

$$h(x,t+\Delta t) = h(x,t) + \Delta t \frac{\partial h}{\partial t} + \frac{\Delta t^2}{2} \frac{\partial^2 h}{\partial t^2} + 0(\Delta t)^3 \qquad \text{(B-3)}$$

From equation (B-2)

$$\frac{\partial h}{\partial t} = -\left[\frac{\partial}{\partial x}\left(\frac{k}{n} h^N\right) - q\right] \qquad \text{(B-4)}$$

and

$$\frac{\partial^2 h}{\partial t^2} = \frac{\partial}{\partial t}\left[\frac{\partial}{\partial x}\left(\frac{k}{n} h^N\right) - q\right] = -\frac{\partial}{\partial x}\left[\frac{\partial}{\partial t}\frac{k}{n} h^N\right] + \frac{\partial q}{\partial t}$$

$$= -\frac{\partial}{\partial x}\left[N \frac{k}{n} h^{N-1} \frac{\partial h}{\partial t}\right] + \frac{\partial q}{\partial t} \qquad \text{(B-5)}$$

Substituting the expression for $\frac{\partial h}{\partial t}$ given by equation (B-4) into equation (B-5)

$$\frac{\partial^2 h}{\partial t^2} = \frac{\partial}{\partial x}\left[N \frac{k}{n} h^{N-1}\left(\frac{\partial}{\partial x}\left(\frac{k}{n} h^N\right) - q\right)\right] + \frac{\partial q}{\partial t} \qquad \text{(B-6)}$$

Therefore:

$$h(x,t+\Delta t) = h(x,t) - \Delta t\left[\frac{\partial}{\partial x}\left(\frac{k}{n} h^N\right) - q\right]$$

$$+ \frac{\Delta t^2}{2}\left\{\frac{\partial}{\partial x}\left[\frac{Nkh^{N-1}}{n}\left(\frac{\partial}{\partial x}\left(\frac{k}{n} h^N\right) - q\right)\right] + \frac{\partial q}{\partial t}\right\} \qquad \text{(B-7)}$$

Equation (B-7) gives a second order approximation for $h(x,t+\Delta t)$ and is the basis of the finite-difference formulation shown in Table 3.

APPENDIX C

Stability Calculations

Stability is one of the properties of a difference scheme that is required before convergence is guaranteed. In an unstable scheme small numerical errors introduced in the computational method are amplified and eventually dominate the solution. Although the following method of stability analysis is not rigorous for nonlinear equations, it does serve to identify those difference schemes that are obviously unsuitable and it also determines appropriate step lengths for conditionally stable schemes.

In a linear stability analysis we assume that instabilities first appear in a very small region of space so that if the coefficients of the derivatives are smooth functions they can be approximated as constants in this region. Accordingly, we linearize equation (11) as shown in equation (C-1) where $\bar{h}$ is a constant.

$$\frac{\partial h}{\partial t} + \beta \bar{h}^{N-1} \frac{\partial h}{\partial x} = q \qquad \text{(C-1)}$$

Now at any point j, k the numerical solution h_j^k is equal to the true solution $h(k\Delta t, j\Delta x)$ plus an error term $\tilde{h}_j^k$.

$$h_j^k = h(k\Delta t, j\Delta x) + \tilde{h}_j^k \qquad \text{(C-2)}$$

where Δt is the time increment and Δx is the distance increment.

Because we are dealing with a linear system, we can consider one term of the Fourier Series expression for the error term.

$$\tilde{h}_m^n = H_0 \exp\left[i(m\sigma\Delta x + n\gamma\Delta t)\right] \qquad \text{(C-3)}$$

where H_0 is a constant, σ and γ are wave numbers in space and time and $i = \sqrt{-1}$. It is assumed that the errors are perturbations added to the solution of the linear system. If we write the linearized finite-difference equation in terms of the correct solution plus the error terms (equation (C-2)) and then subtract the exact equation, we can obtain a differential equation in the error terms. This differential equation is then written in finite-difference form. In a stable scheme the ratio of successive error terms will be smaller than unity, e.g.,

$$\left| \frac{\tilde{h}_j^{k+1}}{\tilde{h}_j^k} \right| \leq 1 \qquad \text{(C-4)}$$

which establishes a stability criterion.

Lax-Wendroff Method

The linearized Lax-Wendroff scheme in the error terms is

$$\tilde{h}_j^{k+1} = \tilde{h}_j^k - \Delta t \left[a \left(\frac{\tilde{h}_{j+1}^k - \tilde{h}_{j-1}^k}{2\Delta x} \right) \right]$$

$$+ \frac{\Delta t^2}{2} \left\{ \frac{a^2}{\Delta x^2} \left(\tilde{h}_{j+1}^k - 2\tilde{h}_j^k + \tilde{h}_{j-1}^k \right) \right\} \qquad \text{(C-5)}$$

where: $a = \frac{Nk\bar{h}^{N-1}}{n}$

If in equation (C-3) we let $m = n = 0$ for point j, k (which we can do with no loss in generality) we obtain the following

$$\tilde{h}_j^k = H_o \; ; \; \tilde{h}_j^{k+1} = H_o \exp\left[i\gamma\Delta t\right]$$

$$\tilde{h}_{j+1}^k = H_o \exp\left[i\sigma\Delta x\right] \; ; \; \tilde{h}_{j-1}^k = H_o \exp\left[-i\sigma\Delta x\right]$$

Substituting these expressions into equation (C-5) and dividing by $\tilde{h}_j^k$

$$\tilde{h}_j^{k+1}/\tilde{h}_j^k = e^{i\gamma\Delta t} = 1 - \frac{a\Delta t}{2\Delta x}\left[e^{i\sigma\Delta x} - e^{-i\sigma\Delta x}\right]$$

$$+ \frac{1}{2}\left(\frac{\Delta t}{\Delta x}a\right)^2 \left[e^{i\sigma\Delta x} - 2 + e^{-i\sigma\Delta x}\right] \qquad \text{(C-6)}$$

with the appropriate trignometric substitutions

$$e^{i\gamma\Delta t} = 1 + a\frac{\Delta t}{\Delta x}(i \sin \sigma\Delta x) + \left(\frac{\Delta t}{\Delta x}a\right)^2 (\cos \sigma\Delta x - 1) \qquad \text{(C-7)}$$

For stability, the quantity $e^{i\gamma\Delta t}$ must lie within the unit circle on the complex plane. Now the real part of equation (C-7) is

$$1 + \left(a\frac{\Delta t}{\Delta x}\right)^2 (\cos \sigma\Delta x - 1)$$

and the imaginary part is

$$a\frac{\Delta t}{\Delta x} \sin \sigma\Delta x \quad .$$

Squaring the real and imaginary parts we obtain the criterion

$$\left| 1 + r^2\left[2(\cos\theta-1) + r^2(\cos^2\theta-2\cos\theta+1) + \sin^2\theta\right] \right| \leq 1 \qquad \text{(C-8)}$$

where $r = \theta\Delta t/\Delta x$ and $\theta = \sigma\Delta x$

Let us consider the most critical condition when the left-hand side of equation (C-8) is evaluated at the following values of $\sigma\Delta x$

$\sigma\Delta x$	$\sin \sigma\Delta x$	$\cos \sigma\Delta x$	Criterion
0	0	1	$\left\|1\right\| \leq 1$
$\pi/2$	1	0	$\left\|1-(a\frac{\Delta t}{\Delta x})^2 + (\frac{a\Delta t}{\Delta x})^4\right\| \leq 1$
π	0	-1	$\left\|1-4(a\frac{\Delta t}{\Delta x})^2+ 4(\frac{a\Delta t}{\Delta x})^4\right\| \leq 1$
$3\pi/2$	-1	0	$\left\|1-(\frac{a\Delta t}{\Delta x})^2 + (\frac{a\Delta t}{\Delta x})^4\right\| \leq 1$

From the analysis, it is clear that the criterion stated above is satisfied when

$$(a\frac{\Delta t}{\Delta x})^2 \leq 1$$

$$a\frac{\Delta t}{\Delta x} \leq 1$$

or

$$\frac{\Delta t}{\Delta x} \leq \frac{n}{Nk\bar{h}^{N-1}} \qquad \text{(C-9)}$$

Equation (C-9) shows that the point $k + 1$, j must lie within the zone of determinacy of the line from k, $j - 1$ to k, $j + 1$. The Lax-Wendroff scheme is linearly stable subject to condition (C-9).

Upstream differencing method

When the upstream differencing method (Table 3) is applied to the linearized equation with the error terms and the exact equations are subtracted we obtain:

$$\tilde{h}_j^{k+1} = \tilde{h}_j^k - a\frac{\Delta t}{\Delta x}(\tilde{h}_j^k - \tilde{h}_{j-1}^k) \qquad \text{(C-10)}$$

where: $a = \frac{Nk\bar{h}}{n}^{N-1}$

After substituting the Fourier expressions for the error terms

$$e^{i\gamma\Delta t} = 1 - a\frac{\Delta t}{\Delta x}(1 - e^{-i\sigma\Delta x}) \qquad \text{(C-11)}$$

For the stability we require

$$\left|1 - a\frac{\Delta t}{\Delta x}(1 - e^{-i\sigma\Delta x})\right| \leq 1$$

or $$\left|1 - a\frac{\Delta t}{\Delta x}(1 - \cos\sigma\Delta x + i \sin\sigma\Delta x)\right| \leq 1 \quad .$$

Squaring the real and imaginary parts,

$$\left|1 - 2a\frac{\Delta t}{\Delta x}\left[a\frac{\Delta t}{\Delta x}(1 - \cos\sigma\Delta x) + (1 - \cos\sigma\Delta x)\right]\right| \leq 1 \qquad \text{(C-12)}$$

Upon simplification, inequality (C-12) becomes

$$a\frac{\Delta t}{\Delta x} \leq \frac{-1 + \sqrt{3}}{2}$$

or

$$\frac{\Delta t}{\Delta x} \leq \frac{n}{2.75Nk\,\bar{h}^{N-1}} \qquad \text{(C-13)}$$

Brakensiek's four-point implicit method

Using the same procedures outlined above, the stability criterion for the implicit method is:

$$\left|\frac{\Delta t}{\Delta x}\frac{(\cos\theta - i\sin\theta + 1)}{\left(1 - \frac{\Delta t}{\Delta x}\right)(\cos\theta - i\sin\theta) - \left(1 + \frac{\Delta t}{\Delta x}\right)}\right| \leq 1$$

which can be put in the form

$$\left|\frac{\sqrt{2\frac{\Delta t}{\Delta x}^2\left[1 + \cos\theta\right]}\, e^{i\theta_1}}{\sqrt{2\frac{\Delta t}{\Delta x}^2\left[1 + \cos\theta\right] + 2(1-\cos\theta)}\, e^{i\theta_2}}\right| \leq 1 \qquad \text{(C-14)}$$

where $\theta = \sigma\Delta t$.

The left-hand side of inequality (C-14) is always ≤ 1 so the scheme is unconditionally stable.

Key Words: Overland flow, Open channel flow, Kinematic, Numerical Methods, Watershed models

Abstract: A kinematic cascade is defined as a sequence of n discrete overland flow planes or channel segments in which the kinematic wave equations are used to describe the unsteady flow. Each plane or channel is characterized by a length, l_k , width, w_k , and a roughness-slope factor, α_k . Outflow from the k^{th} plane, along with the parameters for planes k and k + 1, establishes the upstream boundary condition for plane k + 1 . Nondimensional equations are presented for the k^{th} element in a kinematic cascade. Properties of the solutions for a kinematic cascade with pulsed lateral inputs are examined. Cascade solutions are compared with characteristic-analytic solutions and with experimental data for flow over a linearly converging section.

References: David F. Kibler and David A. Woolhiser, Colorado State University Hydrology Paper No. 39 (March 1970) "The Kinematic Cascade as a Hydrologic Model."

Key Words: Overland flow, Open channel flow, Kinematic, Numerical Methods, Watershed models

Abstract: A kinematic cascade is defined as a sequence of n discrete overland flow planes or channel segments in which the kinematic wave equations are used to describe the unsteady flow. Each plane or channel is characterized by a length, l_k , width, w_k , and a roughness-slope factor, α_k . Outflow from the k^{th} plane, along with the parameters for planes k and k + 1, establishes the upstream boundary condition for plane k + 1 . Nondimensional equations are presented for the k^{th} element in a kinematic cascade. Properties of the solutions for a kinematic cascade with pulsed lateral inputs are examined. Cascade solutions are compared with characteristic-analytic solutions and with experimental data for flow over a linearly converging section.

References: David F. Kibler and David A. Woolhiser, Colorado State University Hydrology Paper No. 39 (March 1970) "The Kinematic Cascade as a Hydrologic Model."

Key Words: Overland flow, Open channel flow, Kinematic, Numerical Methods, Watershed models

Abstract: A kinematic cascade is defined as a sequence of n discrete overland flow planes or channel segments in which the kinematic wave equations are used to describe the unsteady flow. Each plane or channel is characterized by a length, l_k , width, w_k , and a roughness-slope factor, α_k . Outflow from the k^{th} plane, along with the parameters for planes k and k + 1, establishes the upstream boundary condition for plane k + 1 . Nondimensional equations are presented for the k^{th} element in a kinematic cascade. Properties of the solutions for a kinematic cascade with pulsed lateral inputs are examined. Cascade solutions are compared with characteristic-analytic solutions and with experimental data for flow over a linearly converging section.

References: David F. Kibler and David A. Woolhiser, Colorado State University Hydrology Paper No. 39 (March 1970) "The Kinematic Cascade as a Hydrologic Model."

Key Words: Overland flow, Open channel flow, Kinematic, Numerical Methods, Watershed models

Abstract: A kinematic cascade is defined as a sequence of n discrete overland flow planes or channel segments in which the kinematic wave equations are used to describe the unsteady flow. Each plane or channel is characterized by a length, l_k , width, w_k , and a roughness-slope factor, α_k . Outflow from the k^{th} plane, along with the parameters for planes k and k + 1, establishes the upstream boundary condition for plane k + 1 . Nondimensional equations are presented for the k^{th} element in a kinematic cascade. Properties of the solutions for a kinematic cascade with pulsed lateral inputs are examined. Cascade solutions are compared with characteristic-analytic solutions and with experimental data for flow over a linearly converging section.

References: David F. Kibler and David A. Woolhiser, Colorado State University Hydrology Paper No. 39 (March 1970) "The Kinematic Cascade as a Hydrologic Model."

PREVIOUSLY PUBLISHED PAPERS

Colorado State University Hydrology Papers

No. 23 "An Objective Approach to Definitions and Investigations of Continental Hydrologic Droughts," by Vujica Yevjevich, August 1967.

No. 24 "Application of Cross-Spectral Analysis to Hydrologic Time Series," by Ignacio Rodriguez-Iturbe, September 1967.

No. 25 "An Experimental Rainfall-Runoff Facility," by W. T. Dickinson, M. E. Holland and G. L. Smith, September 1967.

No. 26 "The Investigation of Relationship Between Hydrologic Time Series and Sunspot Numbers," by Ignacio Rodriguez-Iturbe and Vujica Yevjevich, April 1968.

No. 27 "Diffusion of Entrapped Gas From Porous Media," by Kenneth M. Adam and Arthur T. Corey, April 1968.

No. 28 "Sampling Bacteria in a Mountain Stream," by Samuel H. Kunkle and James R. Meiman, March 1968.

No. 29 "Estimating Design Floods from Extreme Rainfall," by Frederick C. Bell, July 1968.

No. 30 "Conservation of Ground Water by Gravel Mulches," by A. T. Corey and W. D. Kemper, May 1968.

No. 31 "Effects of Truncation on Dependence in Hydrologic Time Series," by Rezaul Karim Bhuiya and Vujica Yevjevich, November 1968.

No. 32 "Properties of Non-Homogeneous Hydrologic Series," by V. Yevjevich and R. I. Jeng, April 1969.

No. 33 "Runs of Precipitation Series," by Jose Llamas and M. M. Siddiqui, May 1969.

No. 34 "Statistical Discrimination of Change in Daily Runoff," by Andre J. Dumas and Hubert J. Morel-Seytoux, August 1969.

No. 35 "Stochastic Process of Precipitation," by P. Todorovic and V. Yevjevich, September 1969.

No. 36 "Suitability of the Upper Colorado River Basin for Precipitation Management," by Hiroshi Nakamichi and Hubert J. Morel-Seytoux, October 1969.

No. 37 "Regional Discrimination of Change in Runoff," by Viboon Ninmannit and Hubert J. Morel-Seytoux, November 1969.

No. 38 "Evaluation of Effect of Impoundment on Water Quality in Cheney Reservoir," by J. C. Ward and S. Karaki, March 1970.

COLORADO STATE UNIVERSITY

EXPERIMENTAL RAINFALL-RUNOFF FACILITY

Summary of Experiments and preliminary Results of an Experimental Investigation on the Kinematic Theory of Overland Flow

prepared for

U. S. Department of the Interior
Office of Water Resources Research
under matching grant
No. B-030-COLO
and
Colorado State University Experiment Station
Fort Collins, Colorado

November 1969

CER69-70MEH21a

COLORADO STATE UNIVERSITY
EXPERIMENTAL RAINFALL-RUNOFF FACILITY

Initial Data Analyses

The first series of experimental runs were performed during Sept. and Oct., 1969. The primary objective of these experiments was to test the hypothesis that the kinematic wave equations are an adequate mathematical model for overland flow on a linearly converging surface. A second objective was to investigate the effect of spatially non-uniform roughness on the watershed response. The experimental runs completed in 1969 are listed in Table I.

The mathematical model upon which the data analysis is based is the kinematic model for overland flow on a converging surface (Woolhiser, 1969). A definition sketch of the problem is shown in Fig. (1). The equations describing converging overland flow are:

The continuity equation:

$$\frac{\partial h}{\partial t} + \frac{\partial\, uh}{\partial\, x} = q + \frac{uh}{(L_o - x)} \qquad (1)$$

And the friction relationship

$$u = \partial h^{N-1} \qquad (2)$$

where u is the local velocity, h is the local depth L_o is the radius, q is the lateral inflow rate and ∂ and N are parameters. If the Chezy formula is used $\partial = C\sqrt{S_o}$ and $N = 3/2$ when S_o is the slope and C is the Chezy coefficient.

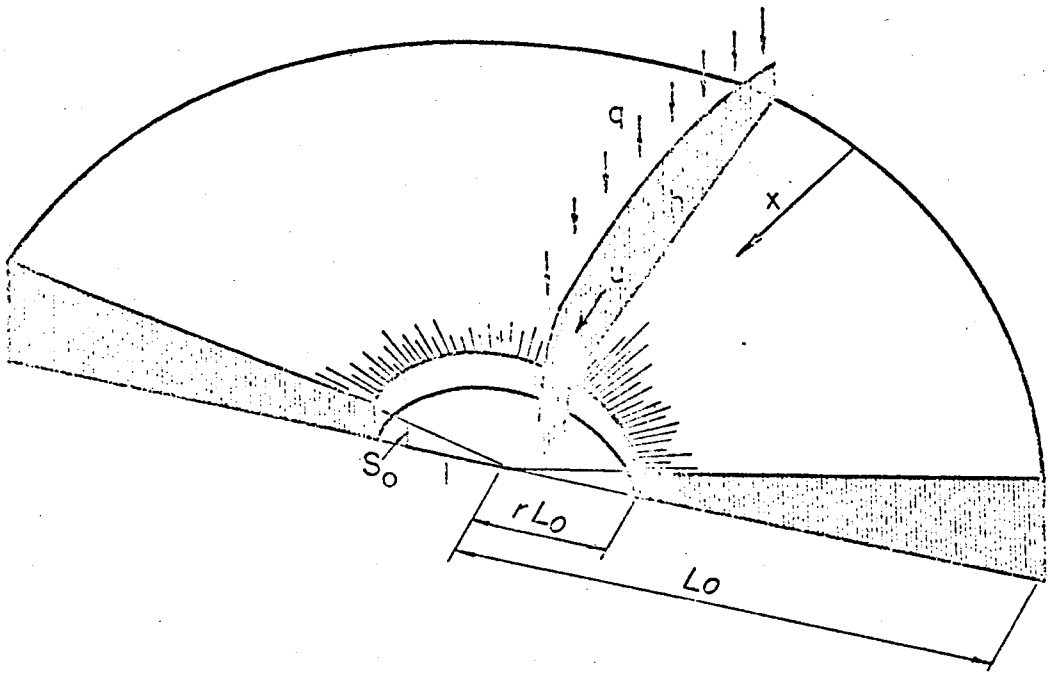

Figure 1. Geometry of Converging Section.

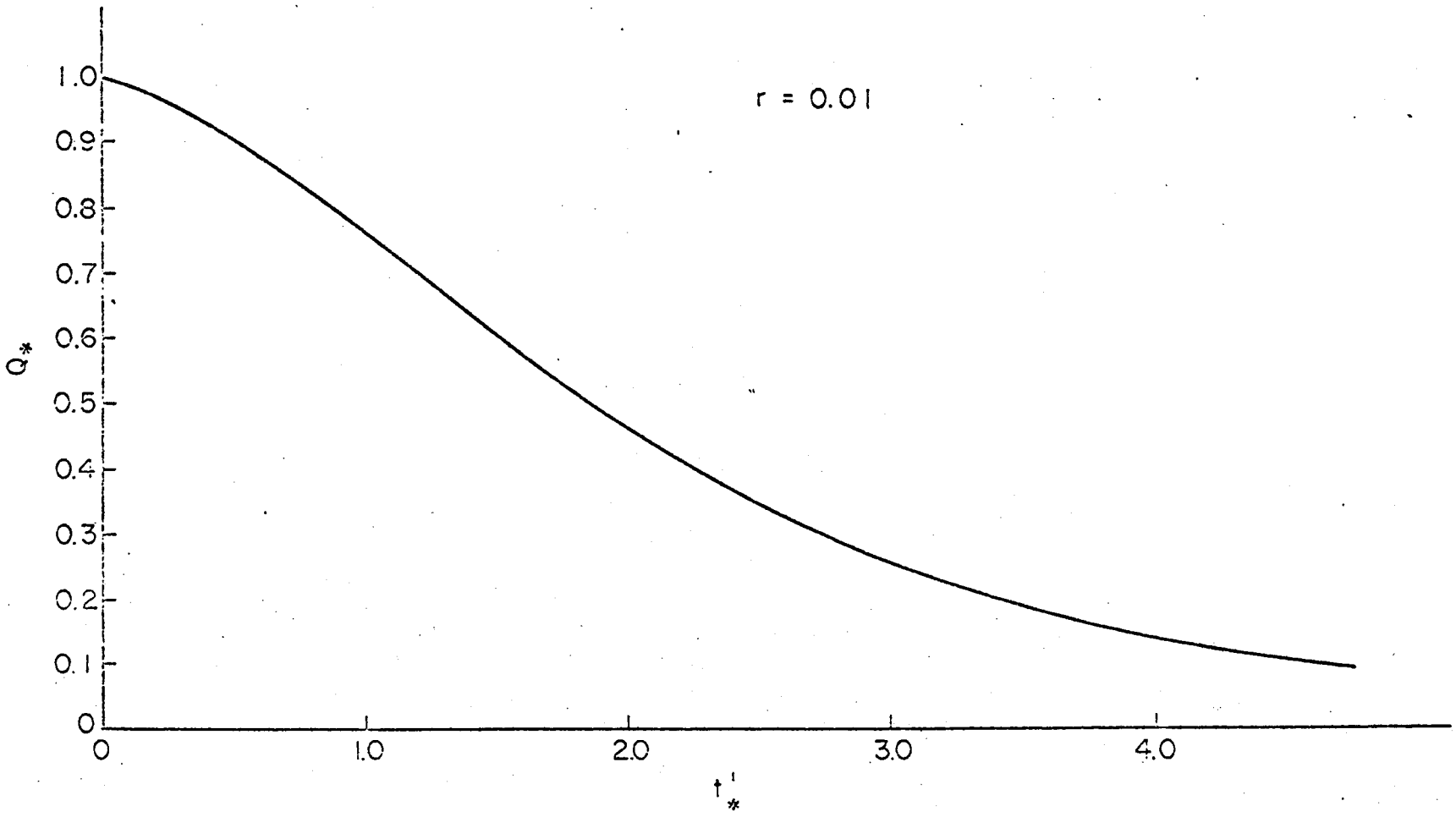

Figure 2. Dimensionless Recession Hydrograph.

where Q_* is the dimensionless discharge, r is the covergence parameter, X_o is the origin of a characteristic beginning at, the time inflow stops in the region $O < X_o < 1$, t_*' is the time after lateral inflow stops until a discharge Q_* appears at the downstream boundary and N is 3/2 for the Chezy equation. This recession hydrograph is shown in Fig. (2). In Fig. (2) note that $t_*^1 = 1$ when $Q_* = 0.76$, $t_*^1 = 2$ when $Q_* = 0.46$ and $t_*^1 = 3$ when $Q_* = 0.26$. Let the time after lateral inflow stops until the dimensionless discharge Q_* is reached be designated as t_{Q_*}. Then an estimate of T_o is given by the average:

$$T_o = 1/3 \left[t_{0.76} + (1/2)\ t_{0.46} + (1/3)\ t_{0.26} \right] \qquad (7)$$

Normalizing times were computed using Eq. (7) and the experimental equilibrium hydrographs were normalized on this basis. Non-dimensional experimental hydrograph are compared with the solution to Eq. (3) in Fig. 3(a) and 3 (b). Agreement between the hydrographs appears quite good, however, the Chezy parameterestimated from Eq. (4) appears not to be constant depending only upon the surface characteristics but appear to vary with the equilibrium flow rate (see Fig. 4). This may be an indication that the Chezy formulation is not appropriate over the range of intensities tested. Undoubtedly flow is initially laminar for all cases and may become turbulent over a substantial portion of the surface as flow rates increase. The Manning formulation may give a more accurate representation for the rough surfaces and this formula will be used in future analysis.

The data analysis reported herein are not complete so no definite conclusions can be made. However, it appears that the Kinematic Model is accurate for the converging flow case with a slope of 5%. The problem

of estimating roughness parameters is an important one and will be investigated throughly. The size of the experimental watershed makes it uniquely suitable for studying effects of spatially variable roughness. The results from the exploratory studies on effects of spatial variations in roughness will assist in the design of new experiments for next summer.

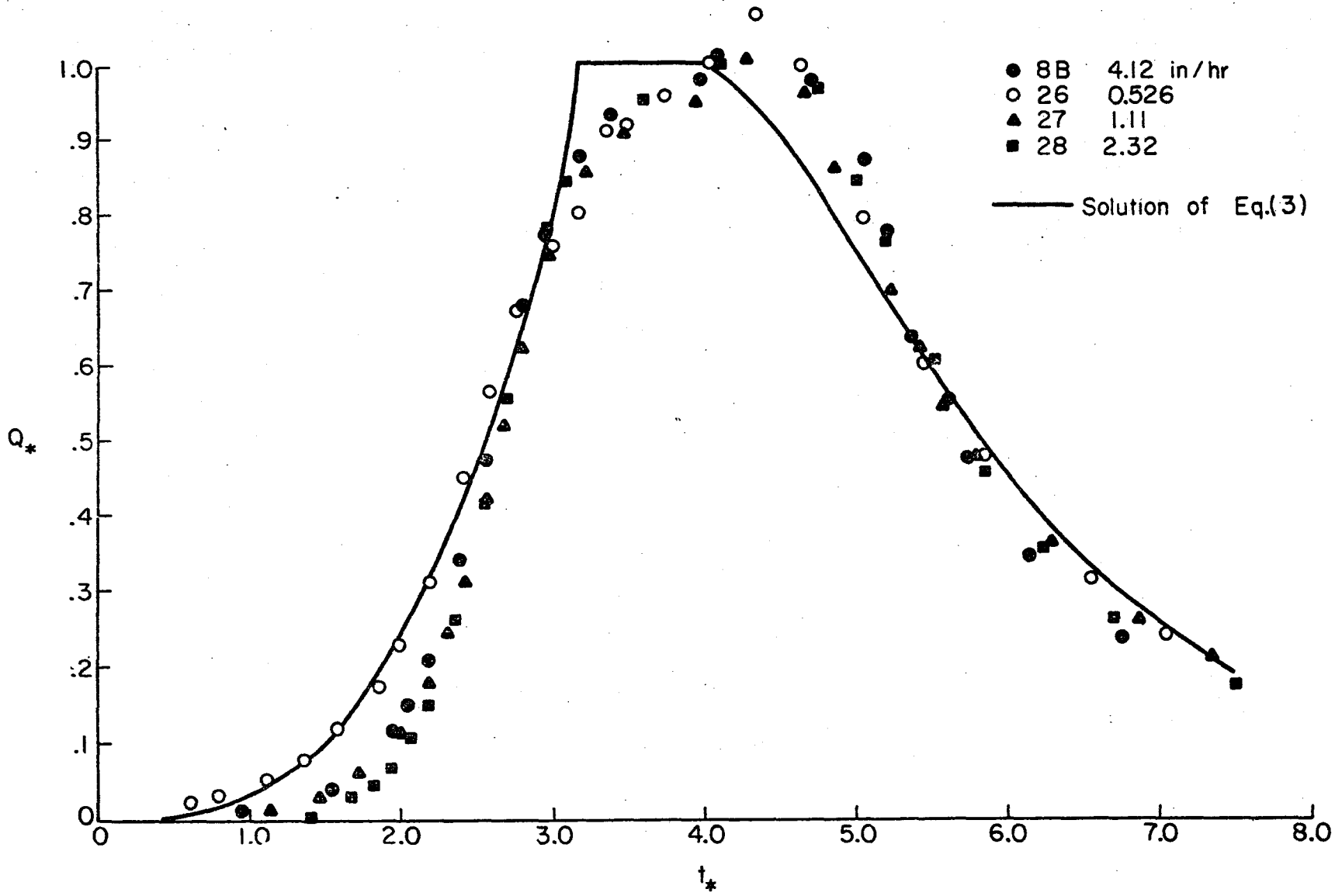

Figure 3A Theoretical and Observed Dimensionless Hydrographs for Butyl Surface

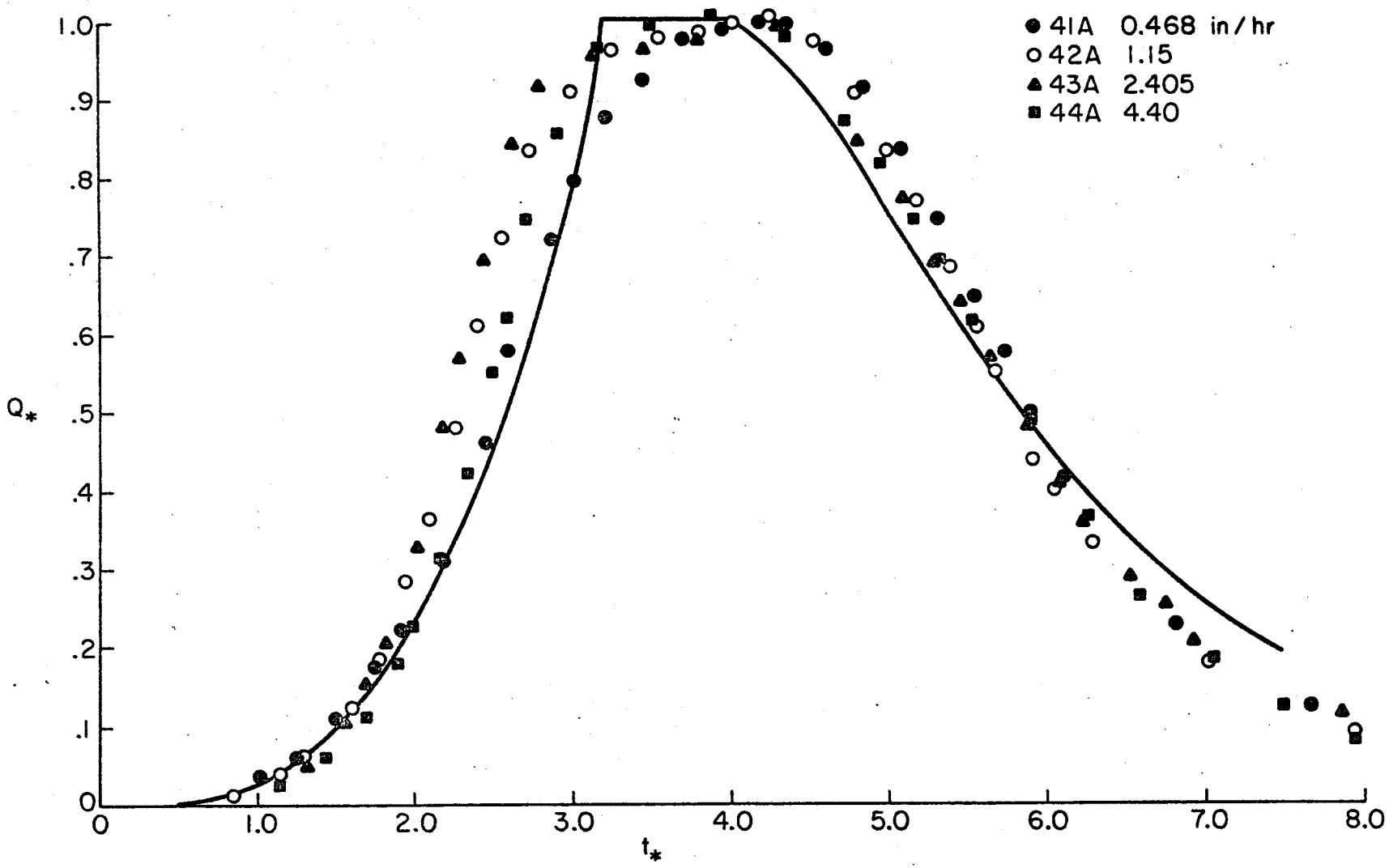

Figure 3B Theoretical and Observed Hydrographs for Graveled Surface

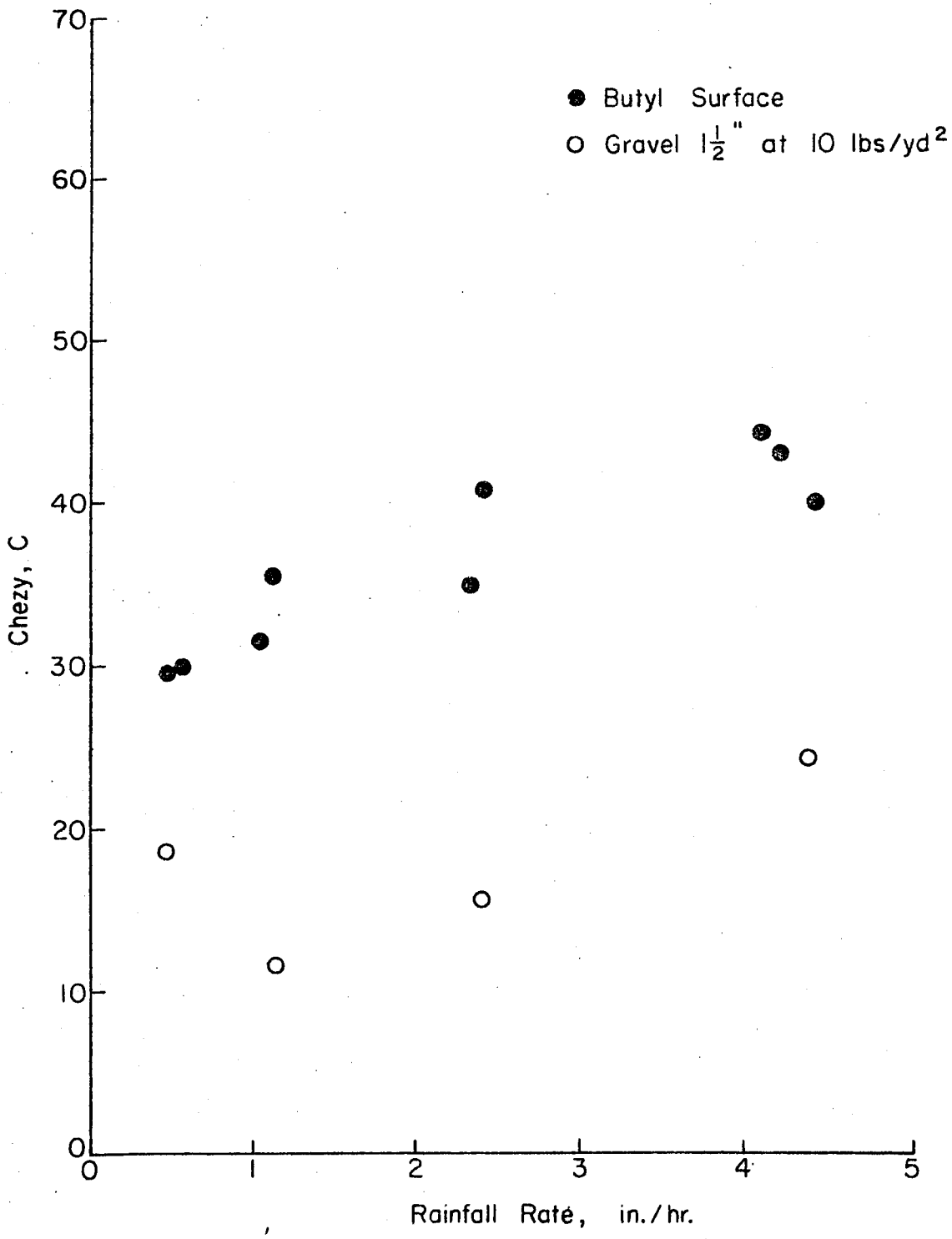

Figure 4 Chezy C vs Rainfall Rate

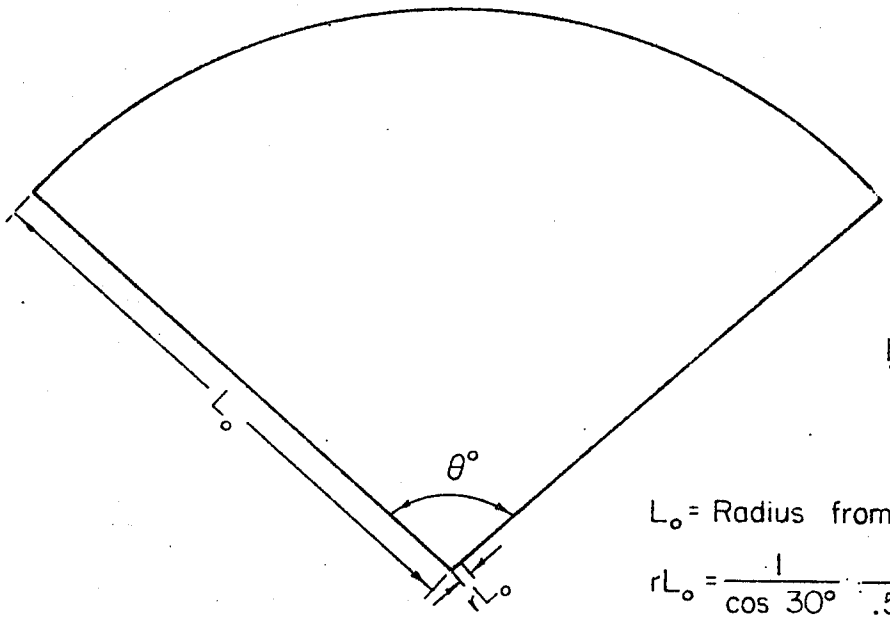

General Configuration

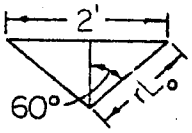

L_o = Radius from Outlet to Rim

$$rL_o = \frac{1}{\cos 30°} \cdot \frac{1}{.557} = 1.17'$$

$$r_1 = \frac{1.17}{110} = .01063$$

$$r_2 = \frac{1.17}{72} = .0163$$

$$r_3 = \frac{1.17}{36} = .0325$$

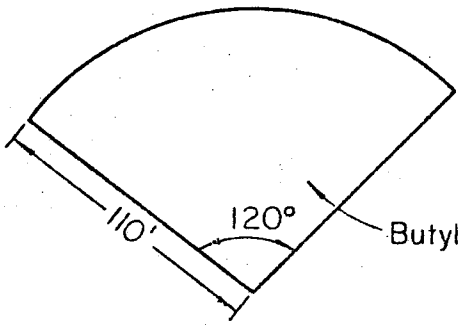

Configuration 1

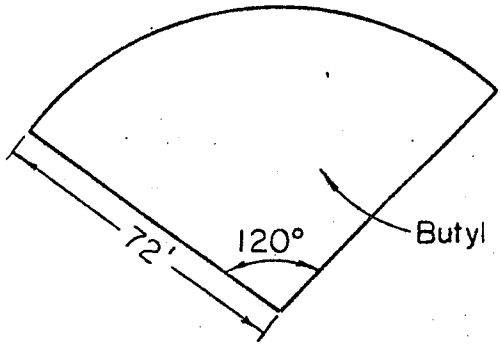

Configuration 2

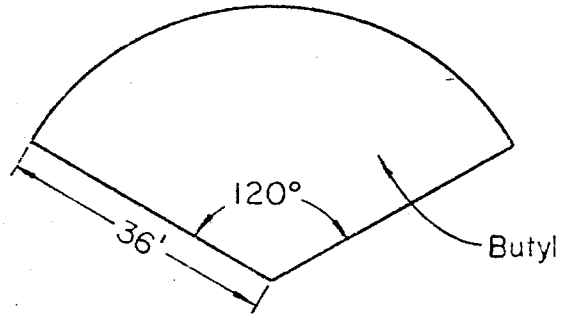

Configuration 3

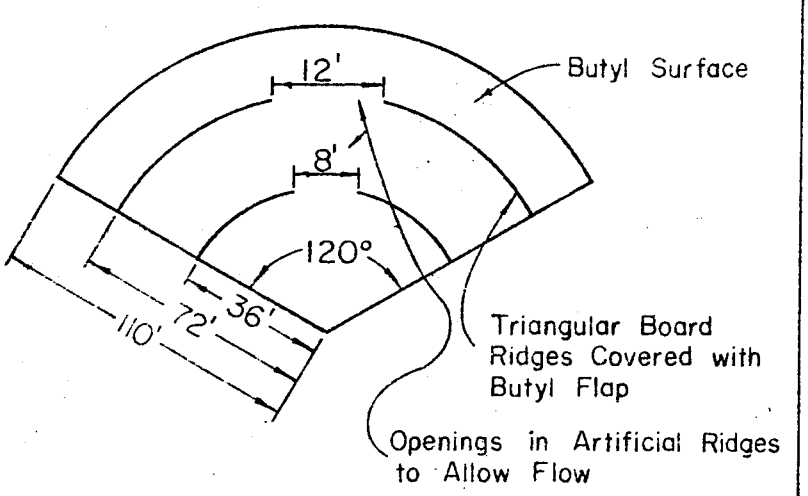

Configuration 4

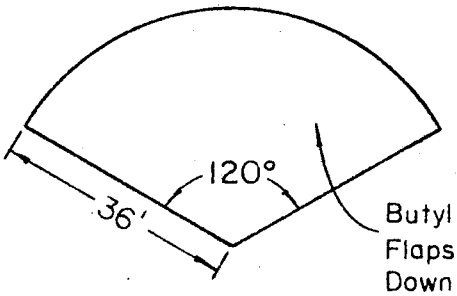

Configuration 5

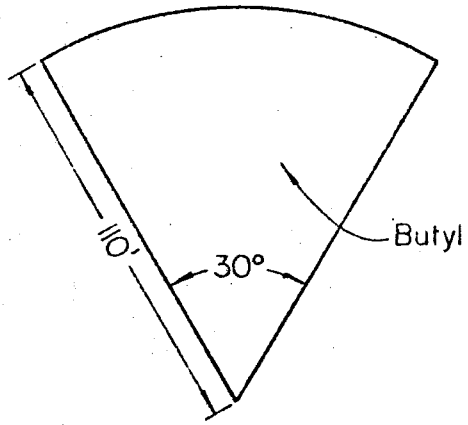

Configuration 6

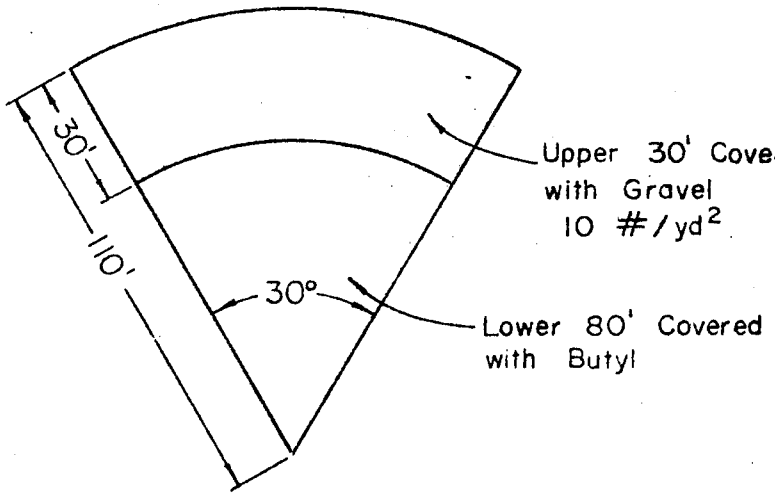

Configuration 7

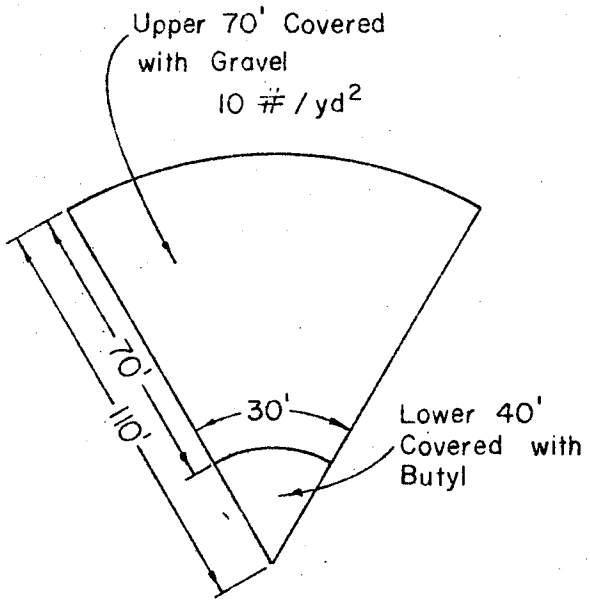

Configuration 8

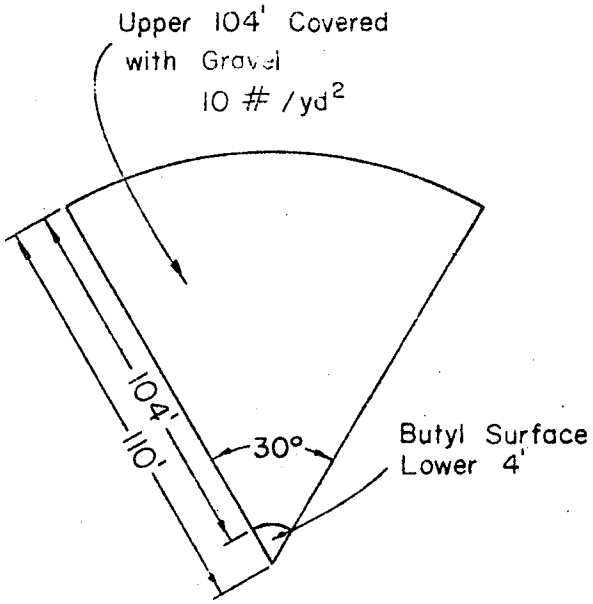

Configuration 9

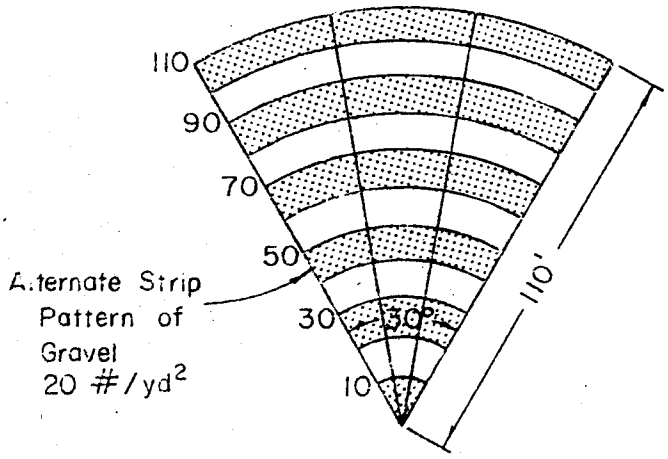

Configuration 10

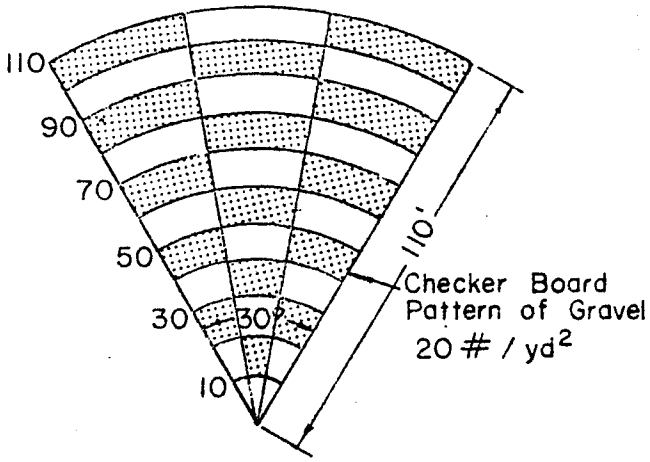

Configuration 11

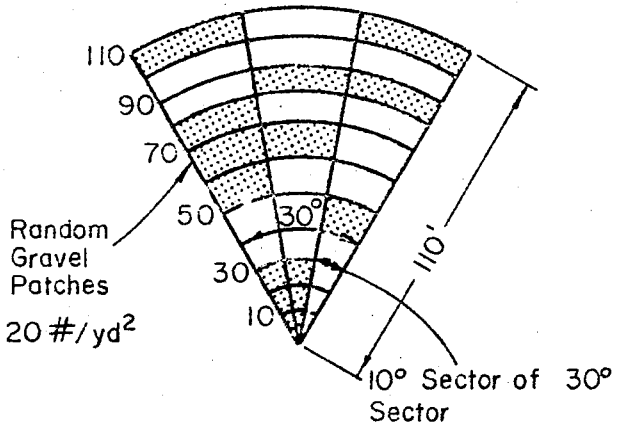

Configuration 12

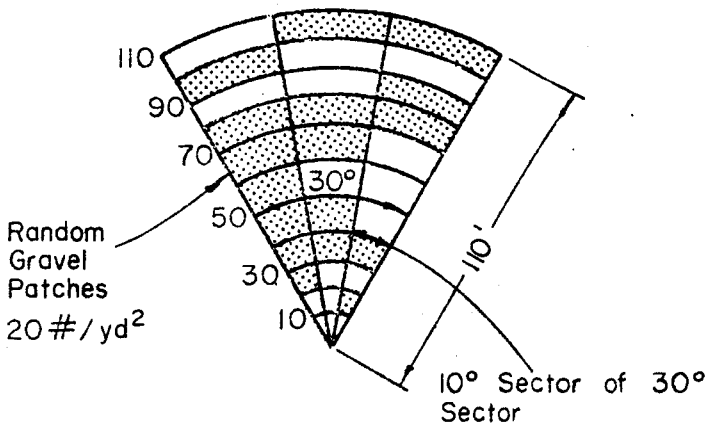

Configuration 13

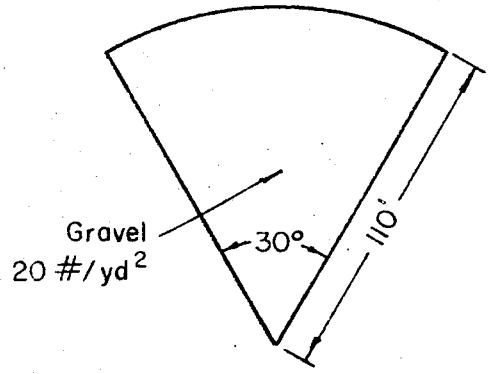

Configuration 14

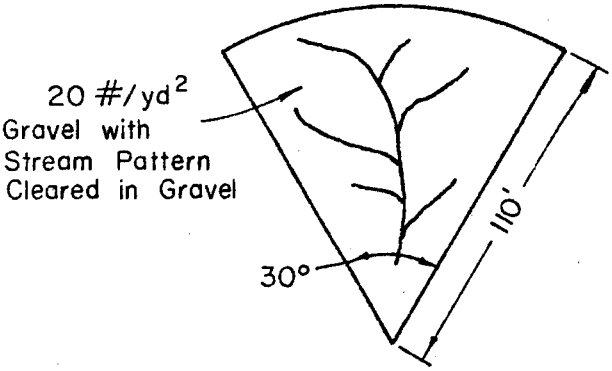

Configuration 15

TABLE I

Colorado State University
Experimental Rainfall-Runoff Facility

EXPERIMENTAL RUNS COMPLETED

Run No.	*Configuration	Surface	! Intensity	Duration-Secs.	Remarks
8A	1	Butyl	RYBG	300	Nozzle Pressure
8B			RYBG	45	variation signifi-
			RYBG	600	cant factor.
9			R	30	
			R	60	
			RY	60	
	1	Butyl	RYG	60	
			R	60	
			RY	60	
10			R	30	
			RYB	60	
	1	Butyl	RYB	60	
			RY	60	
			R	60	
11A			G	15	
	1	Butyl	G	300	Few secs of B rathe
11B				10 90	than G at start of 11B.
12	1	Butyl	G	10	5mph wind
			G	900	
13			R	10	
			R	60	
	1	Butyl	RY	60	
			RYG	60	
			RYB	60	
14			R	20	
			RYB	60	
	1	Butyl	RY	60	
			RYB	60	
15			R	15	
			RYB	60	
	1	Butyl	RY	60	
			RYB	60	
16	2	Butyl	RY	300	Windy day; test stilling well lag
17			Y	135	
			Y	600	
	2	Butyl	Y	20	
			Y	45	
			Y	15	
			Y	300	

No.	*Configuration	Surface	Intensity	Duration-Secs.	Remarks
18	2	Butyl	RY RY RY RY	30 300 75 300	
19			RYG RYG RYG RYG	20 300 60 300	
20	2	Butyl	RYGB RYGB RYGB RYGB	10 300 60 300	Very poor response.
21	3	Butyl	RY RY RY RY	35 300 75 300	
22	3	Butyl	RYG RYG RYG	22 300 75	
23	3	Butyl	RYGB RYGB RYGB	14 300 75	
24A 24B 24C	4	Butyl	RY RY RY RY RY RY	30 720 30 300 30 720	Problem with storage behind the border; should be filled with the wet down stage. Board ridges covered with butyl flap & center opening.
25	4	Butyl	RYG RYG RYG	20 720 120	Board ridges covered with Butyl flap & center opening.
26	5	Butyl	R R R R	20 300 20 90	Plastic flaps laid down.
27	5	Butyl	RY RY RY	30 300 90	Plastic flaps laid down.
28	5	Butyl	RYG RYG RYG RYG	20 300 10 75	Plastic flaps laid down.
29	6	Butyl	R R R R	85 300 15 90	Plastic flaps laid down.

Run No.	*Configuration	Surface	Intensity	Duration-Secs.	Remarks
30	6	Butyl	RY RY	360 90	Wind calm.
31	6	Butyl	RYG RY	300 75	Surface wet evaporation no wet down.
32	6	Butyl	RYBG RYBG	300 45	No wet down needed
33	7	Gravel & Butyl	R R	420 90	Gravel$_2$ for top 30' 10#/yd^2
34	7	Gravel & Butyl	RY RY	300 90	Gravel$_2$ for top 30' 10#/yd^2
35	7	GRavel & Butyl	RY RYG RYG	25 360 75	Gravel$_2$ for top 30' 10#/yd^2
36	7	Gravel & Butyl	RYBG RYBG RYBG	10 240 45	Gravel$_2$ for top 30' 10#/yd^2
37	8	Gravel & Butyl	R R	420 120	Gravel$_2$ for top 70' 10#/yd^2
38	8	Gravel & Butyl	RY RY	60 120	Gravel$_2$ for top 70' 10#/yd^2
39	8	Gravel & Butyl	RYG RYG	360 90	Gravel$_2$ for top 70' 10#/yd^2
40	8	Gravel & Butyl	RYGB RYGB	300 60	Gravel$_2$ for top 70' 10#/yd^2
41	9	Butyl & Gravel	R R	120 120	10#/yd^2 for top 104' Little or no wind.
42	9	Butyl & Gravel	RY RY	480 120	10#/yd^2 top 104'
43	9	Butyl & Gravel	RYG RYG	360 90	10#/yd^2 for top 104' wind calm
44A 44B	9	Butyl & Gravel	RYGB RYGB RYGB	300 60 60	10#/yd^2 for top 104' Run fouled up
45	10	Butyl & Gravel	RYG RYG RYG RYG	365 720 210 75	partial that becomes equilibrium
46	10	Butyl & Gravel	RYBG RYBG	300 90	
47	10	Butyl & Gravel	RY RY	360 120	

Run No.	*Configuration	Surface	!Intensity	Duration	Remarks
48	10	Butyl & Gravel	R R	420 120	
49	11	Butyl & Gravel	RYG RYG	720 90	
50	11	Butyl & Gravel	R R R	420 120 120	Repeat partial equilibrium
51	11	Butyl & Gravel	RY RY	360 120	
52	1'	Butyl & Gravel	RYBG RYBG	305 90	
53	12	Butyl & Gravel	R R	540 120	
54	12	Butyl & Gravel	RY RY RY	360 10 120	wind calm
55	12	Butyl & Gravel	RYG RYG RYG RYG	10 300 10 90	
56	12	Butyl & Gravel	RYGB RYGB RYGB	10 300 90	
57	13	Butyl & Gravel	R R	420 120	
58	13	Butyl & Gravel	RY RY RY	10 360 120	
59	13	Butyl & Gravel	RYG RYG RYG	10 300 90	
60	13	Butyl & Gravel	RYBG RYBG	300 90	
61	14	Butyl & Gravel	R R	540 120	
62	14	Butyl & Gravel	RY RY	420 120	
63	14	Butyl & Gravel	RYG RYG	420 90	
64	14	Butyl & Gravel	RYGB RYGB	420 90	
65	15	Butyl & Gravel	R R	480 120	

Run No.	*Configuration	Surface	!Intensity	Duration	Remarks
66	15	Butyl & Gravel	RY RY	360 120	
67	15	Butyl & Gravel	RYG RYG	420 90	
68	15	Butyl & Gravel	RYGB RYGB	420 90	

* See attached Configuration sketches at end of Table 1.

! See attached coding Table 2 at end of Table 1.

Coding Scheme for Rainfall Intensity

CODE	RAINFALL INTENSITY
R	Approx. 0.5 inches per hour
RY	Approx. 1.0 inches per hour
RYG	Approx. 2.0 inches per hour
RYGB	Approx. 4.0 inches per hour

Equations (1) and (2) can be combined by eliminating u and written in the following dimensionless form:

$$\frac{\partial h^*}{\partial t^*} + Nh^{*N-1}\frac{\partial h^*}{\partial x^*} = q^* + \left[\frac{(1-r)\ h^{*N}}{1-x_*\ )1-r)}\right] \qquad (3)$$

where

$$h^* = h/H_o\ ,\quad t^* = \frac{Lo\ (1-r)}{Vo},\quad X^* = \frac{x}{L\ (1-r)}$$

and

$$q^* = ql_{qo} = \frac{q\ L_o\ (1-r)}{Ho\ \ Vo}$$

The normalizing quantities are defined as follows: H_o is the normal steady-state depth at $x = L_o(1-r)$ V_o is the normal steady-state velocity at $x = L_o(1-r)$, and $L_o(1-r)$ is the length of the converging section.

Equation (3) has only one parameter, r, which is related to the degree of convergence. This indicates that when r is constant and if the kinematic model is adequate there will be a unique equilibrium hydrograph if experimental data are normalized by dividing the discharge by the steady-state discharge and by dividing the observed time by a normalizing time t_o. The normalizing time will be chosen such that it minimizes an error criterion between observed and computed dimensionless hydrographs. In choosing such an optimized t_o we are in fact obtaining an optimized estimate of the Chezy parameter C through the following relationship:

$$C = \left[\frac{L_o\ (1-r)}{T_o}\right]^{3/2} (S_o\ Q_o)^{-1/2} \qquad (4)$$

Where Q_o is the steady-state discharge per foot of width at the outlet.

Two sets of experimental runs with different roughness but the same value of the parameter r have been analyzed so far. The series with a smooth butyl surface are 8B, 26, 27, and 28. The second series, runs 41A, 42A, 43A, and 44A, had a uniform layer of 1-1/2 diameter gravel spread over the butyl surface at a rate of approximately 10 lbs. per square yard.

Experimental runs were performed at each of four rainfall intensities and consisted of two parts: an equilibrium run to established the steady-state input rate and a partial equilibrium run. Each run was started with approximately the same initial condition by turning on the sprinklers for a short time to wet the surface before each test began. Because of the rapid response of the system, accurate timing is of utmost importance. Although the stage recording equipment at the H-flume measuring device had a time resolution of five seconds some of the early runs were subject to substantial timing errors because of procedural problems. These problems were eliminated after sufficient experience was gained and are not present after the first ten runs.

T_o was estimated from the recession side of the equilibrium hydrographs in the following manner. The discharges were first normalized by dividing by the steady state discharge. The analytical recession from equilibrium can be obtained in the following parametric form

$$Q_* = \frac{X_o \left[2-(1-r)\, X_o\right]}{(1+r)} \tag{5}$$

$$t_* = \left(\frac{1+r}{r}\right) - \frac{\frac{N-1}{N}\left\{\left[1-(1-r)\, X_o\right]^{\frac{2N-1}{N}} - (r)^{\frac{2N-1}{N}}\right\}}{(2N-1)\,(1-r)\left\{X_o\left[2-(1-r)\, X_o\right]\right\}^{\frac{N-1}{N}}} \tag{6}$$